# Final Report to


**Title of Project:**

Field Testing and Diagnostics of Radial-Jet Well Stimulation for Enhanced Oil Recovery from Marginal Reserves

09123-03.FINAL

**Performer Name:**
New Mexico Institute of Mining and Technology
New Mexico Petroleum Recovery Research Center

**Performer Address:**
801 Leroy Place
Socorro, NM 87801 USA

**Industry Partners:**
Harvard Petroleum Corporation LLC
Viper Drill LLC

**Principal Investigator:**
Robert Balch, Senior Scientist / Section Head
Petroleum Recovery Research Center (PRRC)
New Mexico Institute of Mining and Technology, Socorro, NM 87801
Phone: (575) 835-5305, Fax: (575) 835-6031, email: balch@prrc.nmt.edu

Date: November 30, 2015

## LEGAL NOTICE

**This report was prepared by the Petroleum Recovery Research Center as an account of work sponsored by the Research Partnership to Secure Energy for America, RPSEA. Neither RPSEA members of RPSEA, the National Energy Technology Laboratory, the U.S. Department of Energy, nor any person acting on behalf of any of the entities:**

**a. MAKES ANY WARRANTY OR REPRESENTATION, EXPRESS OR IMPLIED WITH RESPECT TO ACCURACY, COMPLETENESS, OR USEFULNESS OF THE INFORMATION CONTAINED IN THIS DOCUMENT, OR THAT THE USE OF ANY INFORMATION, APPARATUS, METHOD, OR PROCESS DISCLOSED IN THIS DOCUMENT MAY NOT INFRINGE PRIVATELY OWNED RIGHTS, OR**

**b. ASSUMES ANY LIABILITY WITH RESPECT TO THE USE OF, OR FOR ANY AND ALL DAMAGES RESULTING FROM THE USE OF, ANY INFORMATION, APPARATUS, METHOD, OR PROCESS DISCLOSED IN THIS DOCUMENT.**

**THIS IS A FINAL REPORT. THE DATA, CALCULATIONS, INFORMATION, CONCLUSIONS, AND/OR RECOMMENDATIONS REPORTED HEREIN ARE THE PROPERTY OF THE U.S. DEPARTMENT OF ENERGY.**

**REFERENCE TO TRADE NAMES OR SPECIFIC COMMERCIAL PRODUCTS, COMMODITIES, OR SERVICES IN THIS REPORT DOES NOT REPRESENT OR CONSTIITUTE AND ENDORSEMENT, RECOMMENDATION, OR FAVORING BY RPSEA OR ITS CONTRACTORS OF THE SPECIFIC COMMERCIAL PRODUCT, COMMODITY, OR SERVICE.**

## ABSTRACT

The objectives of this project were to field-demonstrate a radial drilling technology for production enhancement from mature oilfields and to identify the feasibility as well as cost efficiency of using these stimulations for enhanced oil recovery. Specifically, diagnostic methods for tracking the placement of laterals and optimizing the design of lateral patterns were developed and field-validated.

This research targets the recovery of stranded or by-passed pay and a new drilling technology, the ViperDrill, was field-tested for production enhancement in mature oil wells. To optimize the treatment, diagnostic technologies were developed and field-tested for monitoring the lateral placement: Sensors for measuring acceleration and direction were integrated with coiled tubing for monitoring the placement of laterals, laboratory studies with reservoir modeling using flow simulators were carried out to optimize the lateral placement, and the technical feasibility and economic efficiency of using these treatments for production enhancement in different types of reservoirs were evaluated through computer simulation and field demonstration.

Numerical simulation with Eclipse and CMG simulators modeled the effects of emplacing 30 ft long, 1 in. diameter laterals using three grid models utilizing combinations of square and radial grids with refinements along the lateral trajectories. Expected incremental oil was modeled at ~30% for four laterals in one production interval. Field sites in SE New Mexico were selected in the San Andres/Grayburg and Delaware formations and prototype designs of the location sensor were made utilizing durable piezoelectric sensors and chip-based gyroscopes to measure deviations from vertical; these sensors are very similar to those found in many modern electronics devices, such as smart phones. The drilling system and sensors were both tested while placing a total of 29 laterals of up to 32 ft in length in two wells between May and October of 2015.

Submitted and Signed November, 30, 2015 by:

Robert S. Balch
Principal Investigator

This page intentionally left blank.

# TABLE OF CONTENTS

## LIST OF FIGURES AND TABLES

## LIST OF ACRONYMS

| | |
|---|---|
| NMT | New Mexico Tech aka New Mexico Institute of Mining and Technology |
| PRRC | Petroleum Recovery Research Center |
| HLLC | Harvard Petroleum Company LLC |
| SP | Spontaneous Potential |

## EXECUTIVE SUMMARY

This research targeted the recovery of stranded oil from low-permeability zones in which large quantities of hydrocarbons remain in the formation during primary production, such as stripper wells. Well stimulation by radial jet or short radius drilling enhancement is an attractive technology for enhanced oil recovery for both existing and new field developments. By using the most advanced coil-tubing technologies, lateral holes with different geometries can penetrate to compartmentalized formations that are left behind or bypassed during conventional water-flooding or within the less permeable oil zones that cannot be sufficiently drained by conventional processes. Specifically, ViperDrill technology for drilling short radius, fully horizontal, through-pipe boreholes was field-tested for production enhancement. To optimize the radial treatment, diagnostic technologies were developed and field-tested for monitoring the lateral placement and directions. To accomplish this, a sensor based on tri-axial accelerometers and chip-based gyroscopes was developed, which is capable of operating remotely, with no connection to the surface, during the drilling of the laterals. The sensor tracks the path taken by the drilling system and data is reviewed at the surface using custom software. In addition, laboratory studies with reservoir modeling using a reservoir simulator were carried out to optimize the lateral placement. Impact of reservoir characteristics, such as rock mechanics, residual oil distribution, and reservoir properties on lateral patterns were investigated. Finally, the technical feasibility and economic efficiency of using radial jet treatment for production enhancement in different types of reservoirs was evaluated through field demonstration.

The research has multidisciplinary components and systematic approaches to mesh fundamental research with field demonstration for technology validation. The team members, included the Petroleum Recovery Research Center at New Mexico Tech (PRRC/NMT), Viper Drill, an oilfield service company, and a small producer Harvard Oil Company LLC (HLLC), who combined provide a total of 55.3% cost share for the demonstration project. The successful completion of this project validated a cost-efficient technology that can significantly increase communication and flow rates in existing marginal wells, which are mainly operated by small producers.

Field sites in SE New Mexico were used and include: 1) The Barbie State No. 3 well which produces from dolomites and sandstones of the Grayburg formation; and 2) The Federal 00 # 3 well which produces from fine grained sandstones of the Delaware formation. Numerical Simulators were used to forward model production enhancement through adding up to four radial jetted laterals to existing vertical wells. Models were created for both square and radial grid patterns and employed two-inch diameter, 30 ft horizontal segments. All models show an enhancement in ultimate recovery of between 20–30% over a twenty-year span of time and employing radial jet recompletions earlier in the project did not significantly alter the incremental oil, but did significantly accelerate production of that incremental resource. Prototypes and bench scale

led to development of a location sensor, which addresses a key concern of operators, “Where does the lateral go?” The device utilizes compact high temperature batteries, a programmable control chip, a memory chip, and durable piezoelectric accelerometers, gyroscopes, and gravity sensors to measure deviations from vertical; these sensors are very similar to those found in many modern electronics devices, such as smart phones.

# REPORT DETAILS

## *1.0 Experimental Methods*

This work can be divided into three major components: a simulation study to apply sensitivity testing to the emplacement of short radius laterals into a reservoir; development of technology to track the emplacement of laterals using any short radius drilling technology; and field validation of the simulation models and potential for stimulation by short radius laterals via field testing at two wells in southeast New Mexico. Section 1.1 will discuss development of the simulation models, and background on the field test site that was eventually tested. Section 1.2 will discuss the development of a sensor capable of measuring the track of the emplaced laterals. Section 1.3 will discuss field testing of the Viper Drill and the sensors.

### 1.1 Simulation Modeling

This section of the report focuses on reservoir characterization and simulation of a case-study well in Millman field to evaluate the potential efficiency of short radius laterals. The Barbie State No.1 well located in west Millman field, southeastern New Mexico, was chosen as one of two test wells for the project; the reservoir is small in size, shallow in depth and has low pressure and permeability.

Reservoir description relies on limited existing data: Twelve modern logs are the main source of information and provide reservoir data on porosity, permeability and water saturation. A porosity-permeability correlation from an adjacent field study was used to estimate permeability data. Furthermore, PVT data was generated with reasonably assumed parameters using a black-oil model. This is similar to data available for other mature fields that are candidates for this technology.

A 3D simulation model was constructed integrating available reservoir and geologic data. The reservoir boundary was assigned as free with constant pressure and steady-state flow. Average pressure trend and well production are the two main parameters for history-matching. The

initial history-matching yielded barely satisfactory outcomes so adjustments around the Barbie State No.1 were subsequently made for permeability and oil saturation distribution. The major difficulty in validating the model is the lack of field records such as well bottomhole pressure.

Prediction of four distributions of laterals was performed by running the simulation for 10 years from 2013 to 2023. Regardless of the combination of target layer(s), the case with four laterals per level has the greatest potential in enhancing oil production and final recovery. Considering that the previous main perforation sandstone layer showed the largest increase in oil production, a duplicated sixth layer was placed with four lateral patterns to test lateral potential of bypassed pay in a similar un-perforated layer.

### 1.1.1 Objective and Workflow

The objective of the research is to test a newly developed technology for production enhancement from low-permeability reserves. Diagnostic techniques for monitoring lateral direction and placement were also developed and field tested. It was expected that a successful completion of this project would answer the following questions: (1) How to control and diagnose the placement and direction of laterals during a short radius enhancement? (2) Is a short radius enhancement cost-effective for productions of marginal reserves? (3) What are the preferred reservoir conditions and lateral patterns for deployment of this technology from an existing wellbore?

The Millman field, located in the Permian Basin, has a production history of more than 20 years (Figure 1). The target zone in the Millman field is the **Grayburg** (a mix of carbonate and sandstone facies). The Millman reservoir is still in primary depletion and there is no pressure maintenance. The target well, Barbie State No.1, is located in the Millman Field, Eddy County (Township: 19S, Range: 27E, Section 13). The objective was to model the reservoir using well logs, obtain a match of production history, and then model the impact of one to four jetted lateral simulations after a few months' worth of new data has been collected. The stimulation was planned to take place in the summer of 2014, and occurred instead in May of 2015. A detailed sensitivity analysis of four types of jetted laterals was completed, with a goal of optimizing the number of laterals.

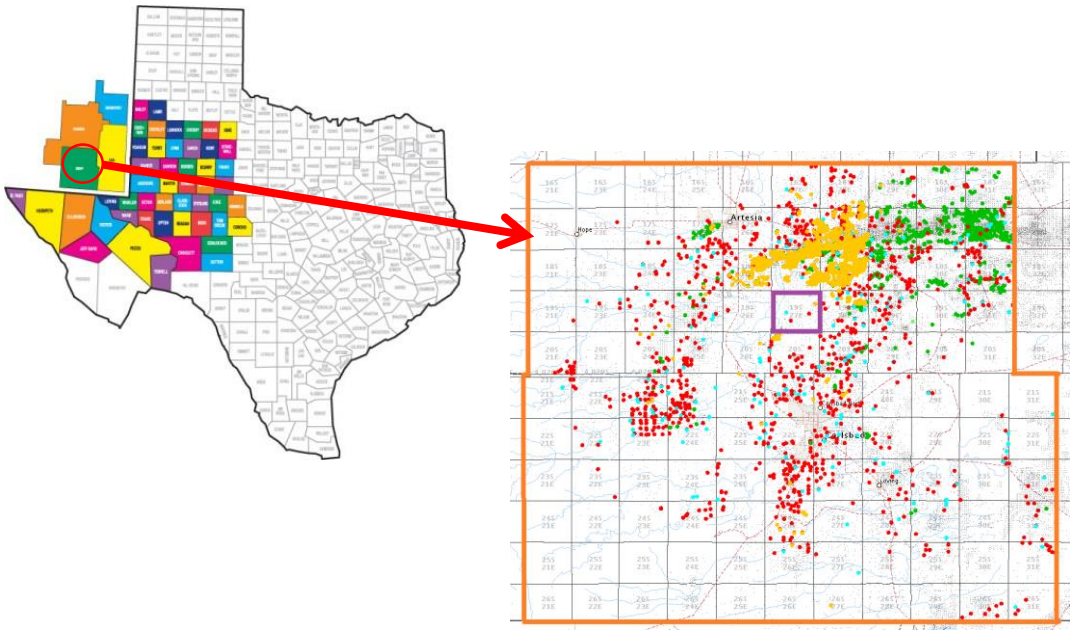

**Figure 1. Location of Millman Field, Eddy County, New Mexico.**

A geological model generated from a well log analysis and correlation was established, and a grid model of the reservoir constructed in which layers are divided based entirely on the well log data. Initial reservoir properties such as permeability, porosity and saturation were available through analysis of well log data in LESA. Other lithology data was obtained from analogue core in a nearby field. Prior to stimulation of the target well, a model of the geological structure with the best available reservoir properties and operator knowledge was constructed. Before the simulation of the proposed stimulation, and with two decades of production data, a sensitivity analysis of the impact of four scenarios for laterals was performed using simulation to optimize the number of laterals. The production response of the stimulation will ultimately be compared to the predicted model.

### 1.1.2 Brief Introduction to Radial-Drilling Technology

Radial drilling is a technology that is advertised to reach reserves which are not economically exploitable with conventional completion techniques (vertical, slanted or horizontal well), and which could also accelerate the recovery of hydrocarbon reserves. It is estimated that 75% to 85% of all known hydrocarbon discoveries remain in the ground (Abdel-Ghany et al., 2011).

Radial drilling represents a family of through-pipe recompletion technologies for drilling horizontal channels out from an existing wellbore (Figure 2). Systems using high pressure water at the end of a coiled tubing are claimed to be able to reach 300 feet away from the wellbore, leaving a channel of 30–50 mm diameter. Other technologies include mechanical short-radius laterals. Radial jet enhancement targets existing oil and gas wells and operates at the end of

coiled tubing units, so there are practical limits on depth. This enhancement technology is advertised as a much more cost-efficient process than conventional re-stimulation techniques. This technology could prolong the productive life of wells and, consequently, an entire field by reducing the need for expensive infill drilling and allowing the targeting of bypassed pay zones that may be too thin to conventionally recomplete. The process is relatively fast and has a reasonable cost. Radial drilling could also be applied in wells when other stimulation techniques are not applicable, and on layers that are close to water saturated layers, which may limit the applicability of hydraulic fracturing stimulation (Abdel-Ghany et al., 2011).

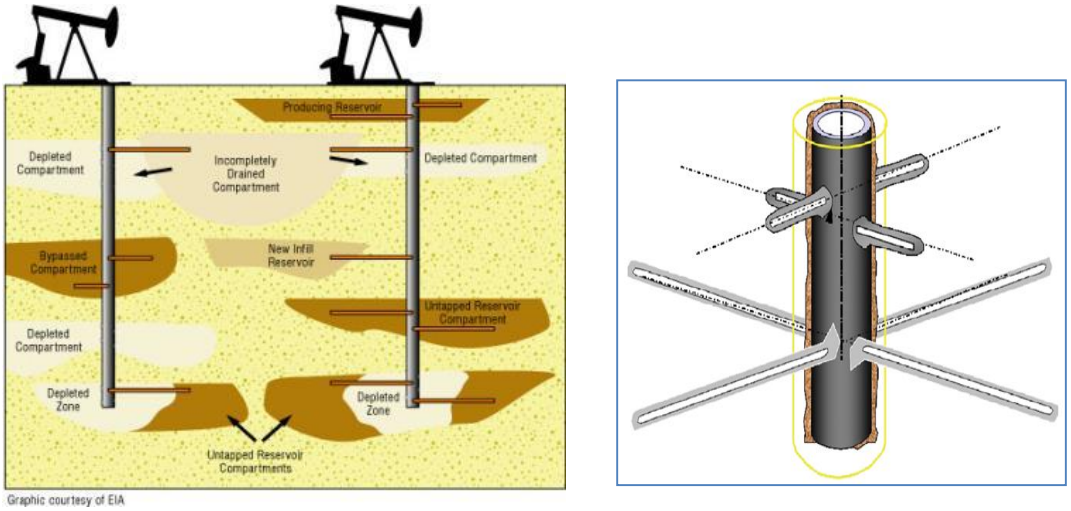


**Figure 2. Potential impact of short radius laterals. Left, accessing compartments and bypassed pay, right ability to leave the wellbore at right angles.**

Performance testing of these short radius laterals has not been adequately studied. The work detailed in this report involves construction of a model, sensitivity studies, and history-matching for one of the test sites, the Millman field, in southeastern New Mexico.

### 1.1.3 The Role of Simulation in the Project

Reservoir simulation has many advantages over a simple analytical method. First, reservoir simulation accounts for space and time variations of geological and rock/fluid data; therefore, the results can be more reliable than other estimation applications. Second, during reservoir characterization and model construction phases, data are gathered and analyzed which leads to a better understanding of the studied reservoir. Third, during the history-matching phase, sensitivity analysis of various parameters can be investigated. Finally, once a simulation model is validated, various development strategies can then be predicted. Thereby, the results ensure that a field is developed with the best solution (Ertekin 2011).

The main objective of this simulation study is to use reservoir simulation to help determine optimal lateral placement and to attempt to predict the measured response of the stimulations. The study workflow includes data acquisition, reservoir description, model construction, validating the model by history match, and sensitivity analysis for four types of lateral emplacements.

In the data acquisition stage, data gathered include: geological data, petrophysical data, production history, and well history. The major difficulty for this study is the limitation and poor quality of the data, but this is not unusual for candidate wells that would use this re-stimulation technology. Well logs of the simulation area lack SP and sonic curves, and some wells do not have a sufficient data source for analysis, though they do provide production history data. For example, the shallow-deep resistivity curves for water saturation determination exists only in BARBIE STATE No.1, JMS STATE No.1, LOCO HILLS STATE No.1 and MARY WOLF STATE No.1. Furthermore, most wells were fractured and acidized during completion in the late 1980s and early 1990s. Even when the skin factor is applied, the near-wellbore flow geometry is difficult to identify.

### 1.1.4 Field Site Overview: New Mexico Permian Basin

Production in the New Mexico portion of the Permian Basin has been obtained from reservoirs located on the Northwest Shelf and on the Central Basin Platform (Figure 3). There are 13 productive zones from shelf, platform and ramp settings. These 13 plays produce from more than 249 reservoirs. In addition there are four plays that are productive from reservoirs deposited in basinal settings (Malone et al., 2000).

A wide variety of advanced management techniques have been applied in the Permian Basin in order to enhance or stimulate production from already discovered reservoirs. Waterfloods have increased recovery and produced substantial volumes of oil in both shelf and basinal reservoirs. Pressure maintenance projects have increased production in solution gas drive reservoirs. More recently, horizontal drilling has been successfully applied to produce oil not in communication with vertical wells in horizontally compartmentalized reservoirs or to produce oil that was upswept by waterfloods in old, mature reservoirs. Other older reservoirs have benefited from new completions in bypassed pay that remained unproduced behind casing. Some other reservoirs did not attain full field development for years after discovery because development was undertaken on the basis of misconceptions regarding trapping mechanisms. In other cases, exploratory objectives were overlooked in favor of drilling targets in other stratigraphic units. It appears that advanced reservoir management techniques have been successful in many plays, but not always widely applied, leaving potentially productive oil in the ground and behind-pipe in mature Permian fields.

### 1.1.5 Geology

Reservoirs of the Artesia Platform sandstone play are stretched across the Northwest Shelf of the Permian Basin and across the western flank of the Central Basin Platform (Figure 3). This play has been in a gradual decline over the past 30 years. Reservoirs are sandstones in the Artesia Group (Permian: Guadalupian). The Artesia Group is subdivided into five formations (descending; Figures 4–5): Tansill, Yates, Seven Rivers, Queen, and Grayburg. Principal productive sandstones are in the Yates and Queen Formations, although sandstones of the Seven Rivers Formation provide significant production in some reservoirs. Reservoirs that produce principally from the Grayburg Formation are considered to be part of the San Andres and Grayburg Mixed Clastic/Carbonate plays. Dolostones of the Queen, Seven Rivers, Yates, and Tansill Formations form secondary reservoirs. Production from the dolostones is generally commingled with production from the more prolific sandstones in many reservoirs.

Reservoirs productive solely from the Queen Sandstones occur along and north of a trend that extends from Hobbs to Artesia (Figure 6). The Queen sandstones were deposited in coastal sandy braided streams, fluvial sand flats and fluvial-dominated coastal sabkhas, and poorly channelized sheet deltas that filled in lagoonal areas. Traps are largely stratigraphic, with porosity plugged in an updip direction by evaporates. Productive Queen Sandstones are fine to medium grained; average reservoir porosities range from 17 to 22 percent.

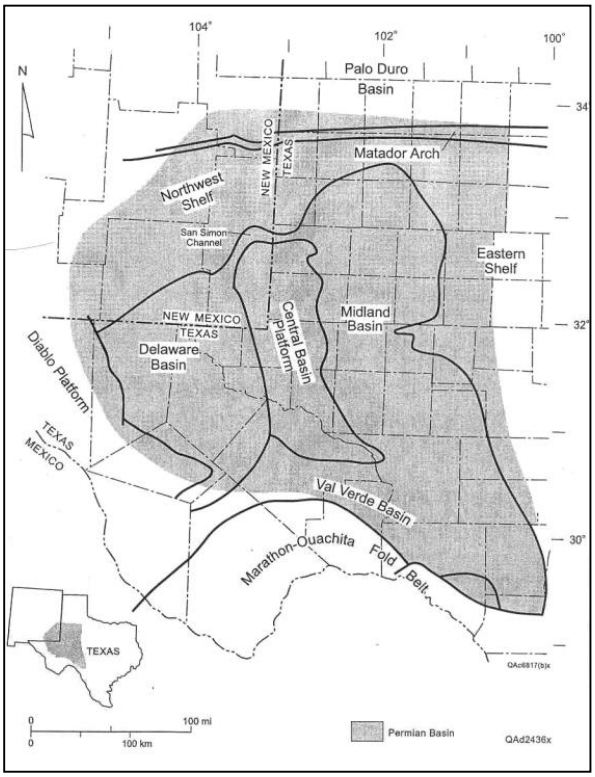


**Figure 3. Major boundaries and subdivisions of the Permian Basin in west Texas and southeastern New Mexico (Broadhead et al., 2004).**

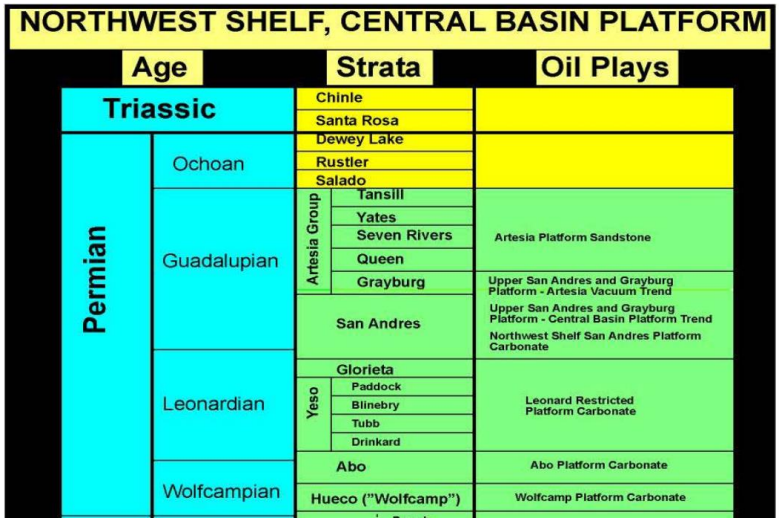


**Figure 4. Stratigraphic chart for the Northwest Shelf and the Central Basin Platform. Plays that are present on the Northwest Shelf and Central Basin Platform are listed next to their appropriate stratigraphic units; the Grayburg zone is the target for this simulation study (Broadhead et al., 2004).**

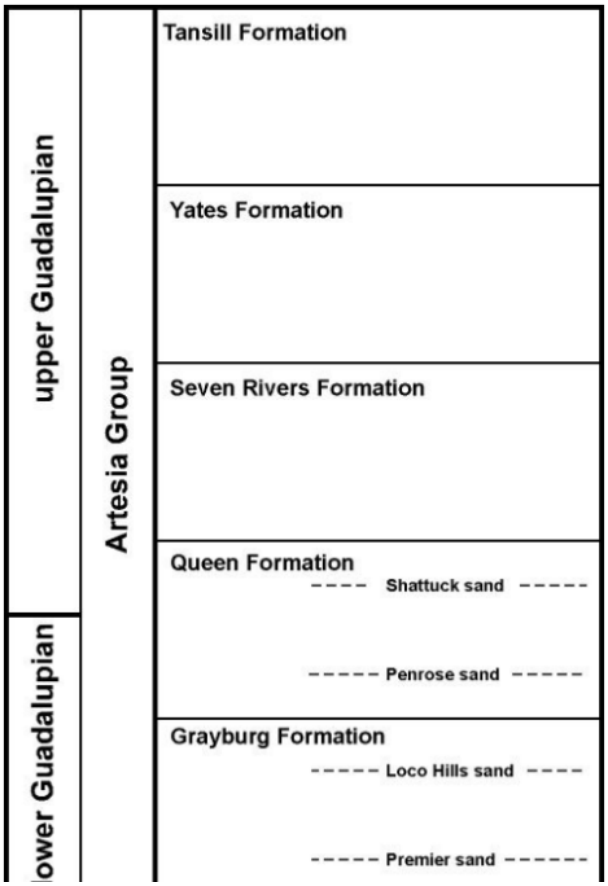


**Figure 5. Stratigraphic column of Guadalupian Artesia Group, Central Basin Platform and Northwest Shelf. Major named productive sandstones and Grayburg formations are indicated (Broadhead, 2004).**

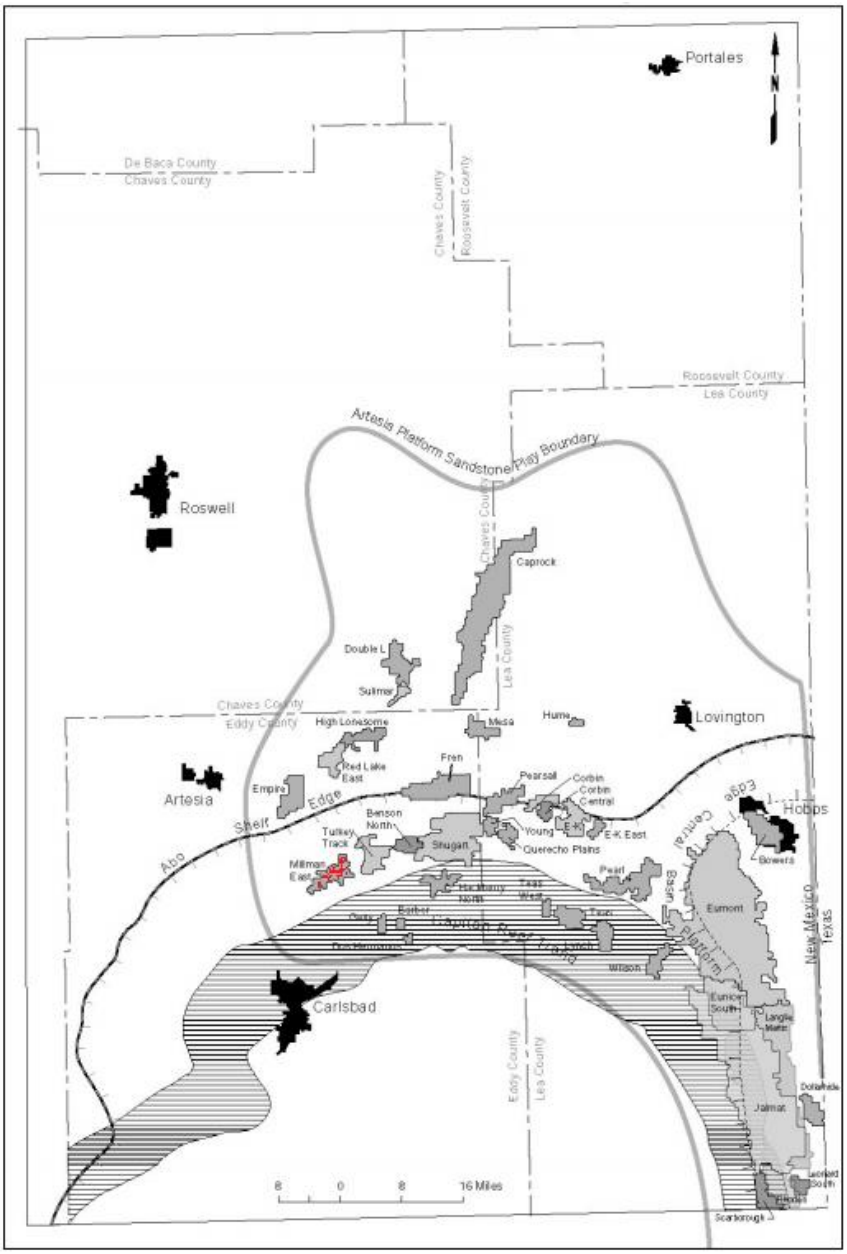


**Figure 6. Location of reservoirs with more than 1 MMBO cumulative production in the New Mexico part of the Artesia Platform Sandstone play (Broadhead et al., 2004).**

### 1.1.6 West Millman Field Review

West Millman field produces from the Grayburg formation. The first field test target well, Barbie State No.1, is an oil well located in Section 13, T19S-R27E. Wells in this area were not able to produce naturally due to low permeability caused by deep burial diagenesis; therefore, stimulation techniques such as hydraulic fracturing and acidizing are required. A pump was chosen to assist the flow. Figure 7 is visualization of well location geometries and Figures 8–9 show log cross-sections in Millman field. Well completion and well production data are summarized in Table 1.

The first well in the simulation area that encountered the Grayburg formation was drilled in October, 1985. The initial GOR was 341.576 scf/bbl. Field peak oil production of about 2055bbl/day was achieved in 1988. From then onwards, oil production showed a steady decline. Cumulative field oil production through 2013 was 6196.63 Mbbl of oil and 10606.5 MMscf gas. The water cut started at 20% and the field ceased to produce water at the end of 1998. Figure 10 shows the field history data, and Figure 11 shows the Field GOR and watercut.

Barbie State No.1 was the discovery oil well for the field; it is located in Section 13, T19S-R27E. The initial test rates were 30 BOPD and 35 BWPD and gas production was too small to measure. Barbie State No.1 was acidized with 5,000 gallons 15% acid and fractured with 100,000 gallons gel $H_2O$ and 190,000 pounds of sand during completion. Well logging was carried out on September 6, 1986, after well completion was accomplished in October 31, 1985.

Oil type for this study area is considered a mixture of dead and live oils. This is shown in the initial well test in which BARBIE STATE showed a poor gas production while MARY WOLF STATE and JMD STATE had high gas production. Furthermore, interval core analysis in Table 2 also supports this conclusion. Figures 12 and 13 show Barbie State #1 production history, and GOR/water cut, respectively.

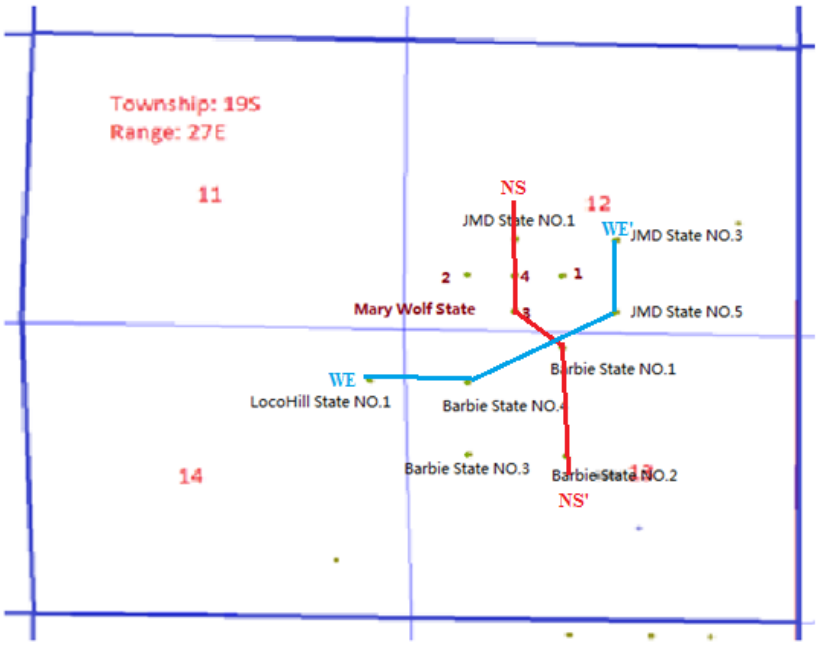


**Figure 7. Well location map of Millman field. Also shown are cross-sections developed for this study.**

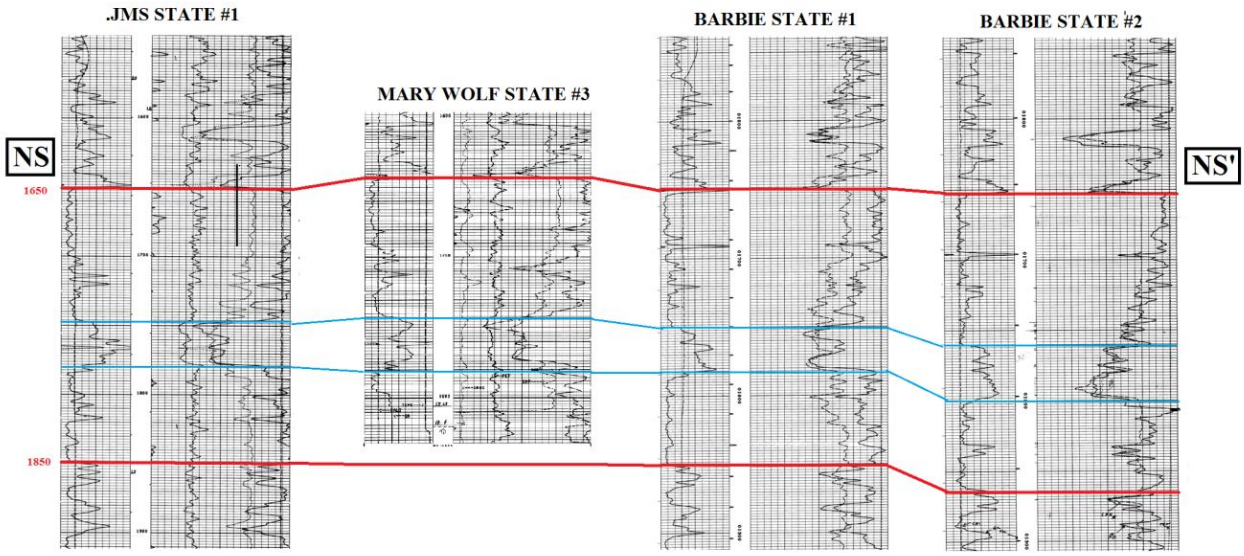


**Figure 8. Cross section NS-NS', Grayburg dolomite/sandstone.**

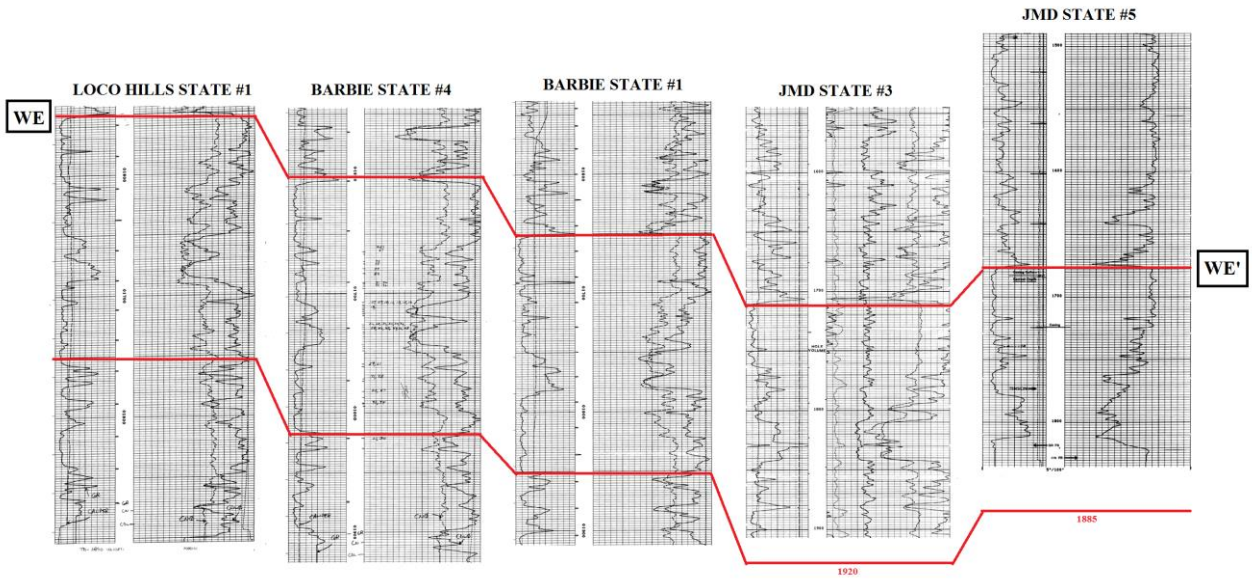


**Figure 9. Cross section WE-WE', Grayburg dolomite/sandstone.**

## Table 1. Summary of Well Completion and Well Production Data for Wells in Millman Field

**TABLE 2.1: WELL COMPLETION DATA**

| API | Lease Name | No. | Main Product | Production Method | TD (ft) | Perforation Interval U Perf (ft) | Perforation Interval L Perf (ft) | Stimualtion Method |
|---|---|---|---|---|---|---|---|---|
| 30-015-25485 | BARBIE STATE | 1 | Oil | Pump | 2800 | 1665 | 1830 | Hudraulic fracturing and acidizing |
| 30-015-25481 | BARBIE STATE | 2 | Oil | Pump | 1940 | 1735 | 1871 | Hudraulic fracturing and acidizing |
| 30-015-25482 | BARBIE STATE | 3 | Oil | Pump | 2005 | 1682 | 1844 | Hudraulic fracturing and acidizing |
| 30-015-25483 | BARBIE STATE | 4 | Oil | Pump | 1920 | 1665 | 1830 | Hudraulic fracturing and acidizing |
| 30-015-25523 | LOCO HILLS STATE | 1 | Oil | Pump | 1900 | 1590 | 1790 | Hudraulic fracturing and acidizing |
| 30-015-25861 | JMD STATE | 1 | Oil | Pump | 2136 | 1733 | 1776 | Hudraulic fracturing and acidizing |
| 30-015-25890 | JMD STATE | 3 | Oil | Pump | 2050 | 1796 | 1840 | Hudraulic fracturing and acidizing |
| 30-015-26237 | JMD STATE | 5 | Oil | Pump | 1830 | 1734 | 1830 | Hudraulic fracturing and acidizing |
| 30-015-25826 | MARY WOLF STATE | 1 | Oil | Pump | 2170 | 1768 | 1810 | Hudraulic fracturing and acidizing |
| 30-015-25883 | MARY WOLF STATE | 2 | Oil | Flowing | 1780 | 1696 | 1707 | Acidizing |
| 30-015-26058 | MARY WOLF STATE | 3 | Oil | Pumping | 1820 | 1700 | 1785 | - |
| 30-015-26059 | MARY WOLF STATE | 4 | Oil | Pumping | 1763 | 1652 | 1763 | Hudraulic fracturing and acidizing |

**TABLE 2.2: INITIAL PRODUCTION WELL TEST**

| API | Lease Name | No. | Main Product | Production Method | Test Date | Choke Size | $P_{TH\ (shut\text{-}in)}$ (psi) | $P_{TH\ (flowing)}$ (psi) | Test Rate Oil (BO/D) | Test Rate Gas (Mscf/D) | Test Rate Water (BW/D) |
|---|---|---|---|---|---|---|---|---|---|---|---|
| 30-015-25485 | BARBIE STATE | 1 | Oil | Pump | 10/14/1985 | OPEN | - | - | 30 | TSTM | 35 |
| 30-015-25481 | BARBIE STATE | 2 | Oil | Pump | 1/15/1986 | OPEN | - | - | 26 | TSTM | 118 |
| 30-015-25482 | BARBIE STATE | 3 | Oil | Pump | 1/24/1986 | OPEN | - | - | 10 | TSTM | 98 |
| 30-015-25483 | BARBIE STATE | 4 | Oil | Pump | 2/6/1986 | OPEN | - | - | 17 | TSTM | 87 |
| 30-015-25523 | LOCO HILLS STATE | 1 | Oil | Pump | 3/6/1986 | OPEN | - | - | 17 | TSTM | 117 |
| 30-015-25861 | JMD STATE | 1 | Oil | Pump | 3/14/1988 | N/A | - | - | 80 | TSTM | 40 |
| 30-015-25890 | JMD STATE | 3 | Oil | Pump | 1/1/1989 | N/A | - | - | 25 | 10 | 0 |
| 30-015-26237 | JMD STATE | 5 | Oil | Pump | 12/14/1989 | N/A | - | - | 20 | 15 | 15 |
| 30-015-25826 | MARY WOLF STATE | 1 | Oil | Pump | 12/1/1987 | N/A | - | - | 80 | N/A | 120 |
| 30-015-25883 | MARY WOLF STATE | 2 | Oil | Flowing | 5/26/1988 | N/A | - | - | 60 | 108 | 2 |
| 30-015-26058 | MARY WOLF STATE | 3 | Oil | Pumping | 2/24/1989 | N/A | - | - | 1 | 2 | 0 |
| 30-015-26059 | MARY WOLF STATE | 4 | Oil | Pumping | 12/13/1989 | N/A | - | - | 70 | 4 | 15 |

**(After Tables 2.1 and 2.2 in Xiao MS Thesis (2013))**

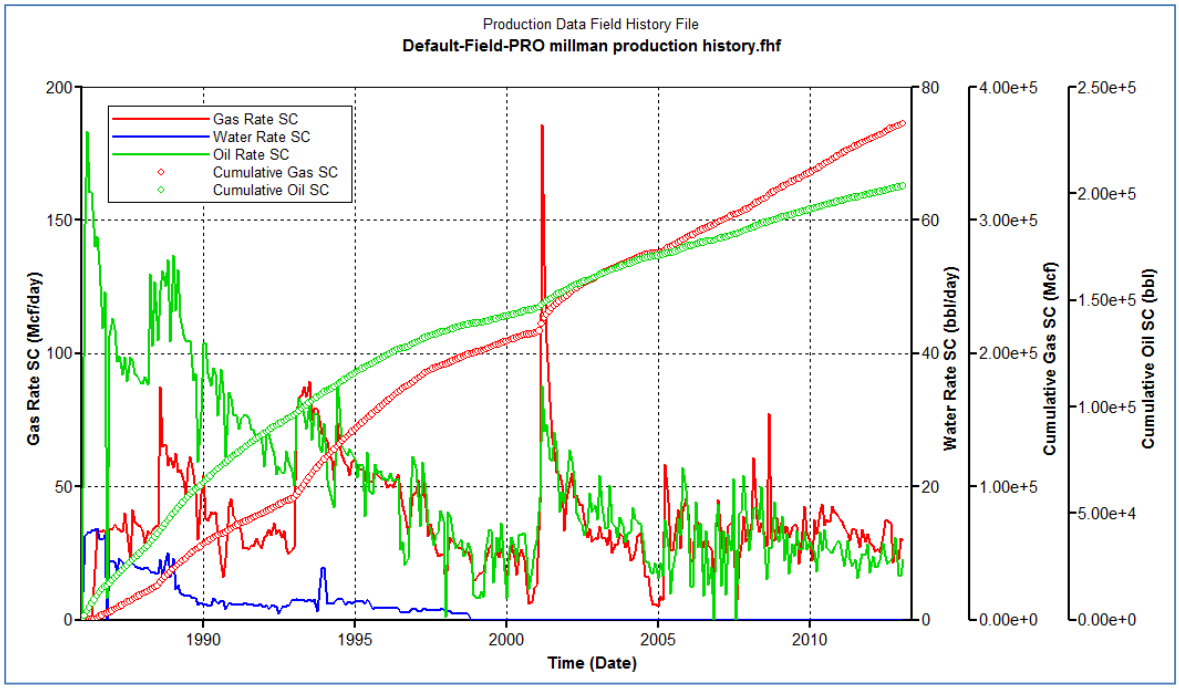


**Figure 10. Millman field production history.**

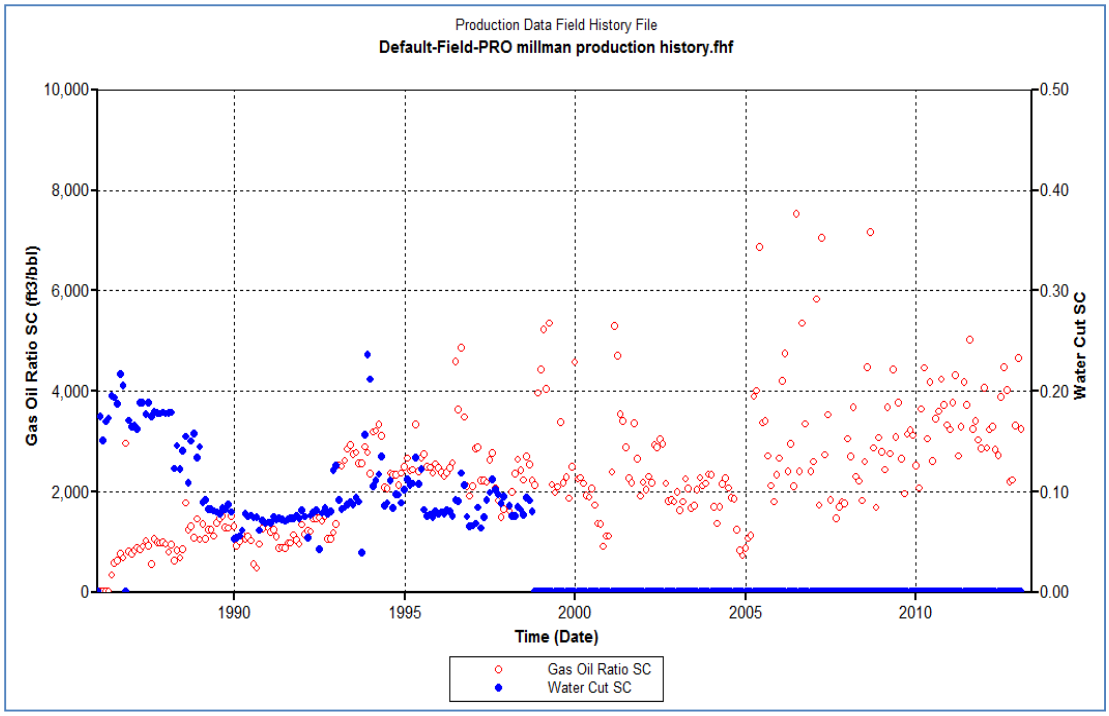


**Figure 11. GOR (ft3/bbl) and Water cut (%) for entire field.**

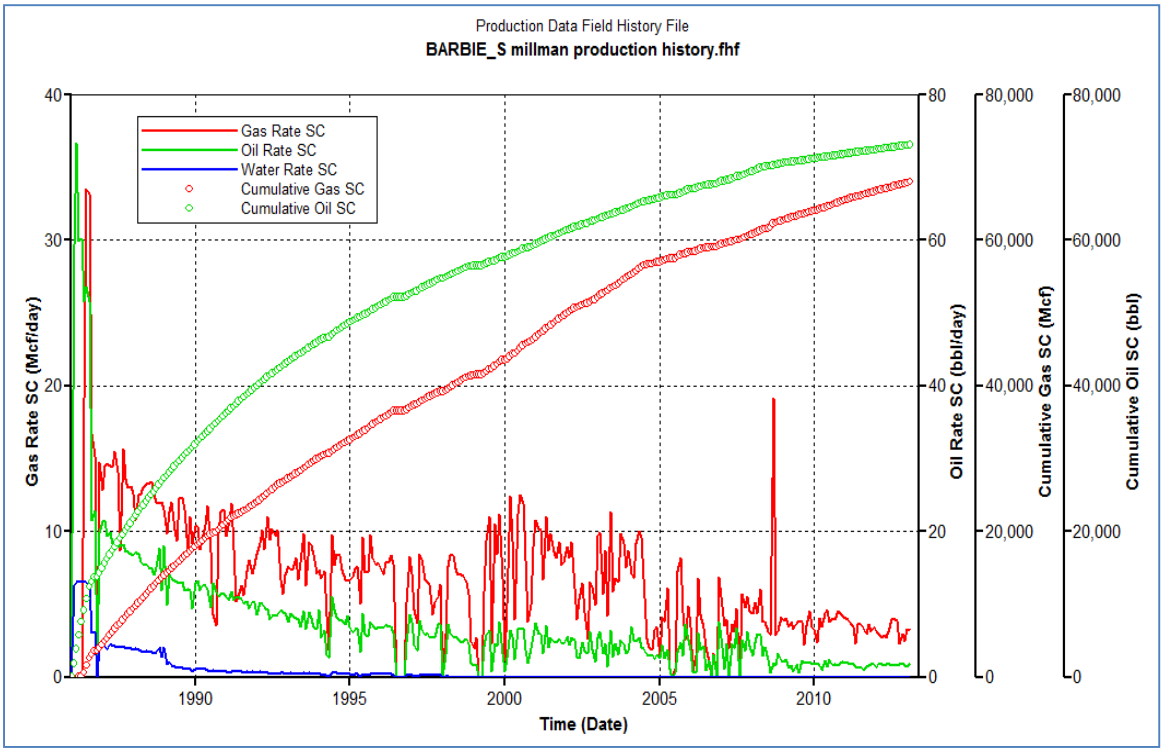


**Figure 12. Production history for Barbie State No.1.**

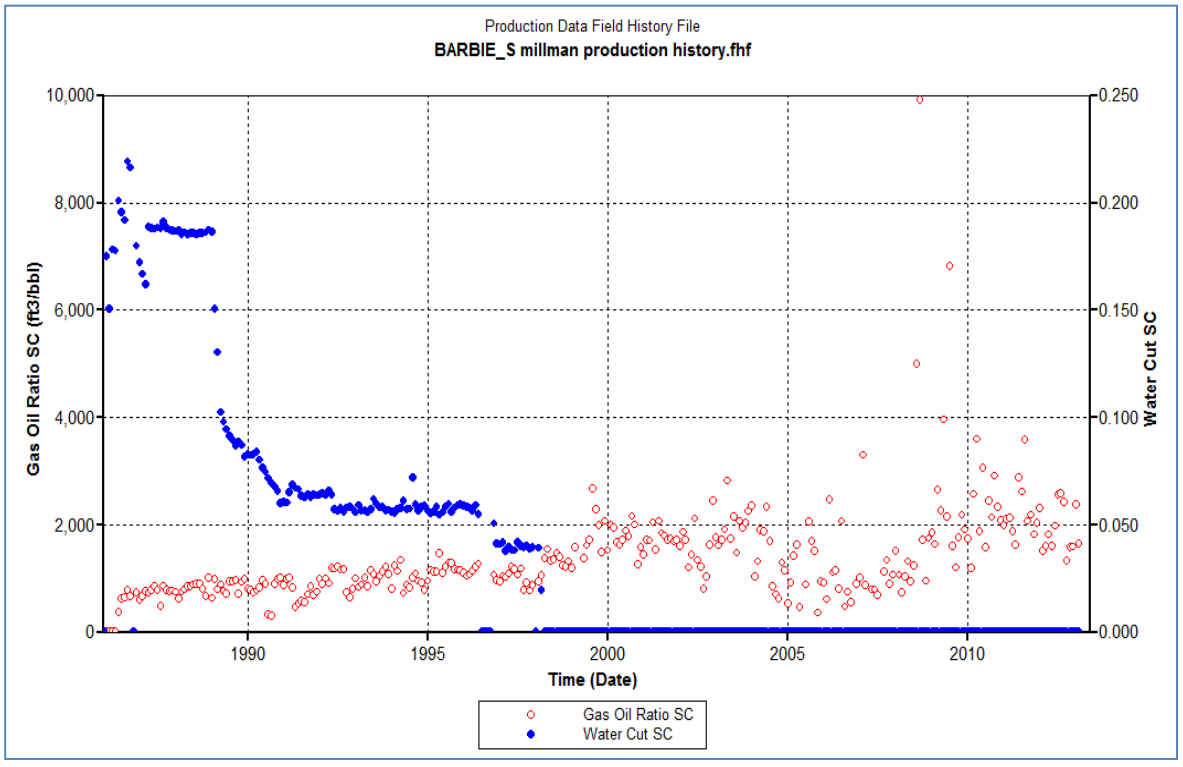


**Figure 13. GOR (ft3/bbl) and Water cut (%) of the Barbie State No.1.**

## Table 2. Sources for Reservoir Data

| Time/Operation | Predrilling | | | | | | |
|---|---|---|---|---|---|---|---|
| | | Seismic | | | | Geology Engineering Study | |
| | Gravity | Time | Velocity | Amplitude | Character | Analogy, Regional Knowledge, and Maps | Depositional Environment |
| Depth markers | | 2 | 2 | | | 2 | 2 |
| Structure and area | 2 | 2 | 1 | 3 | 3 | 2 | |
| Hydrodynamics | | | | | | 1 | |
| Gross thickness | | | 2 | | 3 | 2 | 2 |
| Net thickness | | | | 2 | 2 | 2 | 2 |
| Lithology | | | 2 | 2 | 3 | 2 | 2 |
| Mechanical properties | | | 2 | 2 | 3 | 2 | 2 |
| Contacts | | | 2 | 2 | 2 | 4 | |
| Pressure | | | 2 | 3 | | 1 | |
| Porosity | | | 2 | 2 | 3 | 2 | 2 |
| Permeability | | | | | 4 | 2 | 2 |
| Fluid saturation | | | 3 | 3 | 3 | 4 | |
| Pore sizes | | | | | | 2 | |
| Producing mechanism | | 4 | 3 | 3 | 3 | 2 | 3 |
| Hydrocarbon properties | | | 4 | 4 | | 2 | |
| Water properties | | | | | | 1 | |
| Production rate | | | | | | 2 | 2 |

Code: 1. Best source. 2. Good data source. 3. Average data source. 4. Poor data source.

| Time/Operation | Post-Development | | | | | | |
|---|---|---|---|---|---|---|---|
| | Production | | | | | | Special Studies |
| | Flow Test | Pressure | Water Cut | Gas/Oil Ratio | History | Analogy | Engineering and Geology |
| Depth markers | 2 | | | | | | 1 |
| Structure and area | 2 | 2 | 3 | 3 | 1 | | 1 |
| Hydrodynamics | 2 | 1 | | | 3 | 1 | 1 |
| Gross thickness | 2 | | | | | | 1 |
| Net thickness | 2 | | | | | | 1 |
| Lithology | | | | | | 2 | 1 |
| Mechanical properties | | | | | | 2 | 1 |
| Contacts | 1 | | 2 | 2 | 2 | | 1 |
| Pressure | 1 | 1 | | | | 1 | 1 |
| Porosity | 4 | | | | | 2 | 1 |
| Permeability | 2 | 1 | | | | 2 | 1 |
| Relative permeability | 1 | 2 | 2 | 2 | 2 | 2 | 1 |
| Fluid saturation | 1 | | 1 | 1 | 2 | | 1 |
| Pore sizes | | | | | | 2 | |
| Producing mechanism | | | 1 | 1 | 1 | 1 | 1 |
| Hydrocarbon properties | 1 | 2 | | 1 | | 2 | 1 |
| Water properties | 1 | | 1 | | | 2 | 1 |
| Production rate | 1 | 1 | | | 1 | 2 | 1 |
| Fluids produced | 1 | | 1 | 1 | 1 | 2 | 1 |
| Well damage | 1 | 1 | | | 1 | | 1 |
| Recovery efficiency | | | 2 | 2 | 1 | 2 | 1 |

Code: 1. Best source. 2. Good data source. 3. Average data source. 4. Poor data source.

| Time/Operation | Post-Development | | | | | | |
|---|---|---|---|---|---|---|---|
| | Production | | | | | | Special Studies |
| | Flow Test | Pressure | Water Cut | Gas/Oil Ratio | History | Analogy | Engineering and Geology |
| Depth markers | 2 | | | | | | 1 |
| Structure and area | 2 | 2 | 3 | 3 | 1 | | 1 |
| Hydrodynamics | 2 | 1 | | | 3 | 1 | 1 |
| Gross thickness | 2 | | | | | | 1 |
| Net thickness | 2 | | | | | | 1 |
| Lithology | | | | | | 2 | 1 |
| Mechanical properties | | | | | | 2 | 1 |
| Contacts | 1 | | 2 | 2 | 2 | | 1 |
| Pressure | 1 | 1 | | | | 1 | 1 |
| Porosity | 4 | | | | | 2 | 1 |
| Permeability | 2 | 1 | | | | 2 | 1 |
| Relative permeability | 1 | 2 | 2 | 2 | 2 | 2 | 1 |
| Fluid saturation | 1 | | 1 | 1 | 2 | | 1 |
| Pore sizes | | | | | | 2 | |
| Producing mechanism | | | 1 | 1 | 1 | 1 | 1 |
| Hydrocarbon properties | 1 | 2 | | 1 | | 2 | 1 |
| Water properties | 1 | | 1 | | | 2 | 1 |
| Production rate | 1 | 1 | | | 1 | 2 | 1 |
| Fluids produced | 1 | | 1 | 1 | 1 | 2 | 1 |
| Well damage | 1 | 1 | | | 1 | | 1 |
| Recovery efficiency | | | 2 | 2 | 1 | 2 | 1 |

Code: 1. Best source. 2. Good data source. 3. Average data source. 4. Poor data source.

**(after Table 3.1 in Ertekin, 2011)**

Both the field and the Barbie State #1 showed the same water production trend. Water rate had a constant decline toward zero around the end of 1998. Drive mechanisms for oil production are mainly liquid-rock expansion or solution gas drive. It is assumed that no gas cap is present in this system because the perforation interval of the well was right below the GOC and gas was produced from the gas cap at the same time as oil production. Moreover, as indicated in field production data, no water influx or aquifer exists and field water cut became zero by 1998. Therefore, the water-drive below the any oil water contact is weak or inactive.

Figures 14-15 presents typical pressure and GOR behavior with production for different drive mechanisms. Pressure data and a reservoir factor are not available for this study, but these observations can guide the simulation with a few reasonable assumptions.

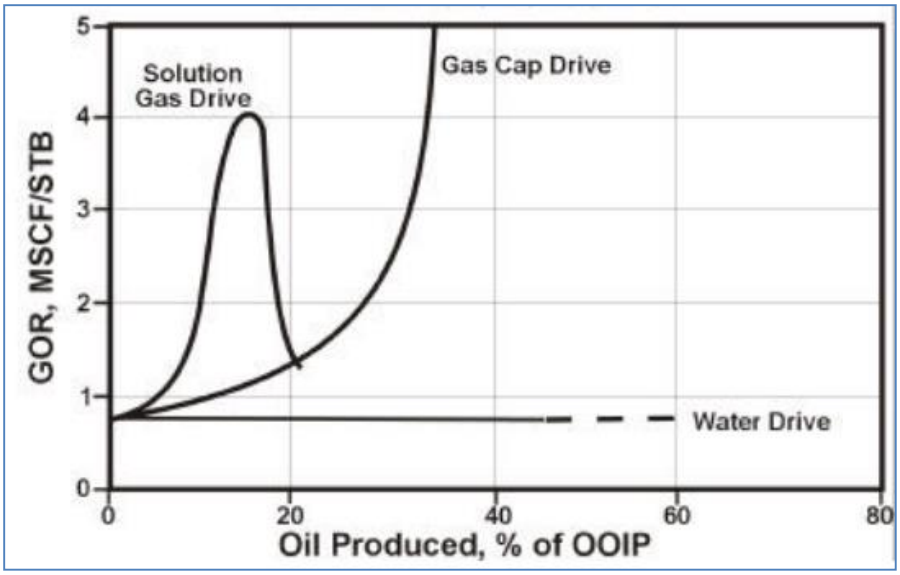


**Figure 14. Gas-oil-ratio trends for drive mechanisms (Chen 2009).**

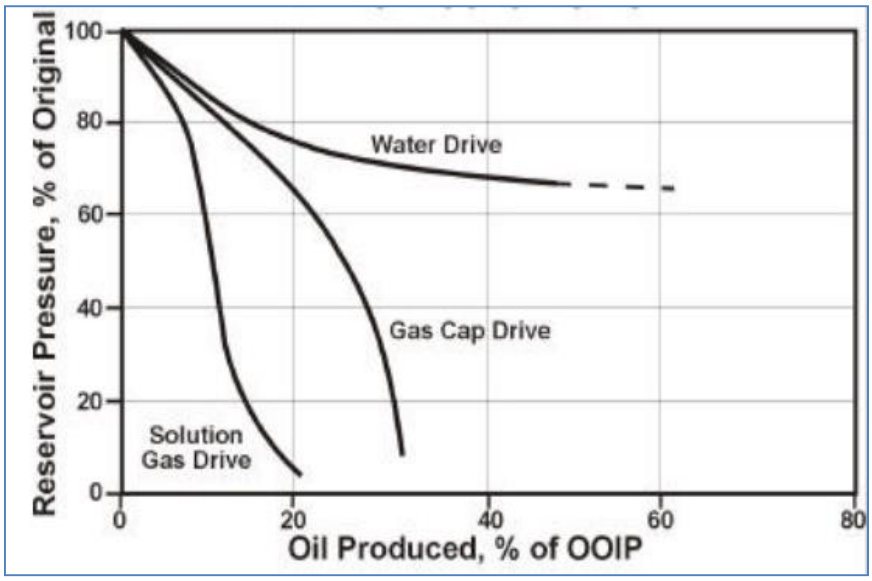


**Figure 15. Reservoir pressure trends for drive mechanisms (Chen 2009)**

### 1.1.7 Reservoir Characterization

As stated, the main objective of this study was to take advantage of reservoir simulation to help determine optimal lateral placement with an attempt to predict the measured response of the stimulations. A limit must be placed on the amount of resources used during a simulation study in order to optimize computational time. Once study objectives are defined, only the resources required to meet these objectives should be used. In this chapter, all available data were analyzed and processed based on various study objectives to characterize the study area of the Millman field.

Before data acquisition, a fundamental rule of reservoir simulation should be clear: always use the simplest model required to meet the study objective. Ertekin (2011) gave a list of data sources available to the reservoir engineer. Table 2 lists all the sources of reservoir data in which numbers 1,2,3, and 4 stand for the quality of these data.

The main difficulty in data acquisition phase is the limited and poor quality of data. This is common across the Permian Basin. Particularly for the West Millman field, regional studies are absent and existing data are typically well logs, general well files and production history. Therefore, reasonable assumptions were made based on information from neighboring fields sharing the same production formation. Expensive capital intensive information such as seismic and advanced wireline loga were not available, all the work in this section depends on existing data or readily available data. Table 3 summarizes accessible data and their sources.

**Table 3. Summary of Accessible Data and Sources**

| Property | | Source(s) |
|---|---|---|
| **Geological Data** | | |
| Structure top | | Structure contour map |
| Layer thickness | | Wireline logs |
| Porosity | | Wireline logs |
| Permeability | | Wireline logs&Φ-k correlation |
| **PVT Properties** | | |
| Oil | | Black Oil default |
| Gas | | production correlation |
| **Petrophysical data** | | |
| Fluid saturation | | Wireline logs |

Table 4 lists the requirements of the geologic model for reservoir simulation purposes. All of the required geologic data sources are mainly sourced from well logs. Optional properties such as vertical permeability and initial saturation are needed to study the fluid distribution around the target well, Barbie State No.1, in order to simulate the impact of an emplaced lateral. All available well logs were downloaded from the New Mexico Oil Conservation Division's

website as image files (*.tif). In order to be further analyzed in commercial log evaluation software, these logs needed to be in digital form. The log images were digitized to a digital format (*.las) using Petra software. Table 5 summarizes available well logs for study. A total of twelve wells in the study area contain useful log data.

The available geological data for the Millman Field consists of contour maps of the top structure, unit thickness, and facies, from well logs. However, the simulation focused only on the production interval, the Grayburg formation. The Grayburg formation was divided into five layers; the top structure or bottom structure of each were acquired through a stratigraphic analysis of well logs as shown in Figure 16. While this data was being interpreted, a preliminary model was formed from a single well log analysis. The entire zone of the structure model is shown in Figure 16, but simulations only focused on a subset of the data (blue square in Figure 16), which used data from twelve wells (well locations detailed in Figure 17).

**Table 4. Requirements of the Geologic Model in Reservoir Simulation**

| Property | Use in Simulation | Status |
|---|---|---|
| Structure top | Reservoir depth<br>Initial reservoir pressure<br>Original oil in place (OOIP) and original gas in place (OGIP) calculations | Required for the top layer<br>Optional for lower layers (defaults may be obtained from the structure top of the top layer and gross thicknesses) |
| Net reservoir thickness, $h_n$ | Assignment of cell net thickness values<br>Horizontal-transmissibility calculations<br>PV calculations<br>Calculation of well geometric factors, $G_w$<br>OOIP and OGIP calculations | Required |
| Gross reservoir thickness, $h_g$ | Assignment of cell gross thickness values<br>Gravity head calculations<br>Initial reservoir pressures<br>Transition-zone calculations<br>Initial saturation distributions<br>Vertical-transmissibility calculations | Optional (default may be obtained from net thickness, $h_n/h_g = 1$) |
| Net to gross thickness ratio, $h_n/h_g$ | Assignment to cell $h_n/h_g$ values | Optional (default may equal one, $h_n/h_g = 1$) |
| Porosity, $\phi$ | Assignment of cell $\phi$ values<br>Development of porosity/permeability transforms<br>Pore volume (PV) calculations<br>OOIP and OGIP calculations | Required for all layers |
| Horizontal permeability, $k_H$ | Assignment of cell permeability values<br>Horizontal-transmissibility calculations<br>Development of porosity/permeability transforms<br>Calculation of well geometric factors, $G_w$ | Required for all layers |
| Vertical permeability, $k_V$ | Assignment of cell permeability values<br>Vertical-transmissibility calculations | Optional (default may be obtained from horizontal permeabilities, $k_V/k_H = 1$) |
| Initial saturations $S_{wi}$, $S_{oi}$, and $S_{gi}$ | Initial saturation distributions<br>Transition-zone heights<br>OOIP and OGIP calculations | Optional (default may be obtained from initial capillary/gravity equilibrium) |
| Endpoint saturations $S_{iw}$, $S_{orw}$, $S_{org}$ and $S_{gc}$ | Saturation normalization<br>Assignment of cell critical saturation values for saturation unnormalization | Optional (default may be obtained from endpoints of input relative permeability data) |
| Fluid contacts, OWC and gas/oil contact (GOC) | OOIP and OGIP calculations<br>Initial saturation distributions<br>Initial reservoir pressures | Required |

Note: One map per simulation layer is required; however, defaults may be used for optional properties.

## Table 5.Available Wireline Logs for the West Millman Field

| | | | | Log Type | | | | | |
|---|---|---|---|---|---|---|---|---|---|
| API | Lease Name | No. | Location | GR | C | R | PE | N | D |
| 0-015-25485 | BARBIE STATE | 1 | 13 19S 27E | / | / | / | | / | / |
| 0-015-25481 | BARBIE STATE | 2 | 13 19S 27E | / | / | | | / | / |
| 0-015-25482 | BARBIE STATE | 3 | 13 19S 27E | / | | | | / | |
| 0-015-25483 | BARBIE STATE | 4 | 13 19S 27E | / | / | | | / | / |
| 0-015-25523 | LOCO HILLS STATE | 1 | 14 19S 27E | / | / | / | | / | / |
| 0-015-25861 | JMD STATE | 1 | 12 19S 27E | / | / | / | / | | |
| 0-015-25890 | JMD STATE | 3 | 12 19S 27E | / | / | | / | | |
| 0-015-26237 | JMD STATE | 5 | 12 19S 27E | / | | | | / | |
| 0-015-25826 | MARY WOLF STATE | 1 | 12 19S 27E | / | / | / | / | / | / |
| 0-015-25883 | MARY WOLF STATE | 2 | 12 19S 27E | / | / | | / | / | / |
| 0-015-26058 | MARY WOLF STATE | 3 | 12 19S 27E | / | / | | / | | / |
| 0-015-26059 | MARY WOLF STATE | 4 | 12 19S 27E | / | / | | / | / | / |
| otal | 12 wells | | | 12 | 10 | 4 | 6 | 9 | 8 |

GR - Gamma ray log R - Resistivity log D - Density log
C - Caliper log PE - litho-Density log N - Neutron log

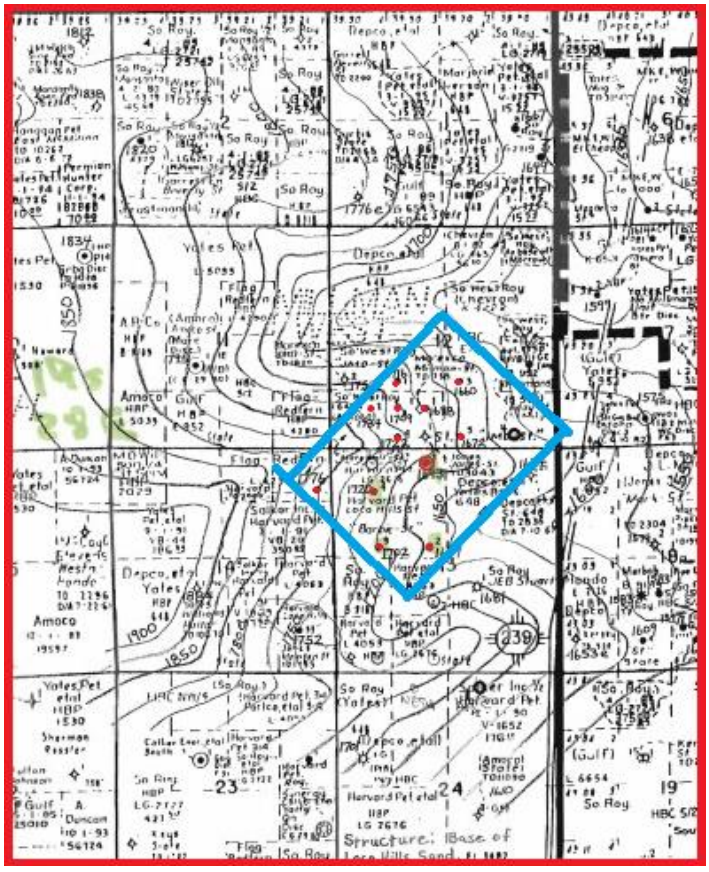


**Figure 16. Structural contours at top of Grayburg formation (Harvard, 2012). The entire area was modeled, but simulations were limited to the subset area contained within the blue box.**

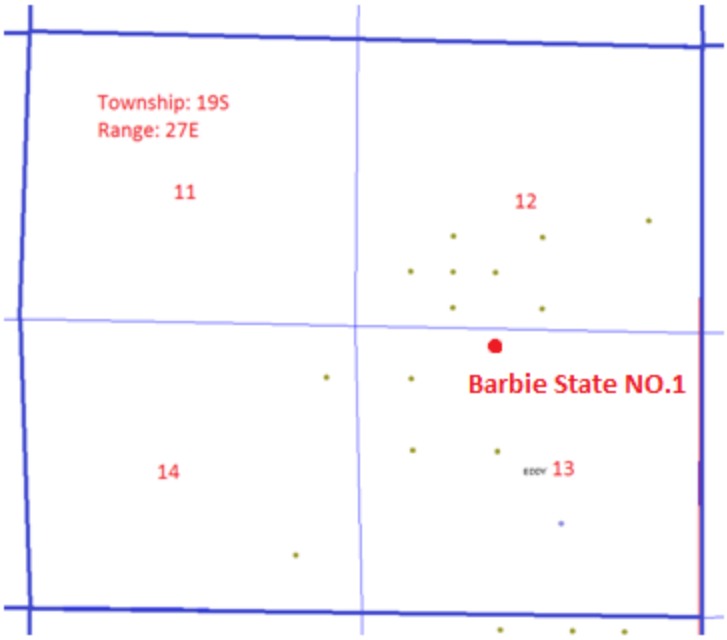


**Figure 17. Detailed well locations in Millman field. This map represents wells inside the blue box in Figure 15.**

Table 6 shows the operator's lithologic analysis results based on depth interval of 20 ft and formations can be separated into four rough segments accordingly: 1640–1700 ft shale, 1700–1740 ft dolomite, 1740–1780 ft sandstone, 1780–1840 ft dolomite. The formation top of the Grayburg is at a depth of 1650 ft and its bottom depth is at 2110 ft.

**Table 6. Lithological Histogram Results for Grayburg Formation of Barbie State No. 1 (Harvard, 2012)**

| DEPTH | | |
|---|---|---|
| TOP | BOTTOM | |
| 1640 | 1680 | CT ORANGE-GOLD RNG,STREAM<br>CT ORANGE-GOLD RNG |
| 1680 | 1700 | CT ORANGE-GOLD RNG |
| 1700 | 1720 | DOL, SL STN LIVE & DEAD, GB, FLS CT BRT YLL & YLL RNG<br>CT YLL & GOLD RNG |
| 1720 | 1740 | DOL, MUCH STN LIVE & DEAR GB, FLS, CT BRT YLL , GLOD RNG<br>CT STREAM, GLOD RNG |
| 1740 | 1760 | SAND SME STN LIVE & DEAD GB, FLS, CLY MTRX, CT STREAM, GOLD RNG<br>CT YLL, YLL RNG |
| 1760 | 1780 | SAND SLI STN DEAD, GB, CLY MTRX<br>CT YLL, YLL RNG |
| 1780 | 1800 | DOL SME VUGS W/DEAD STN (GOOD BROWN LIVE OIL ON PIT)<br>CT YLL, GLOD RNG<br>SAME OIL ON PIT |
| 1800 | 1820 | DOL WHT WME POR<br>SME SMALL BLOBS FREE OIL<br>GOOD CUT GOLD RNG |
| 1820 | 1840 | DOL WHT NOR AS POROUS SME STN, CT NOT AS GOOD GLOD |

Barbie State No.1 is producing from the Grayburg/Premier at an interval from 1710 to 1882 ft. In order to fully understand and specifically study the impact of laterals on mature wells, simulation models were built on production intervals from the Grayburg. After comparing the lithology analysis shown in Table 6 with log interpretations, the Grayburg formation in Barbie State No.1 was divided into five simulation layers.

Figure 18 shows well correlation between Barbie State No.1 and Barbie State No. 4 using gamma ray, neutron log and density log similarity. Top and bottom depth of each layer at well location are summarized in Table 7. Structure top and thickness of five layers were imported into Landmark-Nexus, and maps of structure top and layer thickness were generated in array calculation module. Figures 19–20 show the top structure and thickness contour map of the first layer in the digitized model.

**Table 7. Top and Bottom Depths of Five Simulation Layers in the model**

| | Depth(ft) | | | | | | | | | | | | | | |
|---|---|---|---|---|---|---|---|---|---|---|---|---|---|---|---|
| | 1 | | | 2 | | | 3 | | | 4 | | | 5 | | |
| | h | Top | Bottom | h | Top | Bottom | h | Top | Bottom | h | Top | Bottom | h | Top | Bottom |
| Barbie State 001 | 43 | 1650 | 1693 | 27 | 1693 | 1720 | 30 | 1720 | 1750 | 32 | 1750 | 1782 | 68 | 1782 | 1850 |
| Barbie State 002 | 40 | 1656 | 1696 | 30 | 1696 | 1726 | 34 | 1726 | 1760 | 40 | 1760 | 1800 | 64 | 1800 | 1864 |
| Barbie State 003 | 40 | 1620 | 1660 | 34 | 1660 | 1694 | 36 | 1694 | 1730 | 40 | 1730 | 1770 | 68 | 1770 | 1838 |
| Barbie State 004 | 32 | 1606 | 1638 | 36 | 1638 | 1674 | 32 | 1674 | 1706 | 44 | 1706 | 1750 | 68 | 1750 | 1818 |
| LocoHills State 001 | 30 | 1550 | 1580 | 40 | 1580 | 1620 | 30 | 1620 | 1650 | 40 | 1650 | 1690 | 68 | 1690 | 1758 |
| JMD State 001 | 52 | 1650 | 1702 | 18 | 1702 | 1720 | 28 | 1720 | 1748 | 30 | 1748 | 1778 | 72 | 1778 | 1850 |
| JMD State 003 | 40 | 1710 | 1750 | 34 | 1750 | 1784 | 26 | 1784 | 1810 | 32 | 1810 | 1842 | 78 | 1842 | 1920 |
| JMD State 005 | 41 | 1676 | 1717 | 29 | 1717 | 1746 | 32 | 1746 | 1778 | 34 | 1778 | 1812 | 73 | 1812 | 1885 |
| Mary Wolf State 001 | 54 | 1668 | 1722 | 18 | 1722 | 1740 | 28 | 1740 | 1768 | 38 | 1768 | 1806 | 66 | 1806 | 1872 |
| Mary Wolf State 002 | 22 | 1626 | 1648 | 46 | 1648 | 1694 | 16 | 1694 | 1710 | 34 | 1710 | 1744 | 70 | 1744 | 1814 |
| Mary Wolf State 003 | 38 | 1642 | 1680 | 32 | 1680 | 1712 | 30 | 1712 | 1742 | 40 | 1742 | 1782 | 70 | 1782 | 1852 |

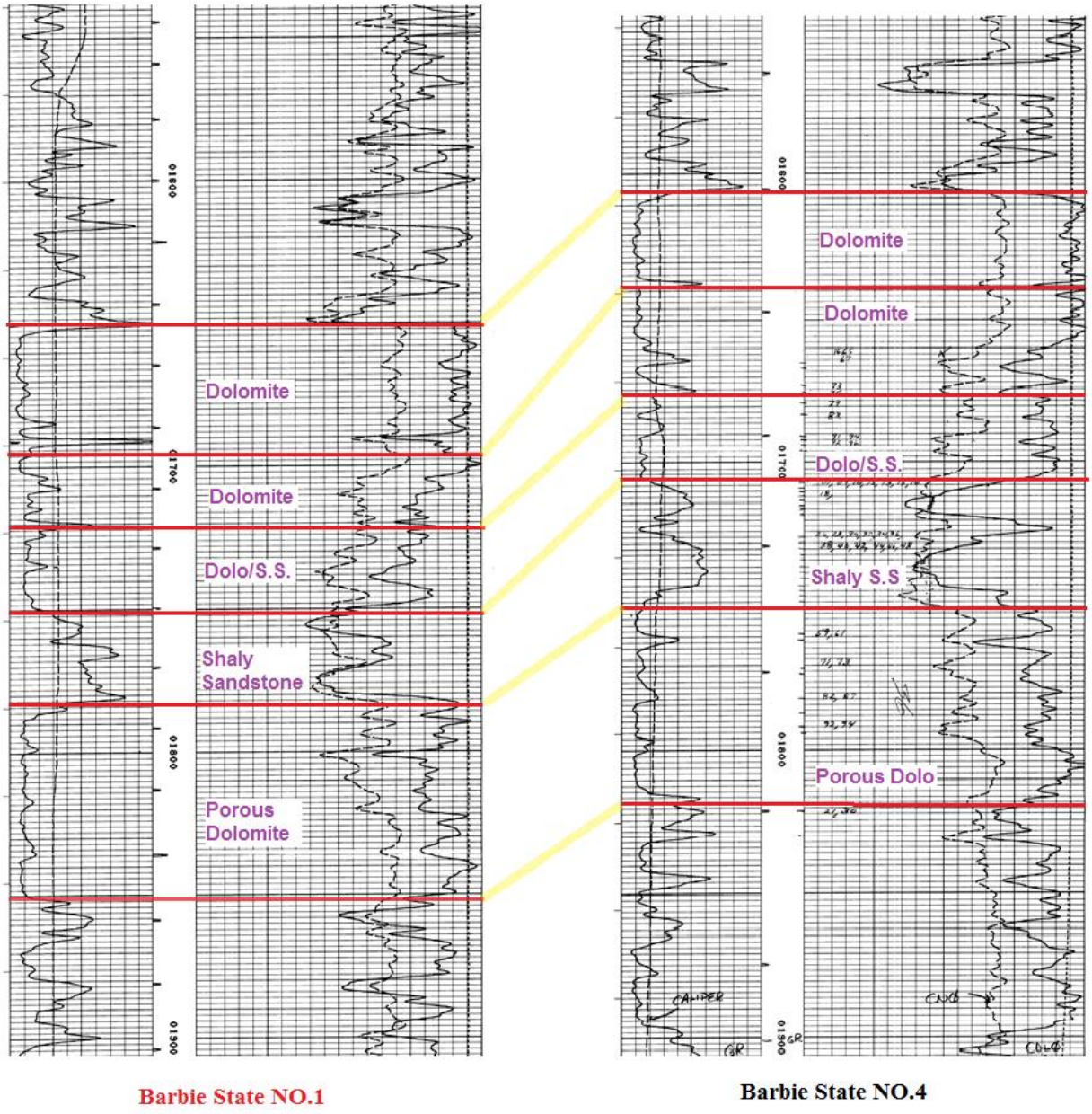


**Figure 18. Correlation of Barbie State 001 with Barbie State 004.**

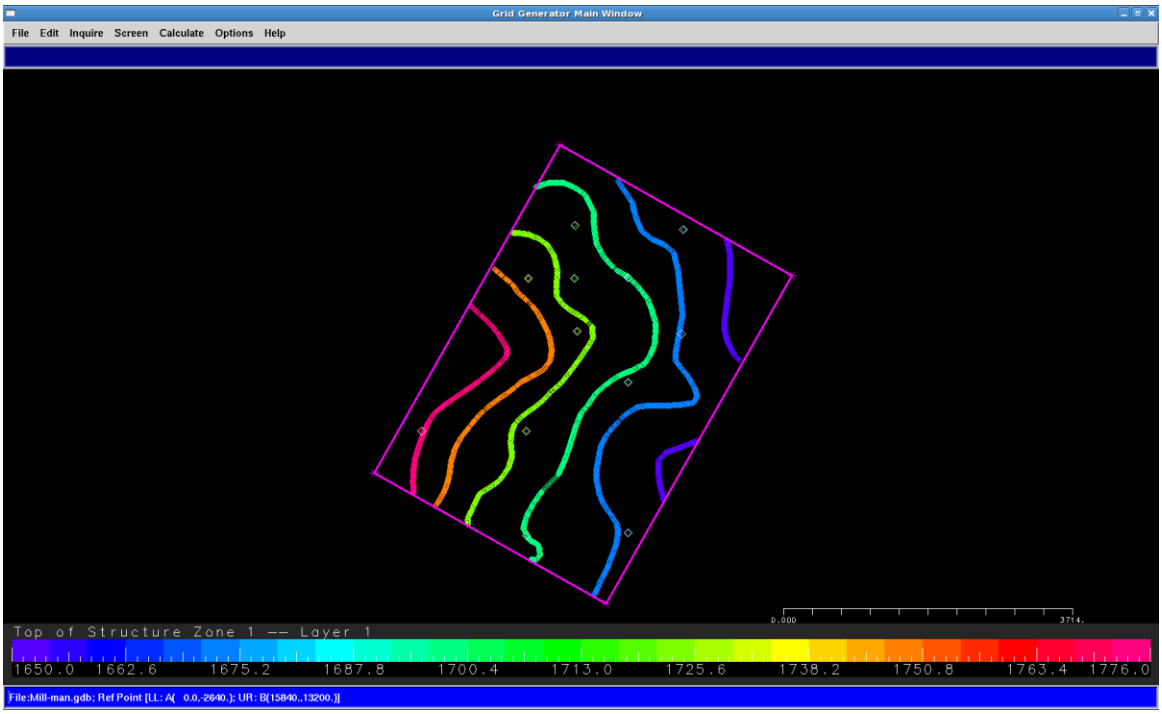


**Figure 19. Top Structure for the Grayburg.**

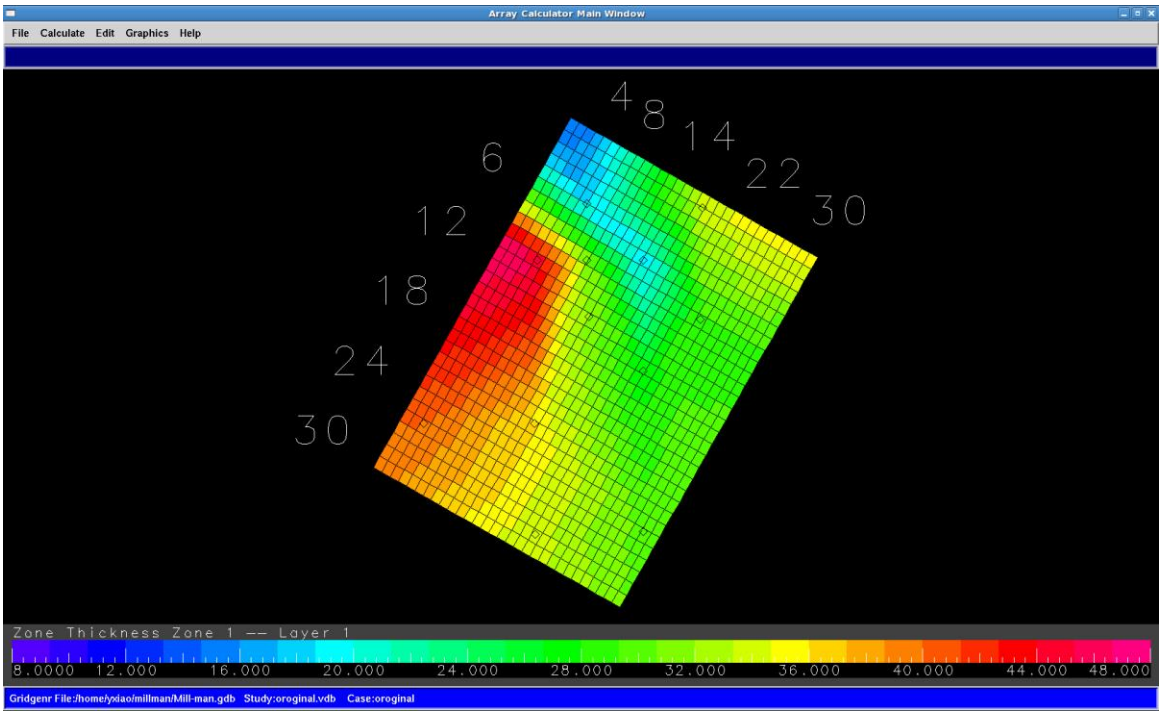


**Figure 20. Computed thickness of Layer 1.**

### 1.1.8 Reservoir Properties

In 1994, Devon Energy Corporation embarked upon a drilling and completion project in the Grayburg-Jackson field of Eddy County, New Mexico, for the purpose of installing a secondary recovery waterflood. The Grayburg-Jackson field produces from the Grayburg and San Andres formations, which comprise several sandstone and dolomite producing intervals within each formation. Historically, these formations have required hydraulic fracture stimulation in order to be economically produced due to their low relative permeability. The low BHST of these formations coupled with the low relative permeability created some unique challenges from a fracture fluid design standpoint. The fracture fluid systems were designed in such a manner as to create long and highly conductive fractures while minimizing polymeric damage to the low perm reservoir. (Malone et al., 2000)

The West Millman field shares the same development issues and production formation as the Grayburg-Jackson field. The target well, Barbie State No.1, was acidized with 5,000 gallons, 15% acid, and fractured with 100,000 gallons of gel $H_20$ and 190,000 pounds of sand in the production interval from depth of 1710 ft. to 1882 ft. Well logs were conducted before stimulation.

Contour maps of porosity, permeability and saturation do not exist for the field. Anecdotal observation from the producer suggest that porosity and permeability are best on high energy depositional features, and that the incised cuts into these, which form "noses" in the top structure have lower porosity and permeability. After the well log data were correlated, porosity and saturation were read from neutron logs and found to be consistent in each layer, and modified within expected variance between high and low energy portions of the reservoir. Input reservoir properties were calculated from LESA well log analysis (Figure 21) and read directly from well logs.

The porosity distribution in the Grayburg is controlled by both depositional facies and diagenesis. The thicker bedded grain-rich facies, most often seen in the high energy shoal portion of each sequence, have the best porosity; whereas, the thinner bedded mud-rich facies, both updip in the lagoon and down-dip in the fusulinid wackestones, have the poorest. Sub-aerial exposure of the individual units, though short-lived, created additional secondary dissolution porosity. Deep burial diagenesis both enhanced and reduced inter-particle porosity and permeability. Anhydrite has been mobile during both the depositional (and early burial) and during the burial diagenetic phase.

The Grayburg Formation is a low permeability Permian dolomite. Horizontal permeability was calculated using a porosity-permeability correlation and no directional permeability was defined. Vertical permeability was assumed using vertical-horizontal permeability correlation with a factor of 0.5. Since no core data can be found on the Grayburg formation, correlation data was collected from analog cores from an East Millman well ~4 miles away.

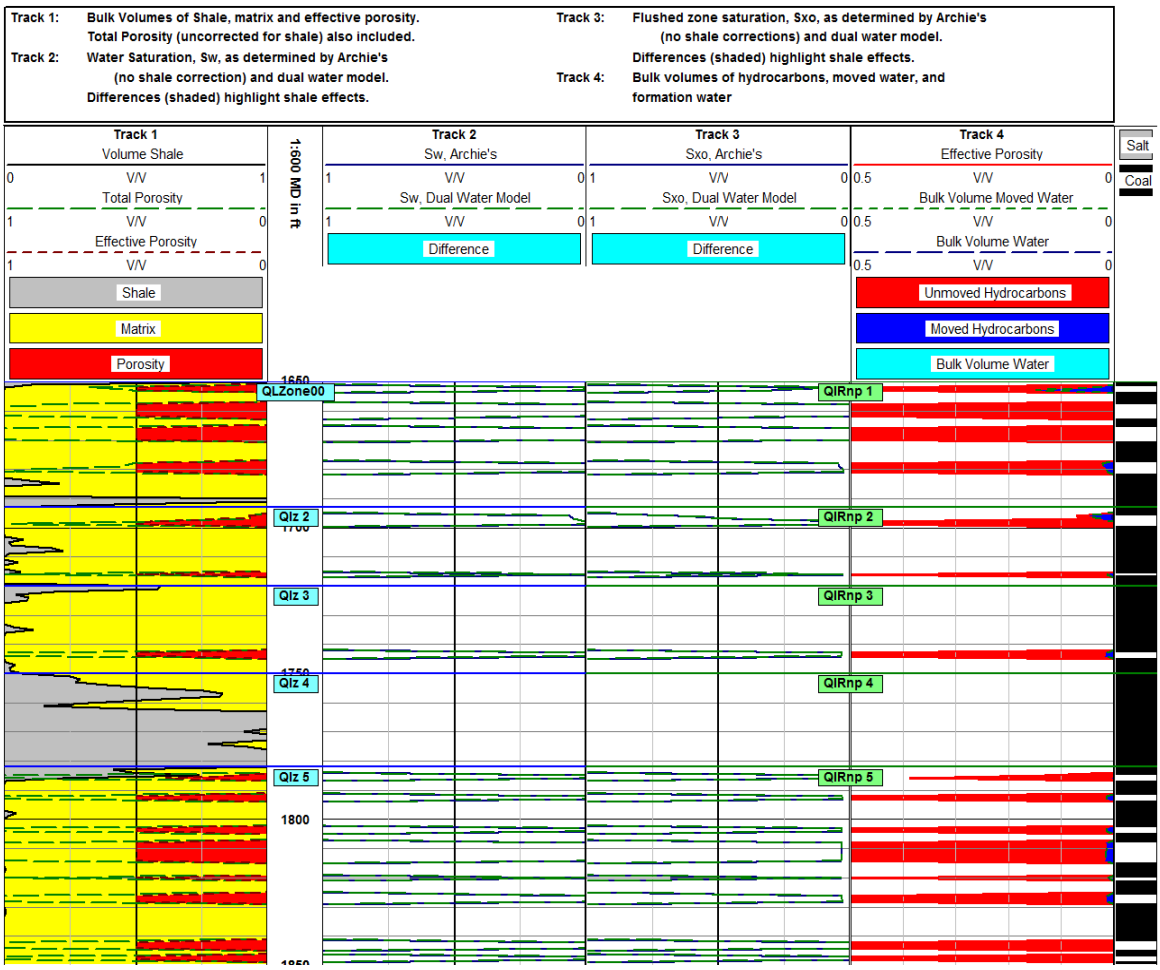


**Figure 21. LESA analysis showing Initial Reservoir Properties-Barbie State 001.**

## Log-estimated permeability

Log-estimated permeability involves solution of the equation:

$$k_{log} = \frac{62500 \times \Phi^6}{S_{wi}{}^2}$$

Additionally, the program compares log-determined $S_w$ with theoretical $S_{wi}$ using a Buckles equation:

$$\Phi S_{wi} = \text{Constant}$$

in which the "Constant" can be edited. However, no core permeability exits for comparison. Otherwise, a fair to good match with $k_{log}$ can be obtained by changing the value of $\Phi S_{wi}$.

Permeability of each layer was calculated using three averaging method: harmonic, geometric and arithmetic. Geometric permeability was then chosen to represent the whole layer. Porosity permeability relationships are illustrated in Figures 22–23.

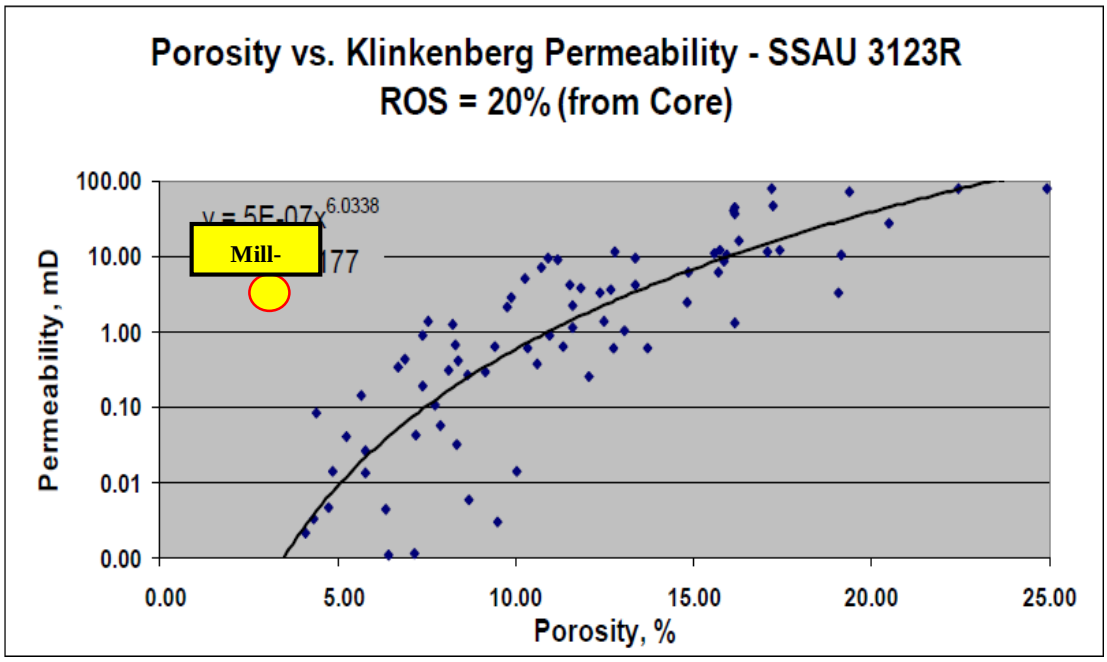


**Figure 22. Permeability-porosity correlation, core plug scale.**

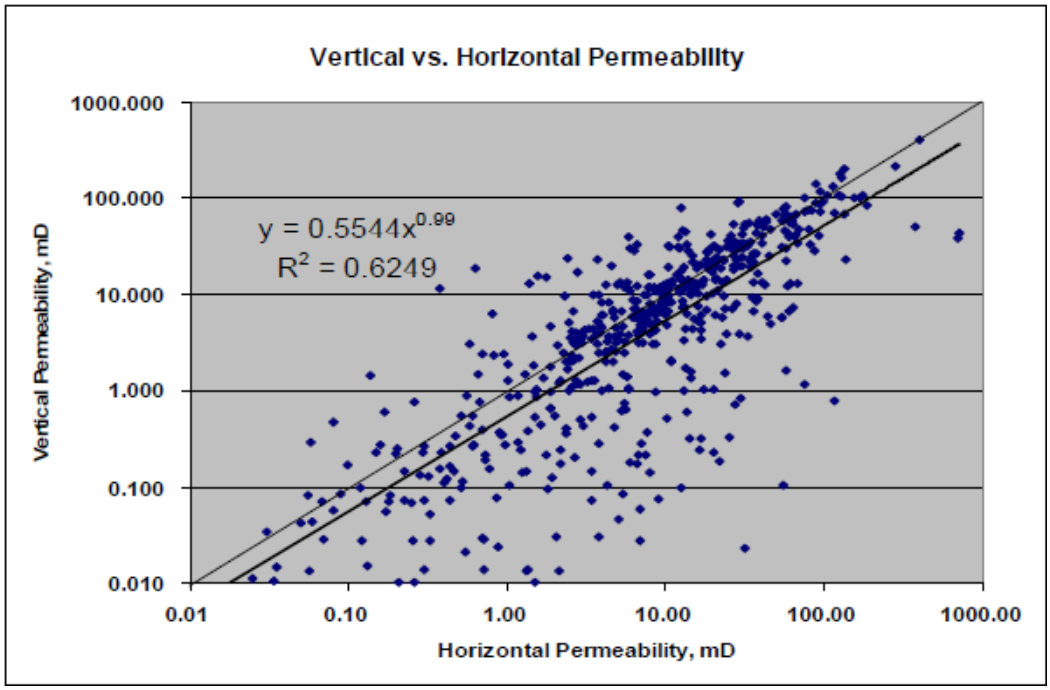


**Figure 23. Vertical to horizontal permeability, full core scale.**

As shown in Table 5, the Deep/Shallow resistivity log is absent except for the BARBIE STATE NO.1, LOCO HILLS STATE NO.1, JMD STATE NO.1 and MARY WOLF STATE NO.1, so fluid saturation could only be calculated in these locations. Analysis results of initial reservoir properties are shown in Figures 21, and 24, and 25 for three wells with adequate logs. Track 4 in Figure 24 demonstrates the vertical distributions of unmoved hydrocarbon, moved hydrocarbon and formation water. Software-generated $S_o$ and $S_w$ were used as input data for reservoir properties.

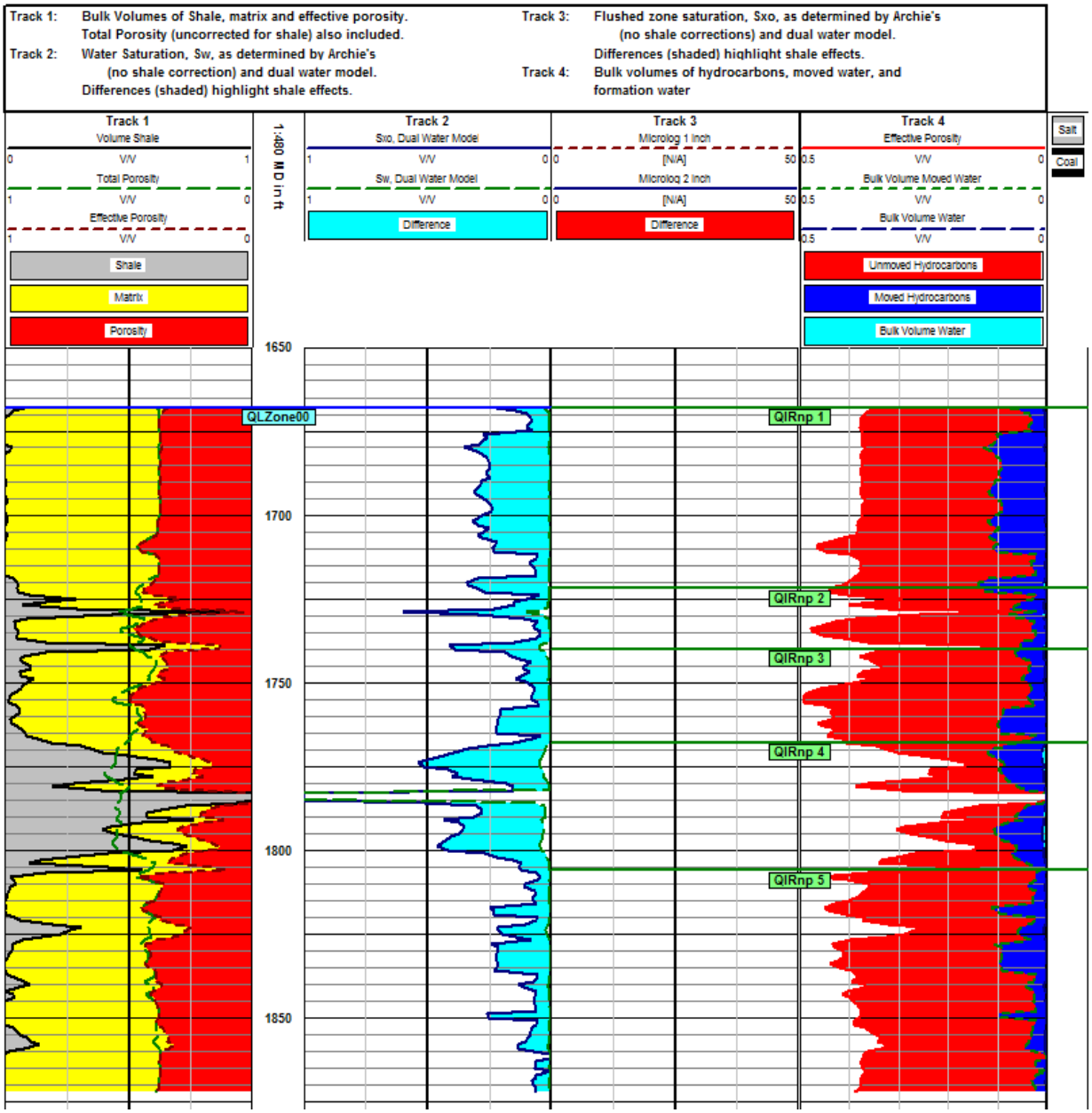


**Figure 24. LESA analysis showing Initial Reservoir Properties-Mary Wolf State 001.**

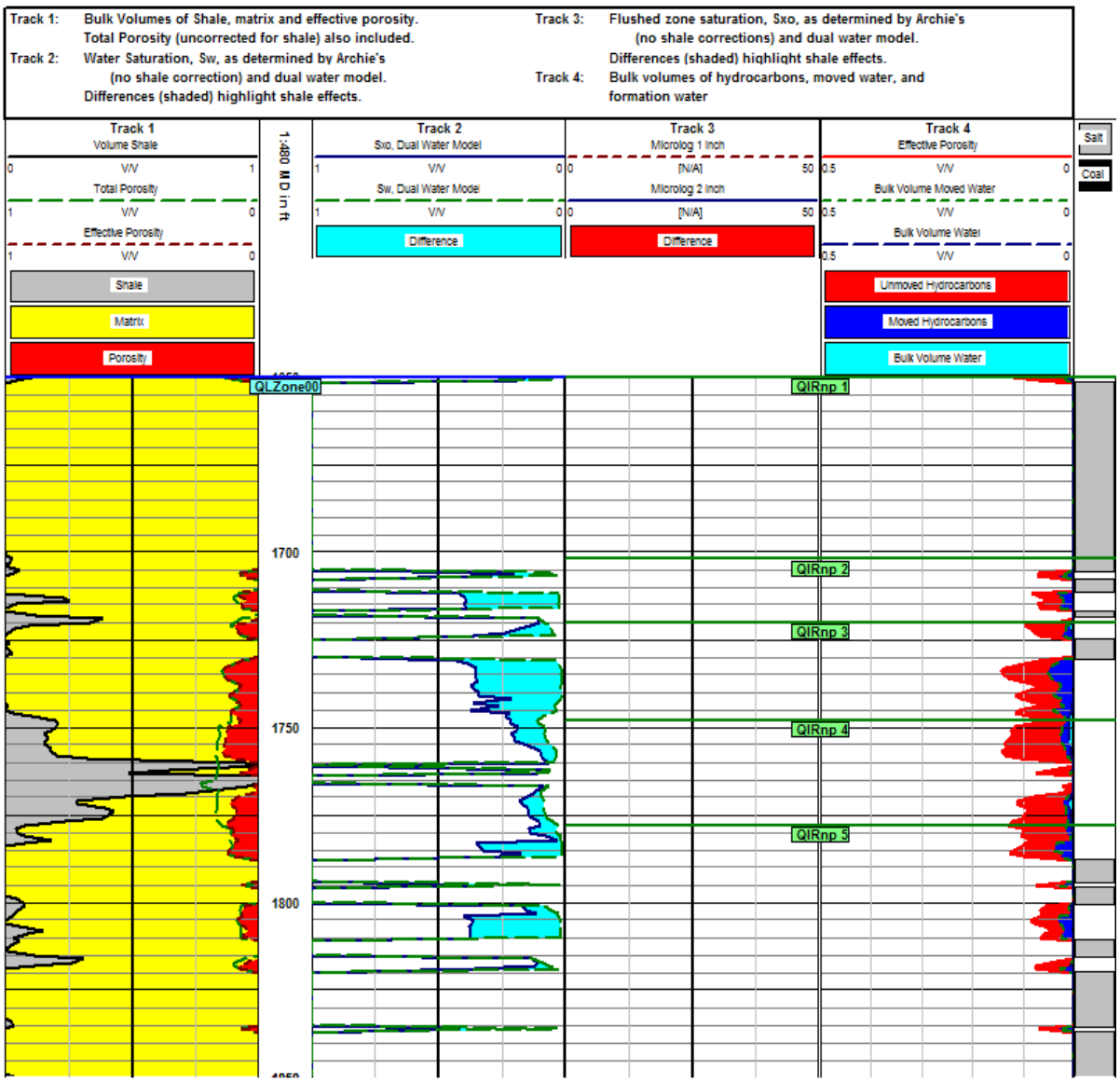


**Figure 25. LESA analysis showing Initial Reservoir Properties-JMD State 001.**

As the relative permeability curve is not available in the West Millman field, information from neighboring fields was borrowed and modified with reasonable assumptions.

### 1.1.9 PVT Analysis

If the producing GOR is relatively constant, then it can be assumed to represent the solution GOR above the bubblepoint. The problem then is to determine black-oil properties by giving (i) stock-tank oil gravity, (ii) surface gas gravity, (iii) BP solution-GOR, (iv) pressure of interest, and (v) the temperature of interest. Figure 26 shows the historical GOR data collected at the beginning of each month during the first 10 years of production (See detailed data in Table 8). It is obvious that the GOR remained relatively constant from 1987 to 1993. The black points are

identified automatically by the CMG simulation software as representatives of the curve trend, and GOR of these points are listed for calculation of initial GOR above and at bubblepoint (BP).

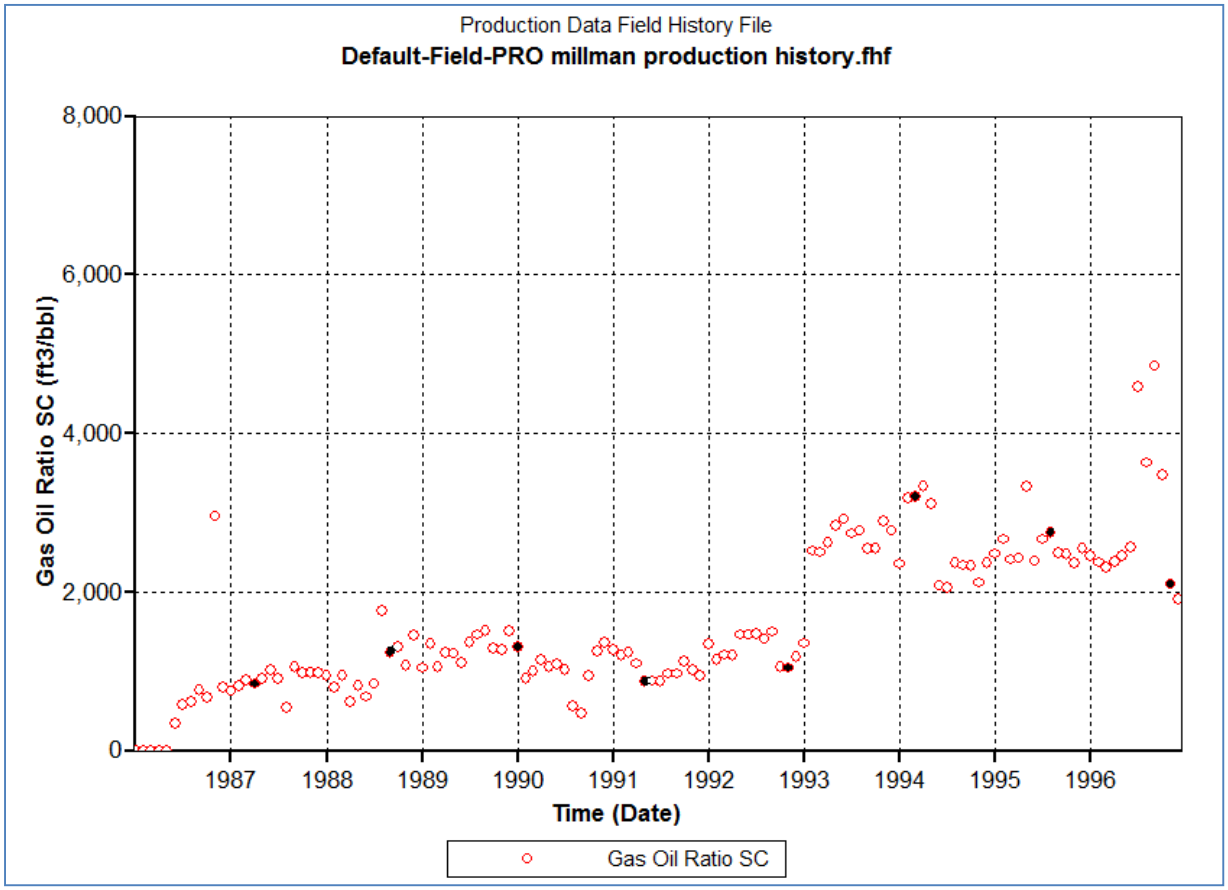


**Figure 26. Historical surface-gas-to-oil ratio (GOR) ft3/bbl.**

**Table 8. Points Involved for Initial GOR Calculation**

| DATA(Y/M/D) | GOR($ft^3$/bbl) |
|---|---|
| 1987-04-01 | 850.409 |
| 1988-09-01 | 1242.464 |
| 1990-01-01 | 1308.412 |
| 1991-06-01 | 887.2469 |
| 1992-12-01 | 1180.866 |
| 1994-03-01 | 3207.709 |
| 1995-08-01 | 2748.715 |

To get initial GOR the following relationship was used:

$$\text{Initial GOR} = \text{AVERAGE}(\text{DATA}_{1987\text{-}1993}) = 1093.879\ \text{ft}^3/\text{bbl}$$

BP pressure can be estimated by the following correlation [Standing 1977]

$$p_b = 18.2(A - 1.4)$$

where

$$A = (R_{sob}/\gamma_g)^{0.83} \times 10^C$$

$$C = 0.00091T - 0.0125\gamma_{API}$$

$P_b$ = BP pressure, psia

$R_{sob}$ = BP solution-GOR, scf/stb

T= temperature, $^0$F

$\Gamma_{API}$ = stock-tank oil API gravity, ◦API

$\Gamma_g$ = surface gas specific gravity (air=1)

Table 9 shows the values for these variables.

**Table 9. PVT Data for Calculation of Bubblepoint**

| Parameters | Unit | |
|---|---|---|
| **Reservoir Temperature** | $^0$F | 160 |
| **Oil Density** | lb/ft$^3$ | 54 |
| **Gas Density/Gravity** | lb/ft3(Air=1) | 0.05345 |
| **Water Density** | lb/ft$^3$ | 62.3664 |
| **Rsob** | scf/bbl | 1093.879 |
| $\gamma_g$ | - | 0.7 |
| $\gamma_{API}$ | $^0$API | 31.92307 |
| **C** | - | -0.25344 |
| **A** | - | 265.9453 |
| **BP** | psia | 4814.725 |

Bubblepoint can also be calcualted in the CMG Builder module. Figure 27 shows the computational results from Builder.

| # | Description | Option | Value |
|---|---|---|---|
| 1 | Reservoir temperature | | 160 F |
| 2 | Generate data upto max. pressure of | | |
| 3 | Bubble point pressure calculation | Generate from GOR value | 1093.876 |
| 4 | Oil density at STC(14.7 psia, 60 F) | Stock tank oil density | 54 lb/ft3 |
| 5 | Gas density at STC(14.7 psia, 60 F) | Gas gravity (Air=1) | 0.7 |
| 6 | Oil properties (Bubble point, Rs, Bo) correlations | Standing | |
| 7 | Oil compressibility correlation | Glaso | |
| 8 | Separator temperature | | |
| 9 | Separator pressure | | |
| 10 | Dead oil viscosity correlation | Ng and Egbogah | |
| 11 | Live oil viscosity correlation | Beggs and Robinson | |
| 12 | Gas critical properties correlation | Standing | |
| 13 | Critical pressure | | |
| 14 | Critical temperature | | |
| 15 | Non-hydrocarbon gas correlation | Not used | |
| 16 | H2S mole fraction (optional) | | |

**Figure 27. PVT Data using correlation; Builder can calculate Rs, Bo, Bg/Eg/Zg, VisO, VisG and optionally Co.**

The black oil and related properties for IMEX are generally carried out using the correlations reviewed by McCain (1991) and the SPE monograph on phase behavior (Whitson, 2000). The actual calculations depend on the choices made by the on the detailed dialog. For the quick PVT generation feature, most of the correlations default to those by Standing and co-authors. The compressibility factor (z-factor) calculation for gas uses the Standing-Katz correlation. The gas viscosity is calculated using the Lee-Gonzalez correlation.

The BP calculated using [Standing, 1977] method is 4814.725 psia, and the value correlated from PVT data in CMG is 4519.95 psia. Using the CMG generated values several important fluid properties were plotted (Figures 28–30).

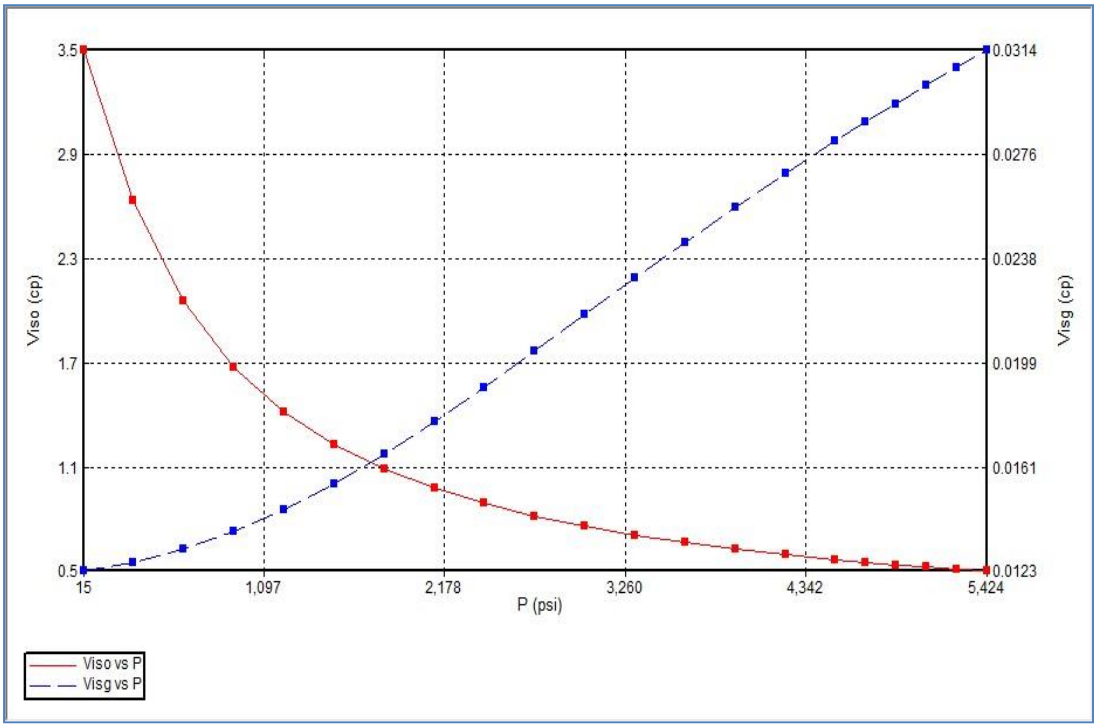


**Figure 28. Viscosity of oil and gas (viso, visg) vs pressure.**

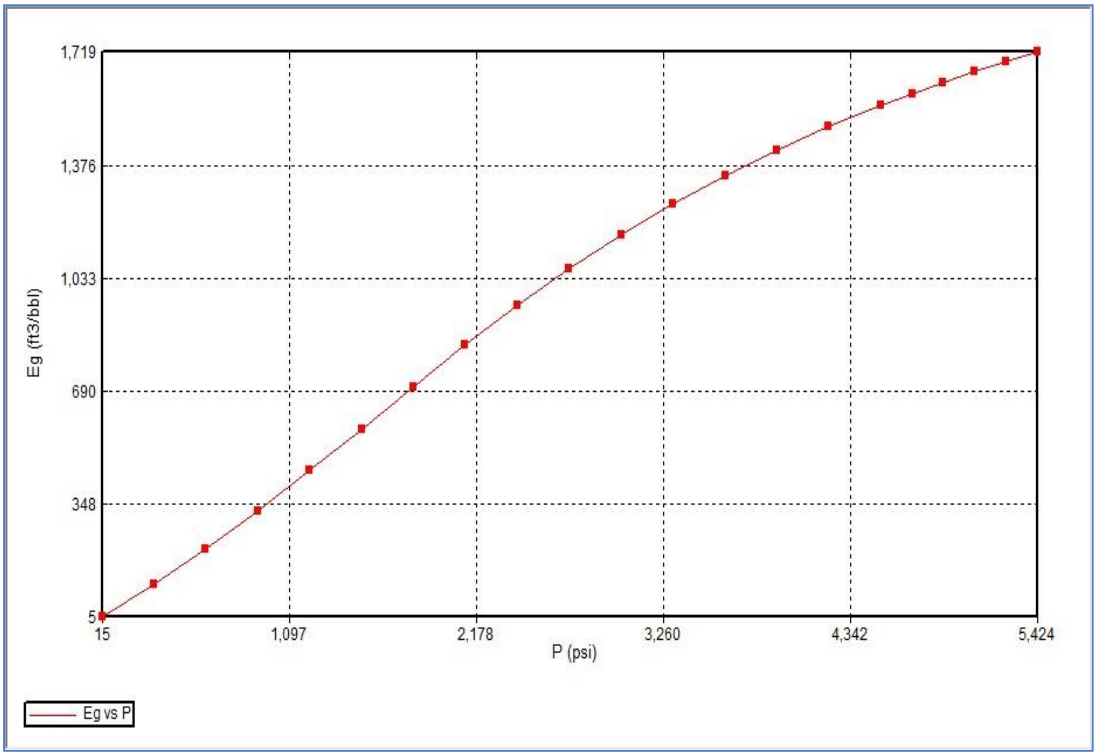


**Figure 29. Gas equivalent of stock tank oil (Eg).**

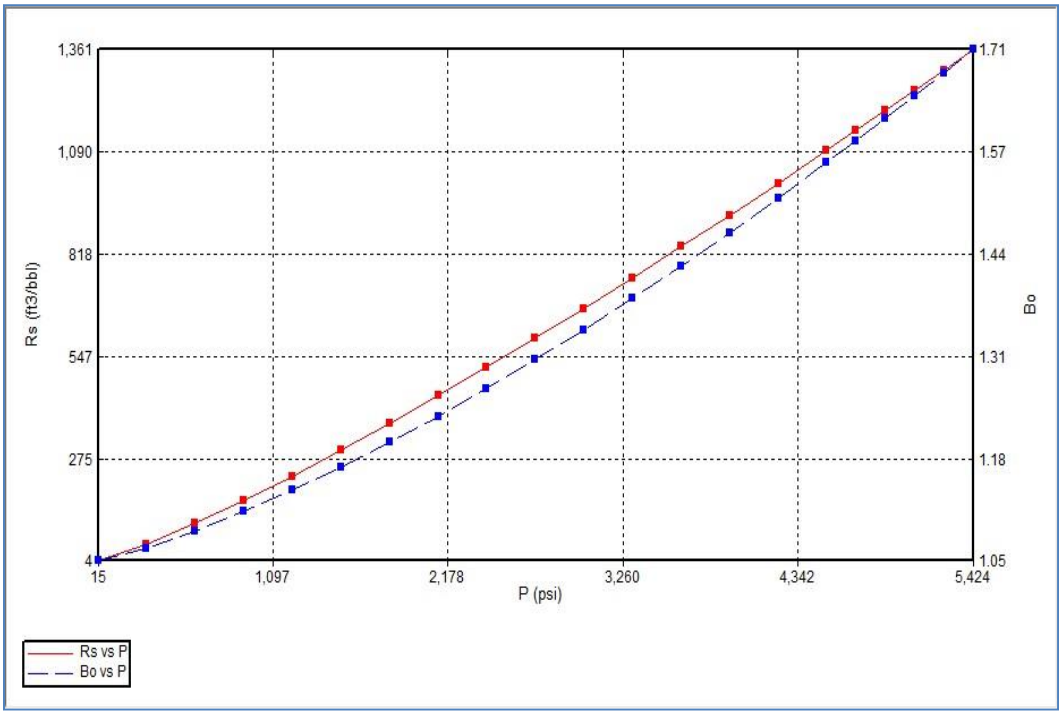


**Figure 30. Solution gas-oil ratio (Rso) and oil formation volume factor (Bo) vs pressure.**

### 1.1.10 Model Construction

The construction of a simulation model requires gathering data to form an integrated, coherent mathematical representation of the subject reservoir. The first step in constructing the simulation model is selection of the modeling approach. This involves making decisions on several key, fundamental aspects of the model. Ertekin (2011) has provided a guideline for selecting the appropriate modeling approach (Table 10).

By restating one objective of the RPSEA project, "*the use of simulation to help determine optimal lateral placement and to try and predict the measured response of the stimulations*," the following decisions can be made. In order to demonstrate and predict scenarios of the simulation block, the model has to be three-dimensional. This study focuses on a single target well, but further simulation work may include other wells in the study area, so both a single well model and full-field model were constructed. Assuming that the practice of fracture and acidification could be measured by a skin factor, the model used a single porosity system with isotropic permeability. Furthermore, the black-oil simulator (IMEX) was selected for this model. After a brief PVT analysis in which initial GOR was calculated, the characteristics of reservoir fluid fell into black oil with an initial GOR less than 1750 scf/stb. It was unnecessary to use a compositional model because the nature of reservoir fluids (dead oil and dry gas) has not been thoroughly studied and no composition report exists.

The nature of the reservoir fluids and the recovery processes occurring in the reservoir aided in the determination of the appropriate fluid description to use in the simulation study. During primary depletion, two approaches to the fluid property description can be used in reservoir simulation. The compositional approach can be used in all situations during primary depletion; however, it is the most difficult and computationally expensive approach to use. On the other hand, the black oil approach, while not as time-intensive, is not universally applicable. For primary depletion, black-oil models are the most commonly used models in the oil industry. The fluids that can be represented by black-oil models are the crude oil discussed in most textbooks on reservoir engineering. In black-oil reservoirs, fluid properties are considered to be strictly pressure dependent. Volatile oils are composed of high concentrations of intermediate hydrocarbons that can partition easily into both gas and oil phases. The presence of these hydrocarbons allows for a high degree of mass transfer between the hydrocarbon gas and liquid phases during primary depletion. When this occurs, fluid properties can become dependent on composition as well as on reservoir pressure and temperature. The simulation of volatile oils and gas condensate, therefore, may require the more computationally intensive compositional formulation (Ertekin 2011).

However, no clear distinction can be observed between black and volatile oils other than the reservoir temperature, which is closer to the critical temperature for volatile oils, Therefore, for borderline cases, the study objectives determine which PVT formulation, black oil or compositional , to use in the simulation study (Table 10).

**Table 10. Decisions Required for Modeling Approach Selection (After Ertekin, 2011)**

| | |
|---|---|
| Modeling philosophy | Conceptual<br>Actual* |
| Fluid description | Black -oil fluid description*<br>Compositional fluid description |
| Reservoir Type | Single-porosity-reservoir description*<br>Naturally-fractured-reservoir description<br>▪ Dual-porosity formulation<br>▪ Dual-permeability formulation |
| Recovery process | Primary depletion*<br>Secondary recovery/pressure maintenance<br>EOR<br>▪ Miscible displacement<br>▪ Chemical flooding |

| | |
|---|---|
| | ▪ Thermal recovery |
| Model scope | Single-well models*<br>Cross-section models<br>Window models<br>Full-field models* |
| Model dimensionality | 0D models (tank-type models)<br>1D models<br>2D models<br>Stacked areal models<br>3D models* |
| Equation solvers | Nonlinear-equation solver<br>▪ IMPES<br>▪ SEQ<br>▪ SS<br>▪ Fully implicit*<br>Linear-equation solver<br>▪ Direct solution methods<br>▪ Iterative solution methods |

Criteria for areal gridding design are as follows: First, the areal grid should cover the reservoir area and its boundary; therefore, the model can represent the actual behavior of the reservoir. Second, the grid size should be fine enough to provide the flow information and the capability to monitor fluid flow between producers.

The practical objectives for designing the areal grid are (1) to provide information on the specific areas of interest in the field, (2) to define the internal and external boundaries of the subject reservoir, and (3) to model the dynamics of the recovery processes occurring in the reservoir.

To meet the first and second criteria, the reservoir boundary needs to be defined. The aim of simulation was to optimize the number of jetted laterals and target layers in Barbie State No.1. Thus it was important to learn about the current oil distribution. A total of twelve wells were involved in the study area and no natural boundary, such as fault or pinchout, exists. A rectangular grid system was applied to the model with the target well at center.

Modeling the dynamics of the recovery process required that the grid spacing be fine enough to model properly the physics of the recovery process. As a rule of thumb, three to five grid-blocks between offset wells are generally adequate to model the physical process associated with primary production. In theory, the finite-difference grids should be oriented in the directions of the principal permeability axes. In practice, however, principal permeability axes are

usually not known in the field, so they cannot be used as an aid for defining the orientation of the grid. According to Ertekin (2011), other frequently used considerations for grid orientation include selecting the orientation that minimizes the total number of active cells in the model. As a result, a rotated rectangular areal grid system of 30×30 was constructed to model the single well area (Figures 31–32).

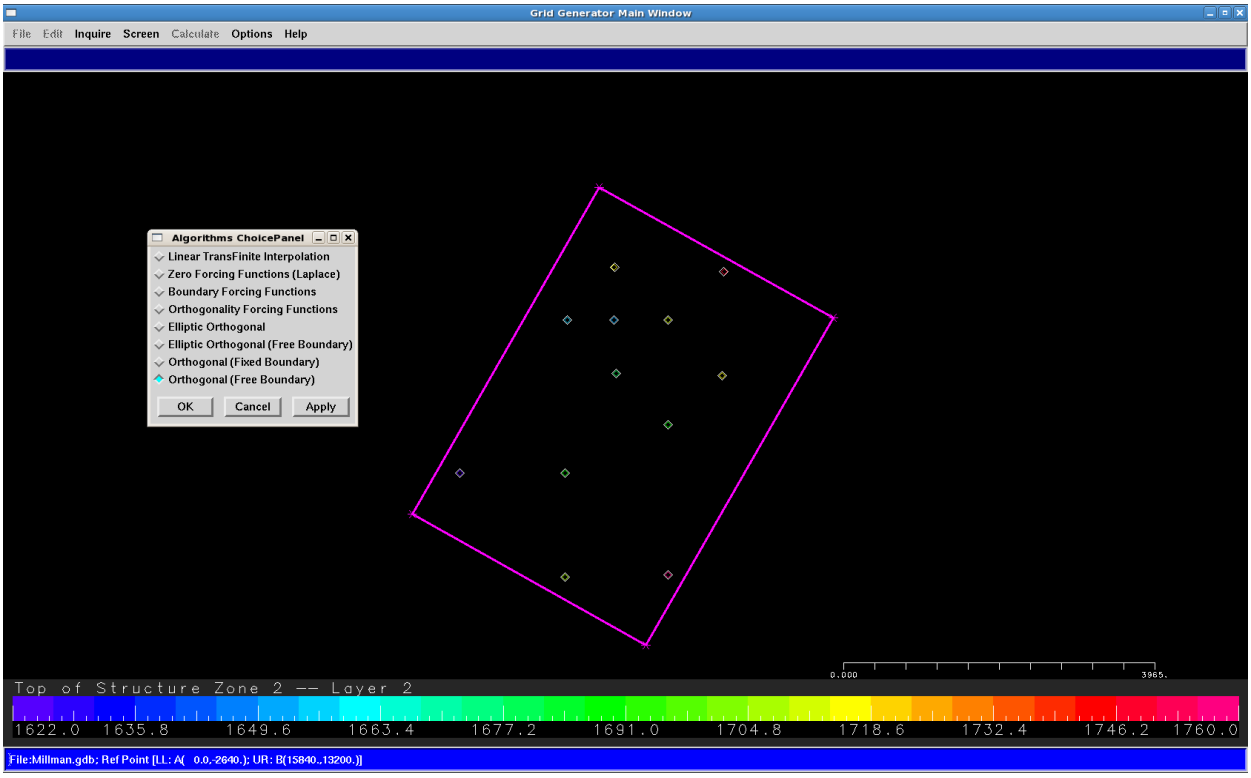


**Figure 31. An orthogonal free boundary covering the study area.**

The practical objective for vertical discretization is to provide enough simulation layers (1) to provide an appropriate description of the stratigraphy and geology of the reservoir under study, (2) to provide additional definition to thick reservoir flow units, (3) to match initial fluid contacts, (4) to match completion and perforation intervals, and (5) to provide adequate in-place-fluid-volume estimates in reservoirs with significant transition zones. As stated in section 1.1.7, the selected model uses five layers. Layer thicknesses from each well were obtained from well log correlations. Figure 33 shows a 3D view of the five-layer model.

Time step design was based on two key points. First, time steps were placed at key times in the reservoir history such as stimulation, first production, shut-in and work-over. Then time steps were placed at monthly intervals for simulation model and therefore, the simulation results were written at regular monthly intervals.

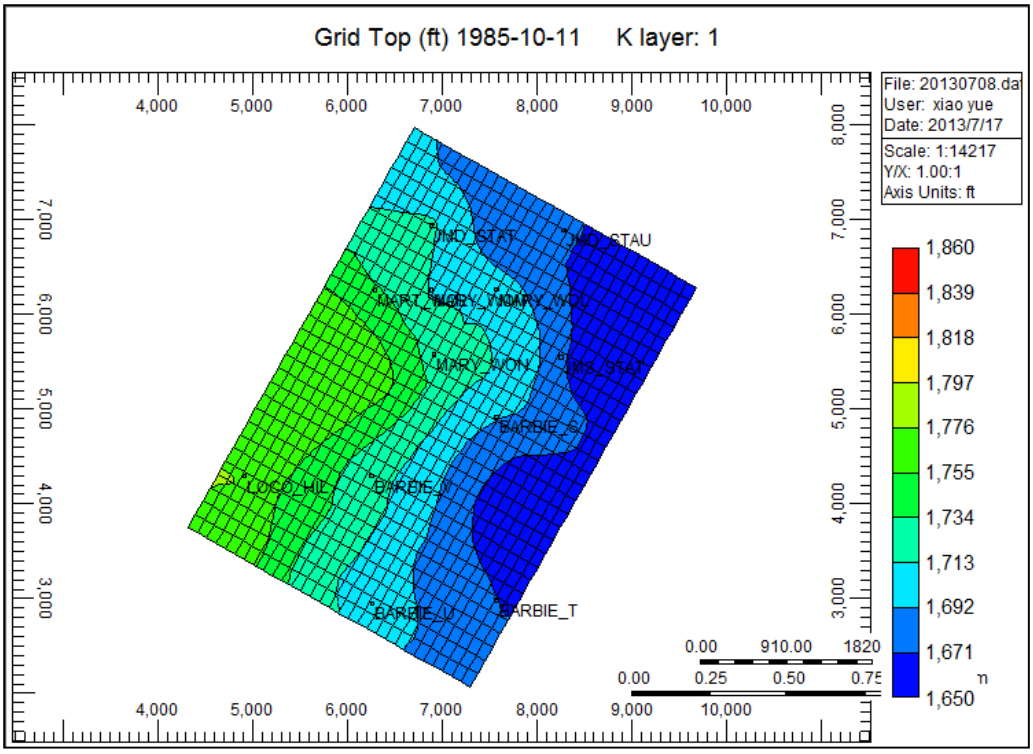


**Figure 32. Areal grid block system showing grid top.**

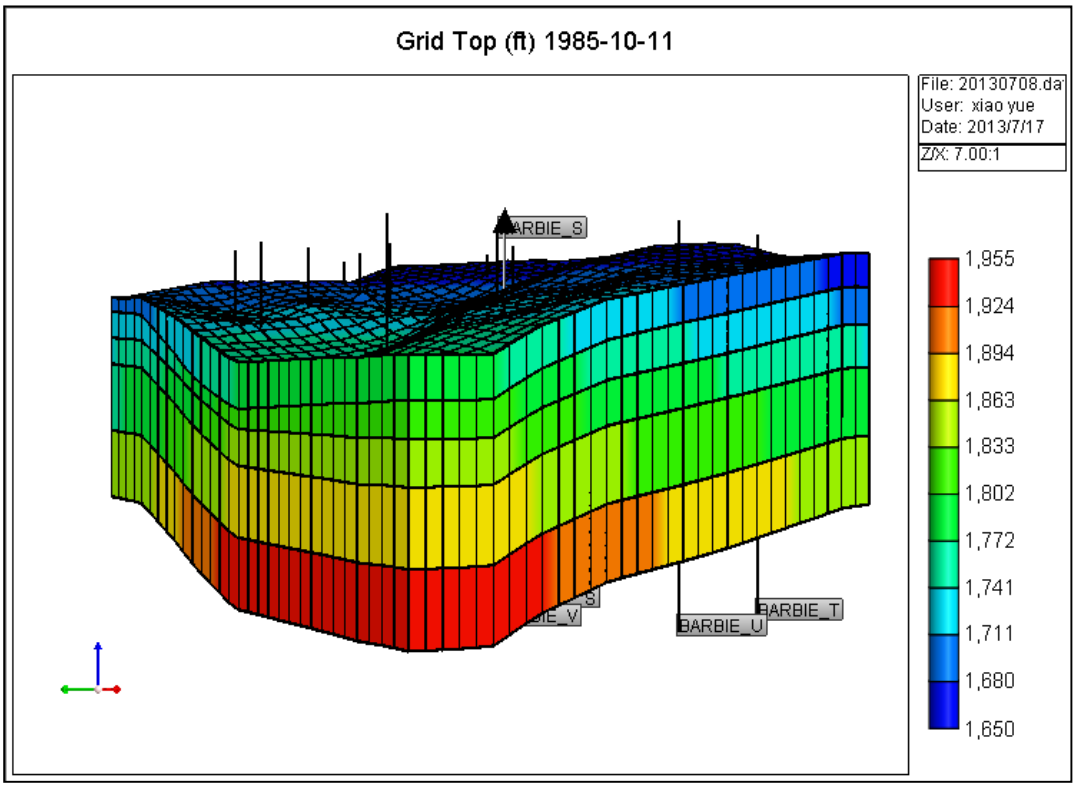


**Figure 33. Vertical grid system showing all five model layers.**

Each grid cell must be assigned with reservoir-geologic properties in order to complete model construction in the simulator. For geologic and petrophysical properties, layer thickness, porosity, permeability and saturation were analyzed at each well location. In-situ permeability was obtained by applying the porosity/permeability correlation with the in-situ porosity. Distributions of these properties' maps were then generated in Landmark's Nexus-Array Calculator. Figures 34–35 show sample initial reservoir properties for the field scale model and Figure 36 shows porosity and oil saturation by layer. Figures 37–38 show the subset area for detailed simulation for the single well stimulation.

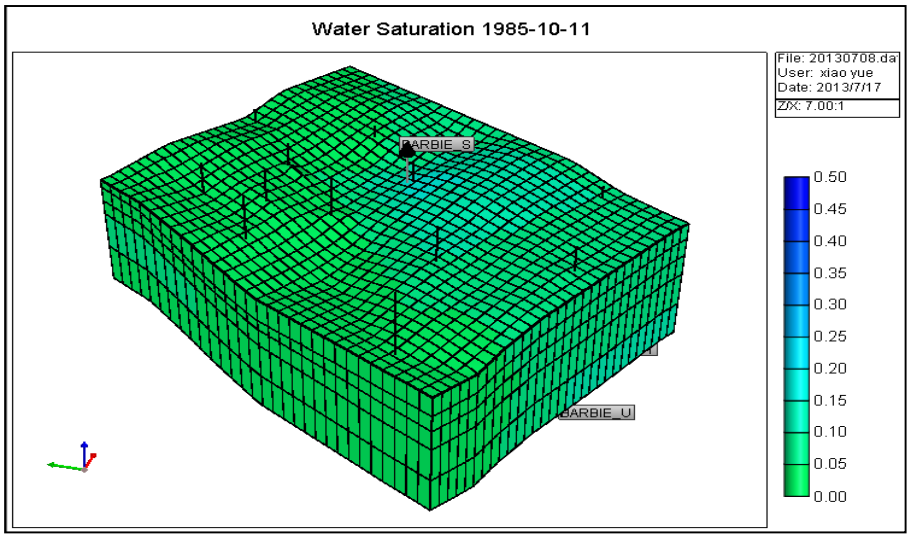


**Figure 34. Simulation model of study area in Millman, showing initial water saturation.**

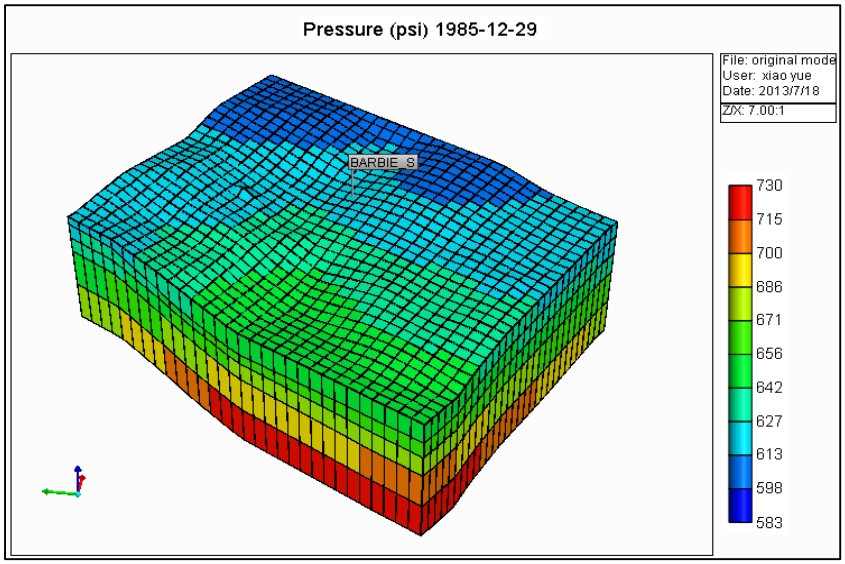


**Figure 35. Simulation model of study area in Millman, showing initial pressure distribution.**

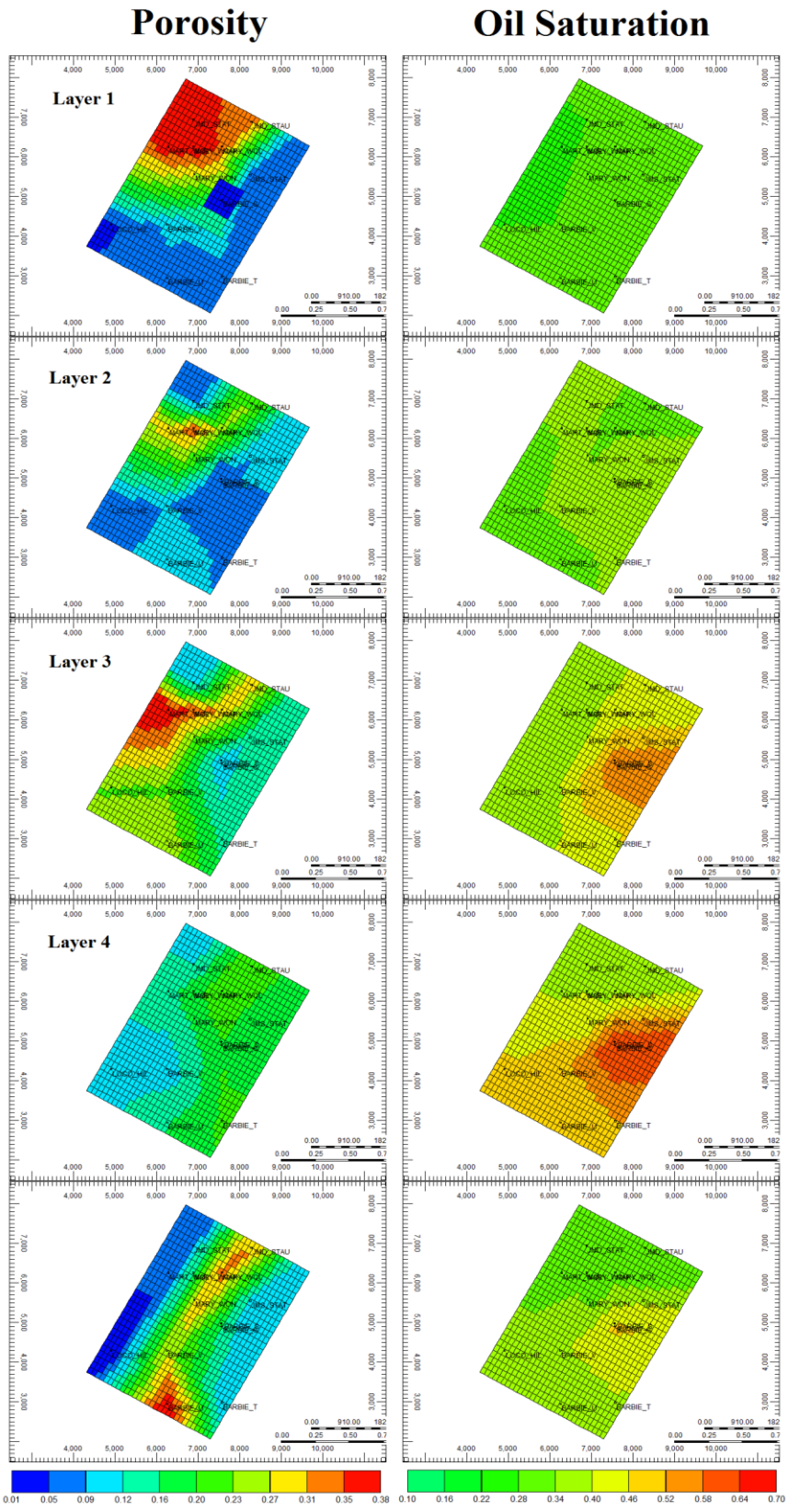


**Figure 36. Porosity and initial oil saturation distributions by layer.**

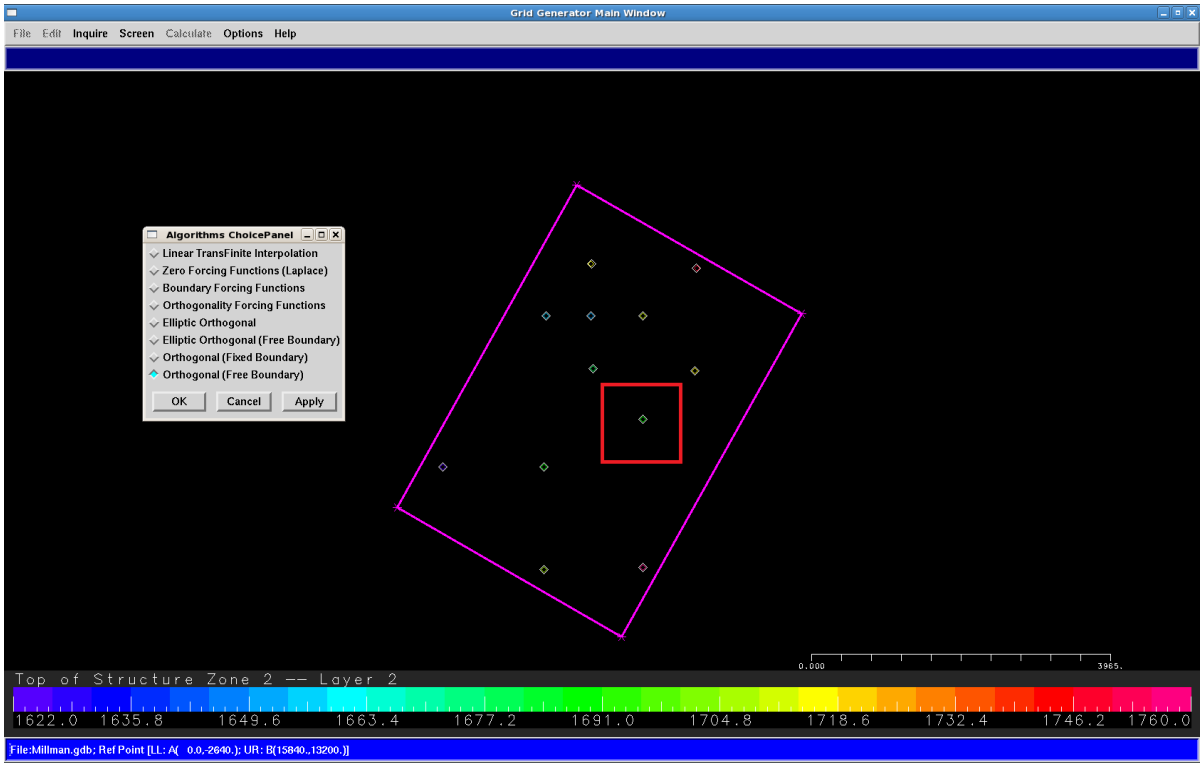


**Figure 37. The scale of the single well model compared with the full-field model. The red square represents the sub area of the single well model.**

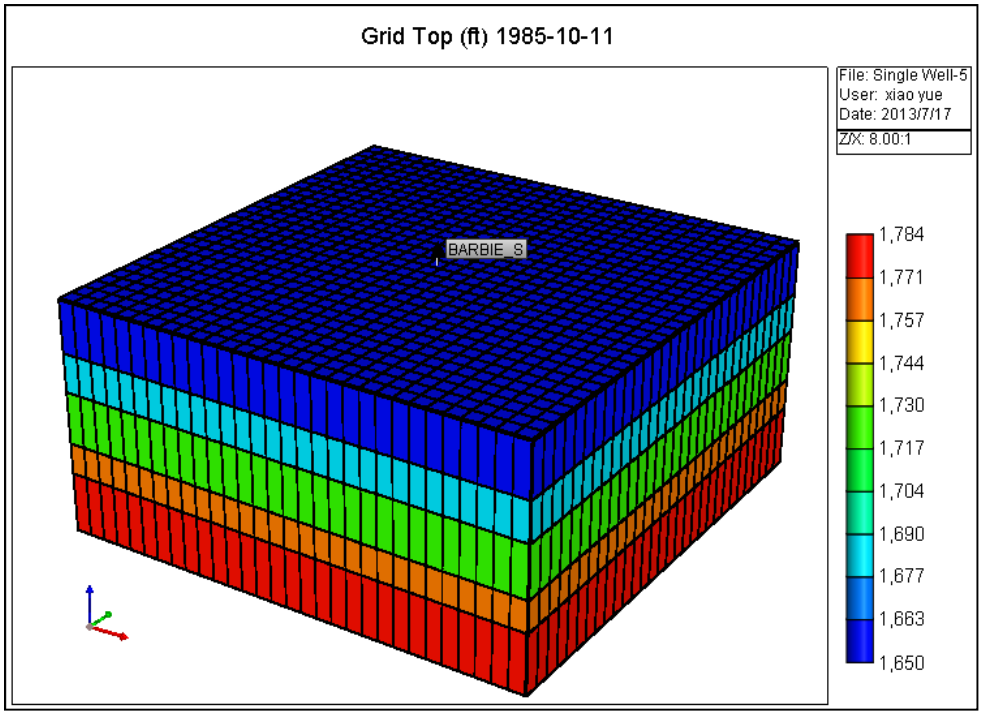


**Figure 38. 3D view of the single well model.**

The distance between Barbie State 001 and Barbie State 004 is about 1500 ft, so a single well model with area of 3000×3000 $ft^2$ was built with the same PVT properties as the full-field model. The model uses a square 30×30 grids system and has homogeneous reservoir properties, with layer thickness of 43, 27, 30, 32 and 68 ft respectively. Reservoir properties of the single well model were all from the results of parameter adjustment during the process of history-matching in the full-field model. Further lateral efficiency prediction was carried out using the single well model (Figure 38).

Before history-matching, uncertainties should be studied and analyzed regarding their influence on the model so that reasonable adjustments can be made to avoid aggravation in reservoir model. Factors that contribute to model uncertainty include:

**Effective porosity**: The model was constructed based on the assumption that total porosity is equal to effective porosity, which neglects the effect of clay content on total porosity. However, it is unknown exactly what the percentage of clay minerals to the total rock composition is. As a result, the pore volume of the model may have been overestimated.

**Permeability**: Porosity-permeability correlation specifically for the simulation zone of the Millman field is not available. Furthermore, correlated permeability exists only at each well location grid. Other grid-cell permeability was obtained by interpolating and extrapolating current values.

**Relative permeability curve:** No experiment has been carried out for collected core samples. Due to the lack of a fundamental rock physics study for this area, a relative permeability curve was applied considering the rock to be a typical sandstone.

**Rock compressibility:** Without core samples available for measurement, researchers relied on Hall's correlations to determine compressibility (Figure 39). His correlation is reported to be valid for any type of consolidated rock; however, it is limited to reservoirs at shallow depths. Note that a relationship exists between pore compressibility and porosity; however, there is a wide range in compressibility for a particular porosity. Lithology of reservoir rock in the study area varies from sandstone to dolomitic sandstone and porosity fell into the range of 0.051–0.357 at the well location. Thus, an average porosity of 0.212 was used and a correlation result of $3.5\times10^{-6}$ was achieved.

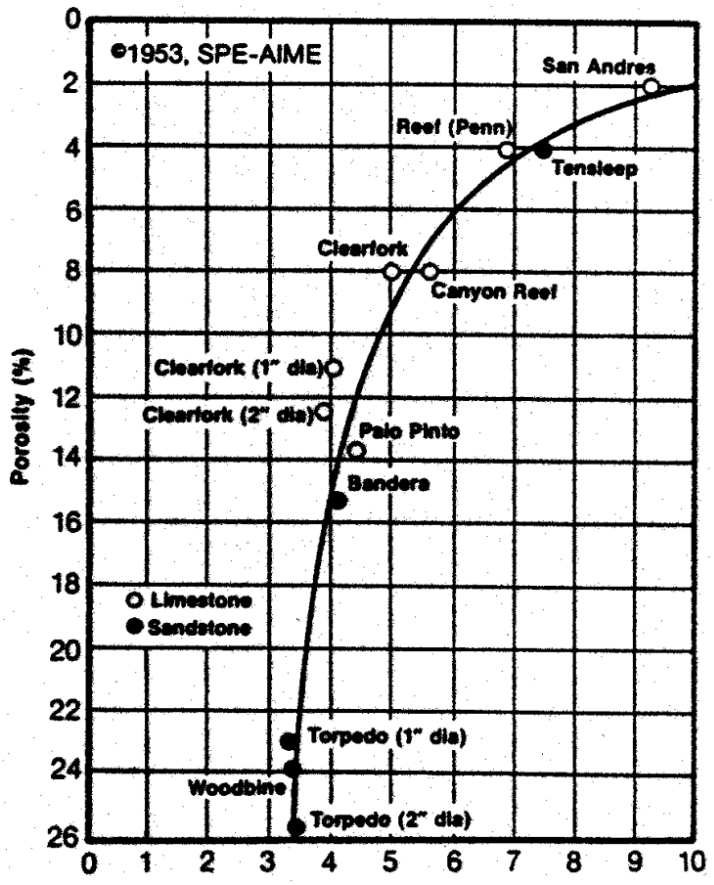


**Figure 39. Hall's correlation of porosity and effective pore compressibility, Pore Vol/Pore Vol/psi ($10^{-6}$ $PSI^{-1}$) (Hall 1953).**

### 1.1.11 Pre-Stimulation History Match

Previous sections discussed the sources of the raw data required for a simulation model and the techniques for handling these data in the construction of a reservoir model. These techniques, however, can be used only for data available from the relatively few wellbores that penetrate the reservoir. Before the simulation model could be utilized to predict reservoir performance adequately, this initial data needed to be adjusted during the history match phase of the study. To validate the model, GOR (gas rate), and reservoir pressure are the two main parameters for history match. Considering that available pressure data was collected at only two points–initial production and present day production, pressure was matched only to a trend scale. Assumption of reservoir pressure at reference depth of 1650 ft. was 500 psi. In addition, historical oil production rates were used in the model to constrain operating conditions when running the simulation.

Figures 40–44 show the simulation results using the initial model based on the field-wide model. Figure 45 shows the pressure simulation results of the target well, Barbie State No.1.

Even though the oil rate is perfectly matched, this model produced far less gas than actual production and simulated reservoir pressures are significantly higher than expected. In these diagrams, solid lines show the simulation results while points represent the production history.

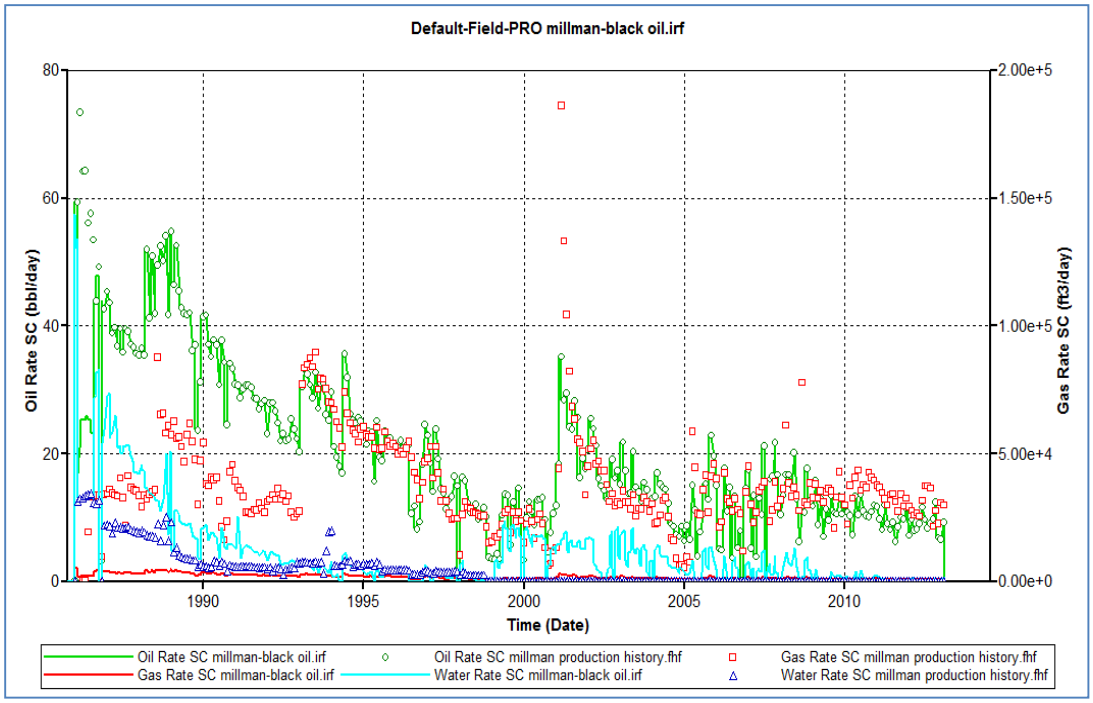


**Figure 40. Field production rates for initial history match.**

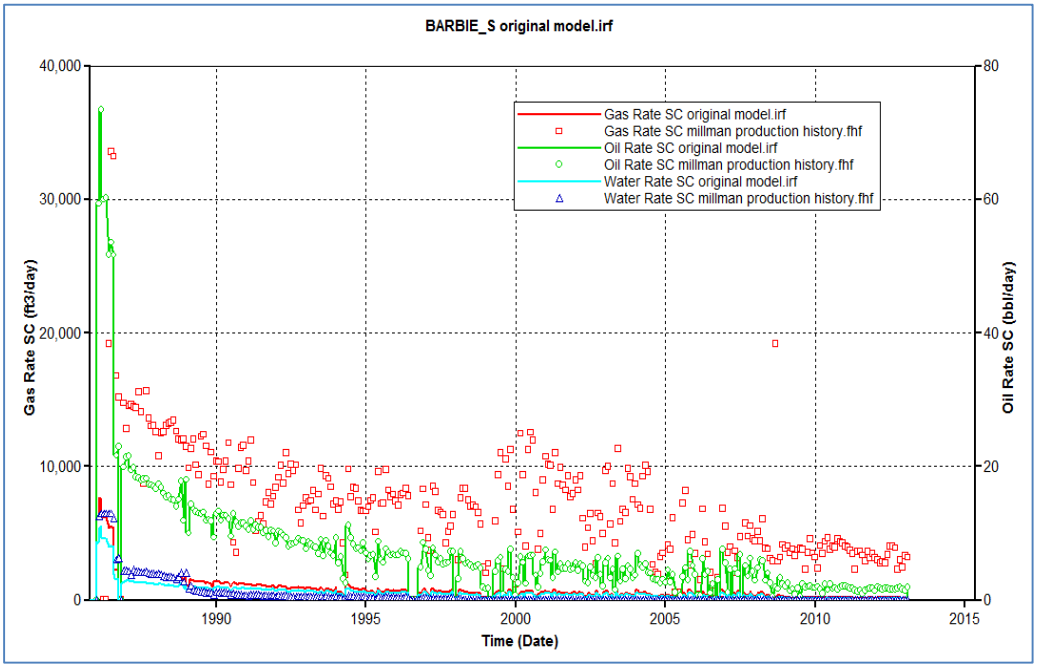


**Figure 41. Production rates of Barbie State No.1 for initial history match.**

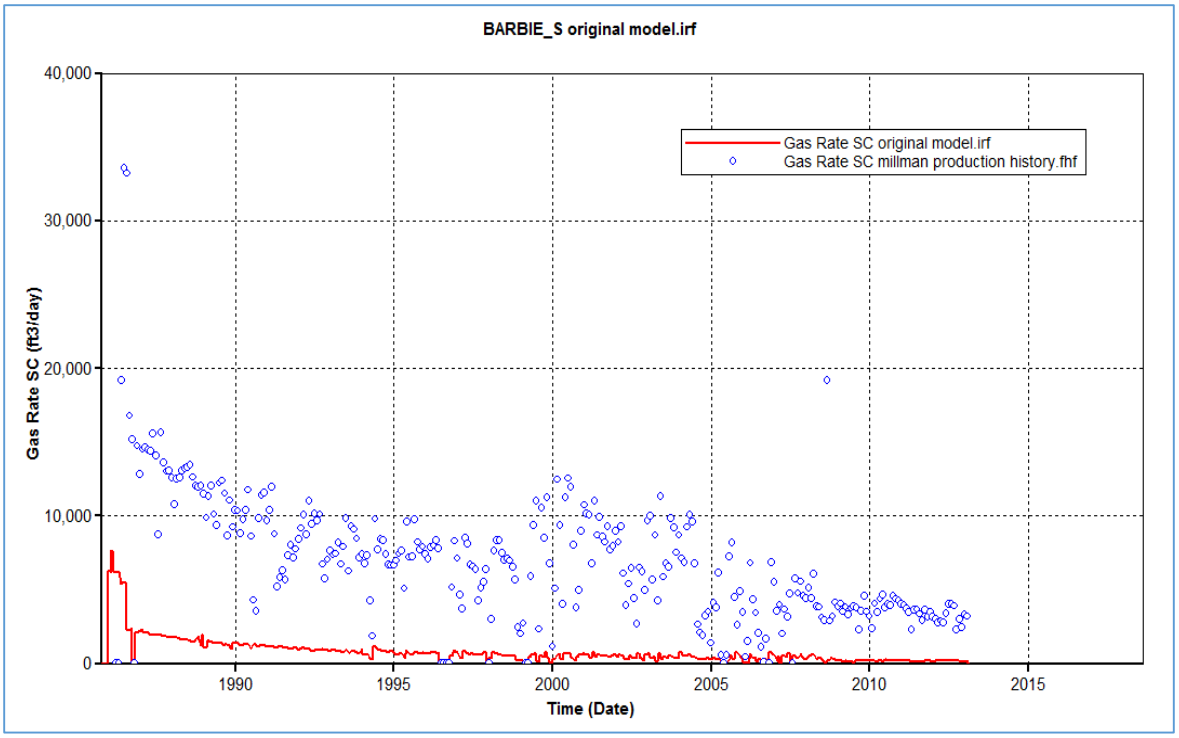


**Figure 42. Gas production of Barbie State No. 1 for initial history match.**

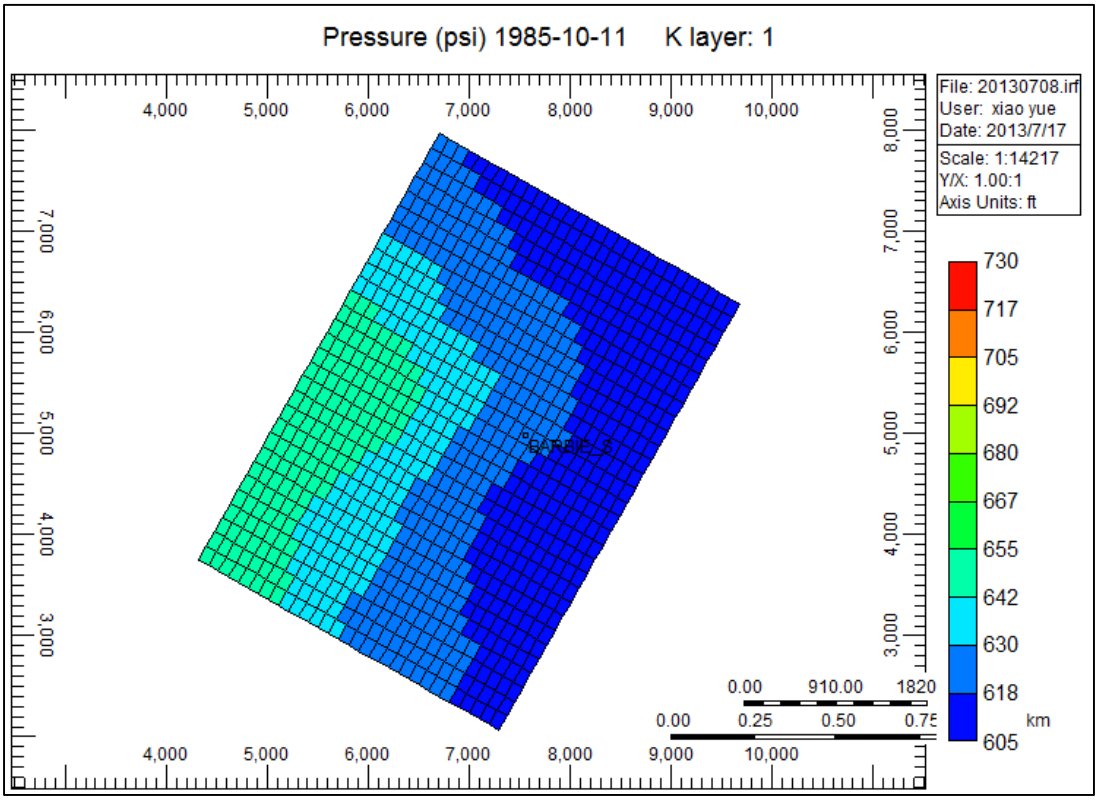


**Figure 43. Pressure distribution at start of first production.**

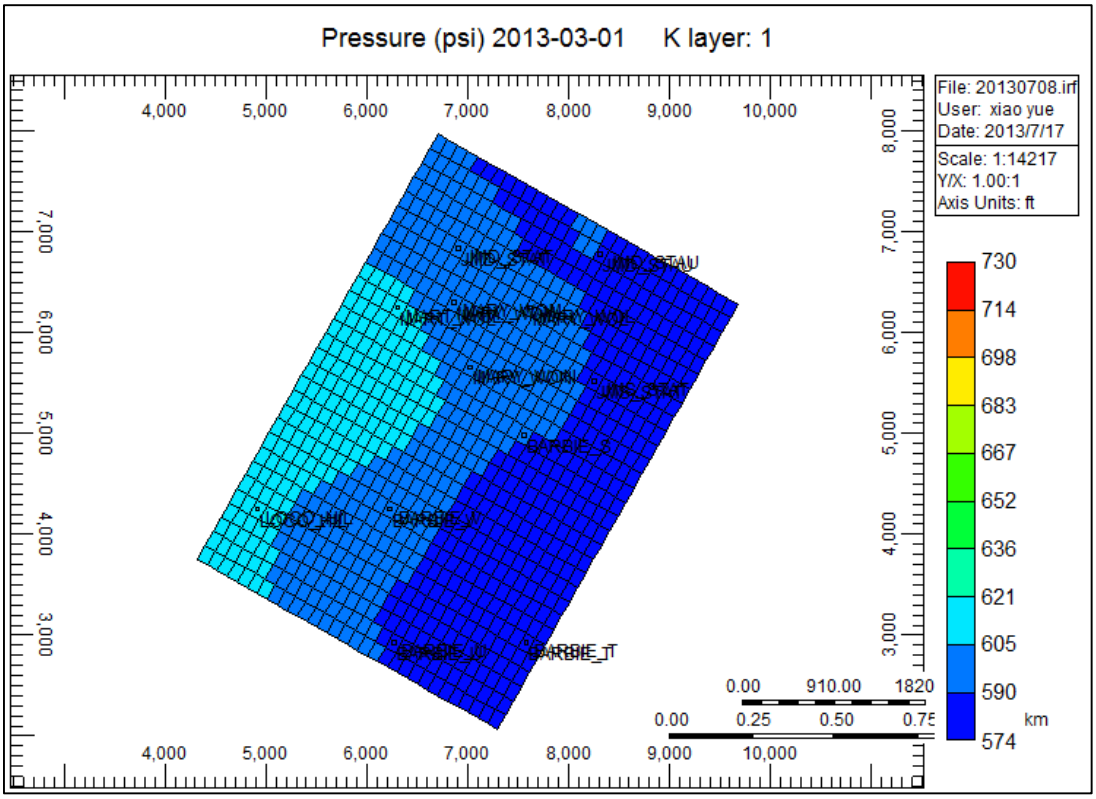


**Figure 44. Pressure distribution at year 2013.**

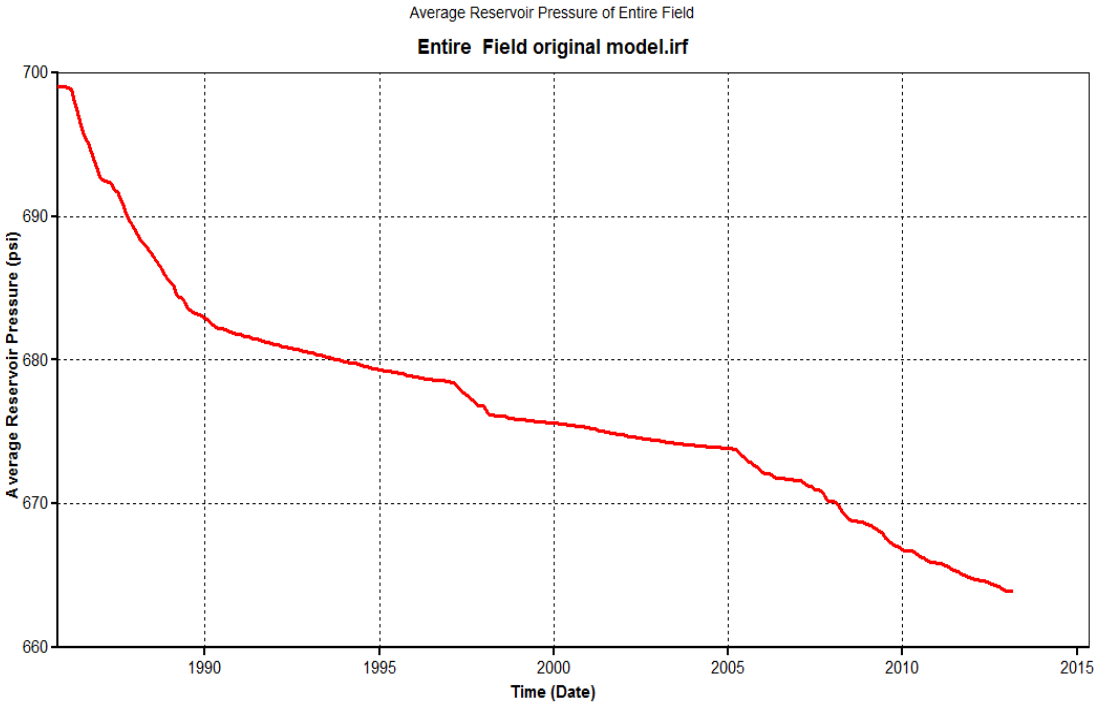


**Figure 45. Average reservoir pressure through time from initial history-matching.**

The study area contains four leases. Gas production for these four leases is shown in Figure 46. It could be observed that Barbie State has most consistently high gas production. However, for study objectives, only the target well Barbie State No.1 was history matched (Figure 47). Figure 42 and Figure 48 show the gas production rate before and after the initial history-matching. In the original model, the gas rate was too small to match the historical production. In order to refine the history match, a closer look was taken at severable variables to try and determine if the original history match could be reasonably improved without violating the understanding of the rock and fluid physics developed during the close study of the field. Of the examined variables, the following were considered for minor adjustments:

***Porosity.*** Porosity of layer 1 was reduced by 88%. This large reduction reflects an observed high percent of clay minerals observed in the analog core, which could cause a very low effective porosity.

***Permeability.*** Permeability of layer 5 was reduced by 93%. With this reduction of permeability, the simulated bottomhole pressure was reduced to expected levels at the end of the simulation. The permeability reduction was limited to the point where production rates are still matched with the actual record. Even though layer 5 is a porous dolomite for a large part, it appears to have poor connectivity and was rarely perforated as a production interval.

***Fluid Saturation***. Water saturation and oil saturation were calculated directly from LESA by analyzing the Shallow-Deep resistivity curves at each well location. Reservoir pressure data does not exist whereas gas saturation is highly pressure-sensitive. Thus the LESA analysis resulted in low estimates of Sw and So. To counter this, the reservoir initialization model was changed from water-oil-gas equilibrium (keyword: VERTICAL DEPTH_AVE) to user-specified saturation (keyword: USER_INPUT) and oil saturation was set as a constant value at each layer. For the Barbie State No.1, small variations were applied as near-wellbore refinements according to regional elevation. The result gas history match was improved as a result (Figure 48).

***Rock Compressibility.*** As previously discussed, gas solution is the major drive mechanism. Compared with water drive and gas cap drive, gas solution drive has the fastest and greatest pressure drop with production. However, in the initial simulation model, the pressure drop was not consistent with current production. Rock compressibility was adjusted from $1\times10^{-5}$ $psi^{-1}$to $3.5\times10^{-5}$ psi-1 to help match average reservoir pressure (see Figures 45 and 49 for comparison). After the compressibility adjustment, the reservoir pressure drops from 650 psi to 100 psi, which falls within a reasonable estimation (Figure 50).

All values modified during history-matching are shown in Tables 11 and 12.

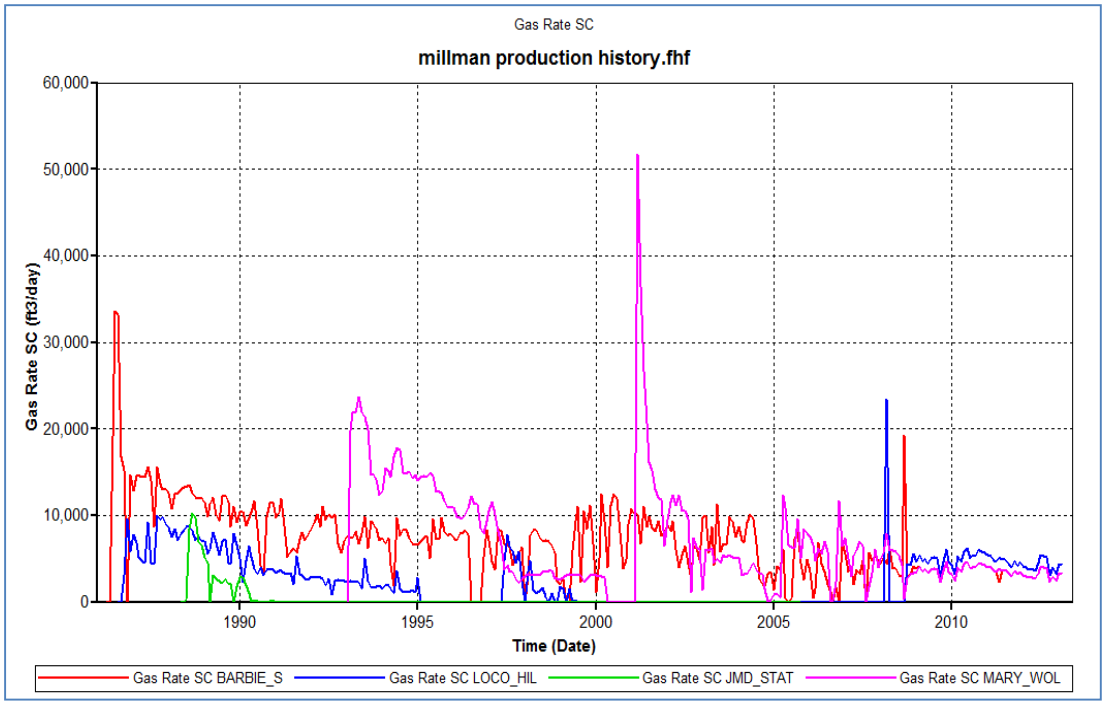


**Figure 46. Gas history productions for the four leases: Barbie State, Loco Hill State, JMD State and Mary Wolf State.**

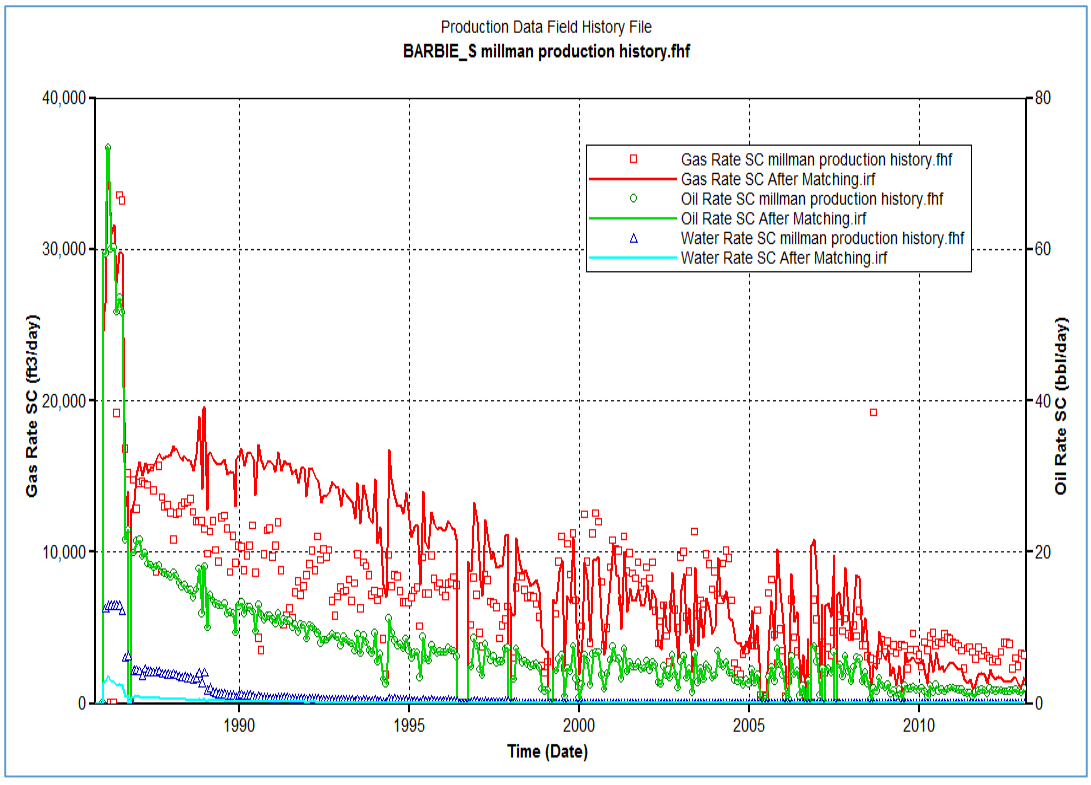


**Figure 47. Production rates for the Barbie State No.1 after initial history match.**

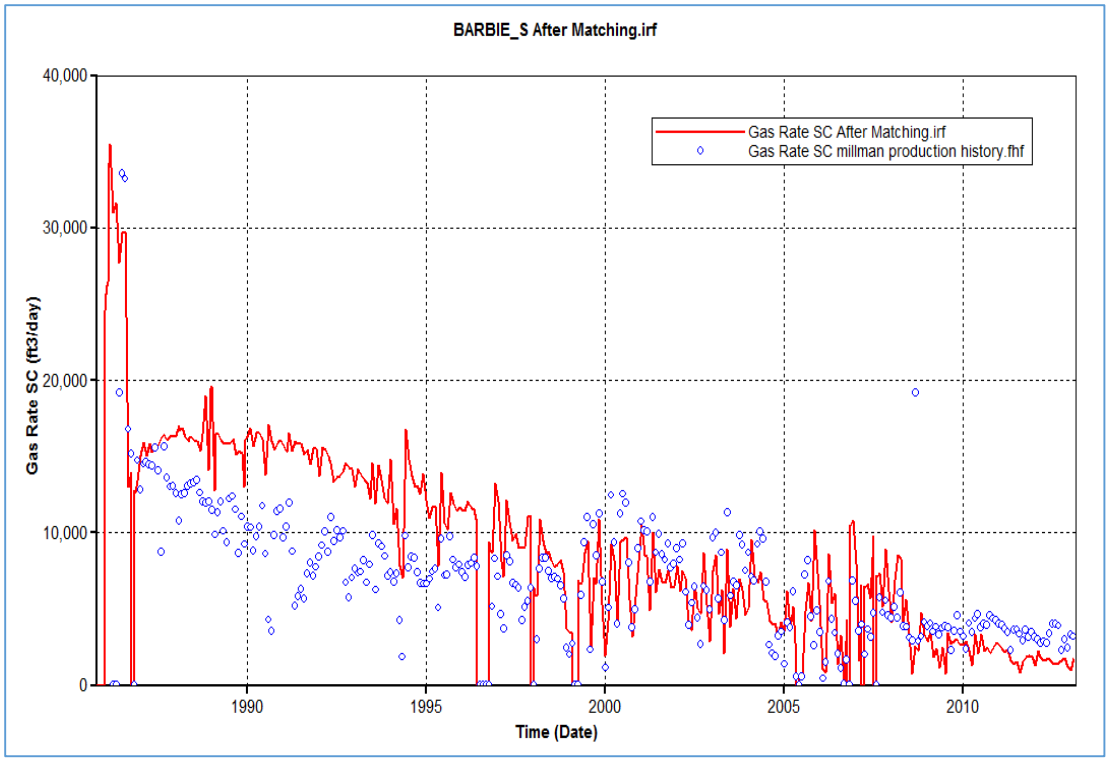


**Figure 48. Gas production for the Barbie State No.1 after initial history match.**

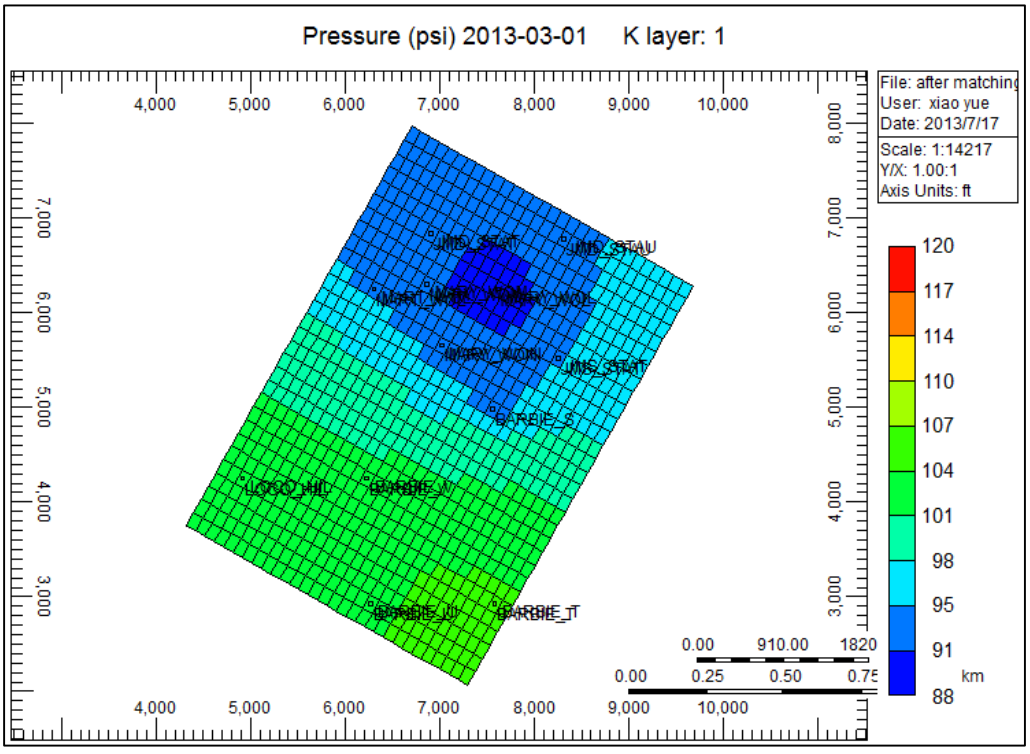


**Figure 49. Pressure distributions at year 2013 after adjusted history-matching.**

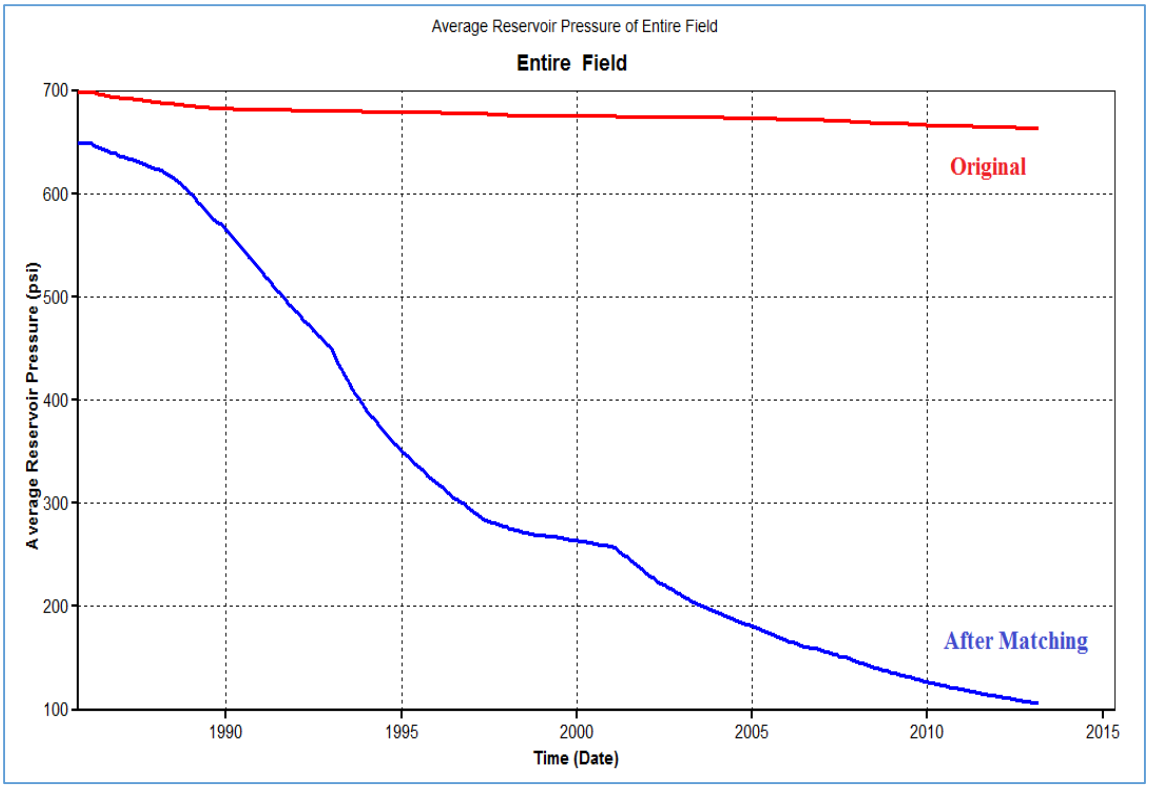


**Figure 50. Average reservoir pressure for the initial (original) and modified (After) history matches.**

**Table 11. Reservoir Properties for Initial History Match**

| | Φ(frac) | k(mD) | $S_w$(frac) | $S_0$(frac) |
|---|---|---|---|---|
| **layer 1** | 0.181 | 2.027 | 0.01 | 0.5 |
| **layer 2** | 0.06 | 7.63 | 0.09 | 0.29 |
| **layer 3** | 0.098 | 54.71 | 0.121 | 0.555 |
| **layer 4** | 0.195 | 47.752 | 0.102 | 0.637 |
| **layer 5** | 0.155 | 30.162 | 0.22 | 0.17 |

**Table 12. Reservoir Properties for Adjusted History Match**

| | Φ(frac) | k(mD) | $S_w$(frac) | $S_0$(frac) |
|---|---|---|---|---|
| **layer 1** | 0.02 | 2.027 | 0.37 | 0.5 |
| **layer 2** | 0.06 | 7.63 | 0.39 | 0.49 |
| **layer 3** | 0.098 | 54.71 | 0.33 | 0.56 |
| **layer 4** | 0.195 | 47.752 | 0.18 | 0.75 |
| **layer 5** | 0.155 | 2 | 0.32 | 0.57 |

### 1.1.12 Lateral Efficiency Prediction

With the history match in place it became possible to forward predict models. The single well model for lateral efficiency prediction was developed and used the reservoir properties shown in Table 13, with each layer having homogenous properties.

**Table 13. Comparisons of Lateral Efficiency in Enhancing Oil Production**

| | Φ(frac) | k(mD) | $S_w$(frac) | $S_0$(frac) |
|---|---|---|---|---|
| **layer 1** | 0.02 | 2.027 | 0.37 | 0.5 |
| **layer 2** | 0.06 | 7.63 | 0.39 | 0.49 |
| **layer 3** | 0.098 | 54.71 | 0.33 | 0.56 |
| **layer 4** | 0.195 | 47.752 | 0.18 | 0.75 |
| **layer 5** | 0.155 | 2 | 0.32 | 0.57 |

Figure 51 shows the lateral patterns to be simulated and Figure 52 is a side view of those layers. The purpose of these models was to establish the optimal number of laterals to stimulate the formation. Layer 4 was chosen as the target layer for lateral stimulation, as it is sandstone and has the highest potential for residual oil. More than half of the existing perforations were located in this layer.

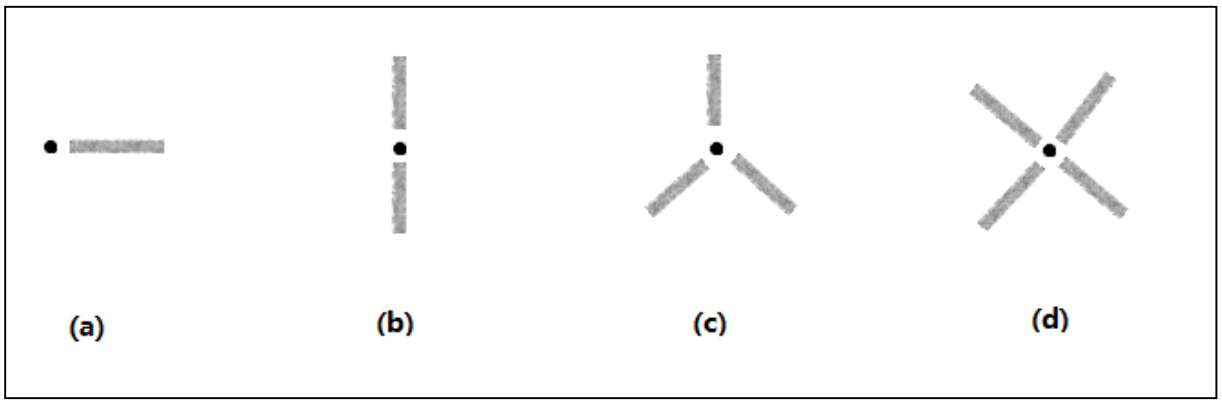


**Figure 51. 30 ft long short radius laterals with 2 in. diameters.**

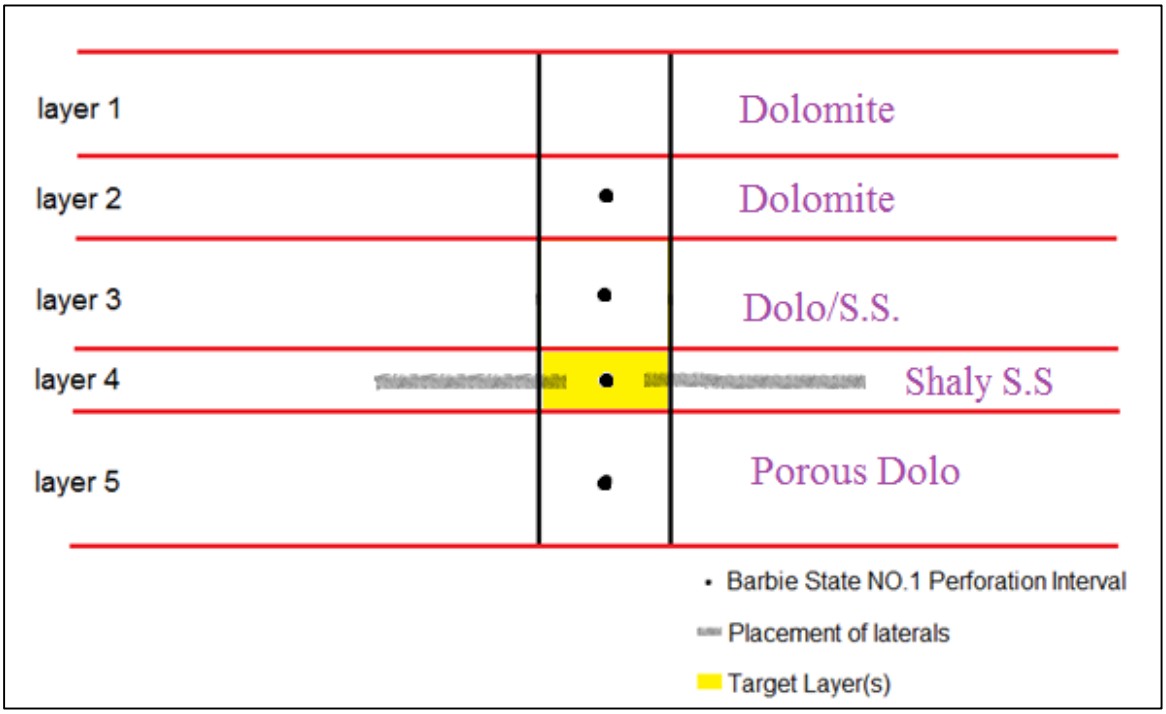


**Figure 52. Target layers for radial drilling.**

Two sets of tests were performed: 1. Add (a), (b), (c), (d) laterals from Figure 51 to layer 4 and simulate from year 2013 to 2023; and 2. Add lateral(s) with best efficiency from Set 1 to a duplicated layer 4 that had not seen initial production to simulate a previously unperforated zone and simulate from year 2013 to 2023.

In order to optimize the type and duration of laterals that were to be emplaced in the target Barbie State No.1 well, a series of simulation were run using CMG. The start time of simulation was the first production data, 10/11/1985, and Barbie State No.1 was treated with four types of lateral patterns on 3/1/2013, and operated for 10 years afterwards. In all other aspects the target well worked under the same operating constraints after 3/1/2013 as it did before. Figure 53 demonstrates the four types of lateral emplaced in a Cartesian refined grid system. Each lateral was assigned to be 30 ft long and 2 in. in diameter. The permeability impact of each lateral was assumed to be 300 mD using the following correlation:

$$k = \sqrt{\frac{8r}{\Phi}}$$

in which:

Porosity $\Phi$=16%

Tube radius r = 1inch

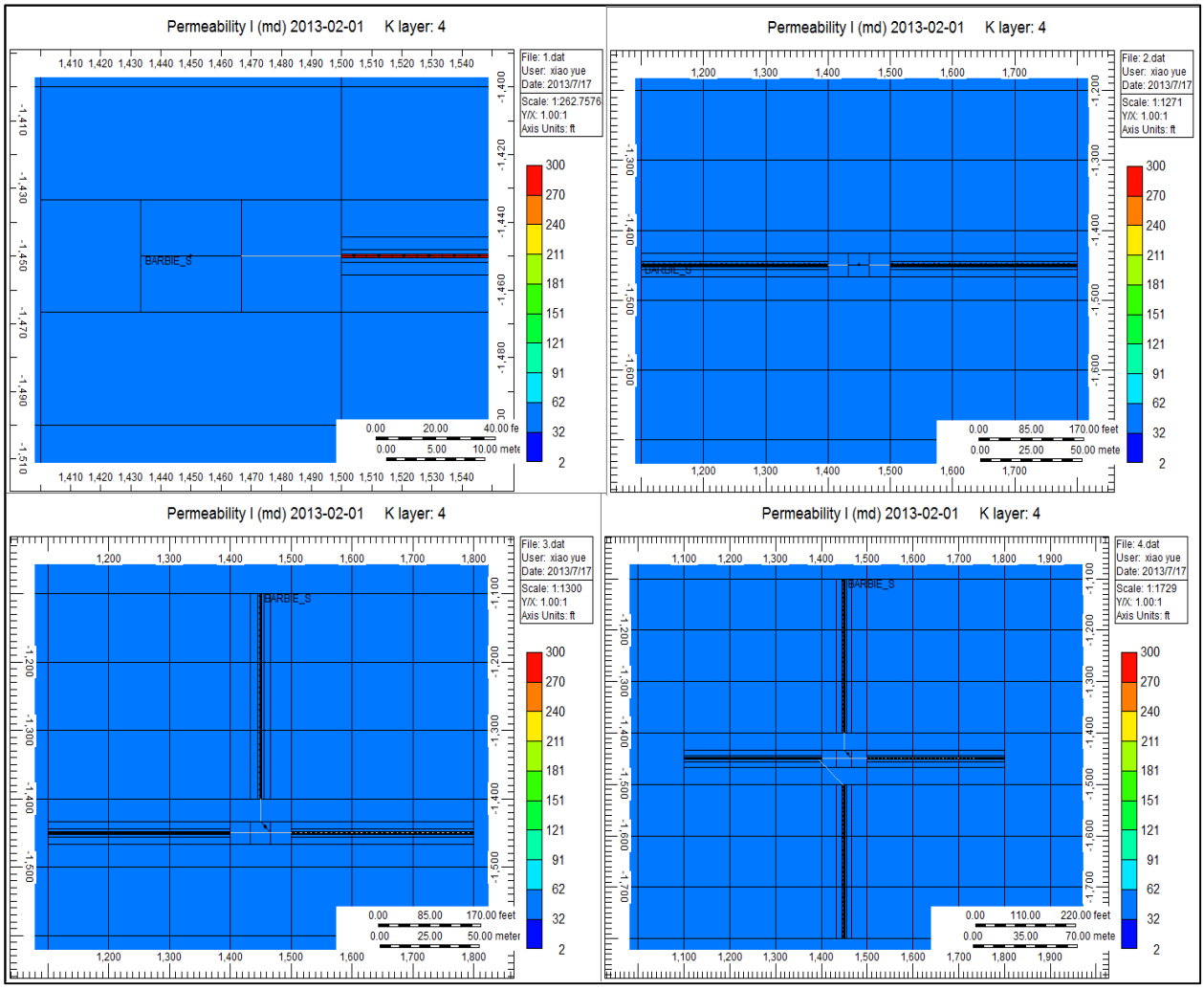


**Figure 53. Local grid refinement- Cartesian refinements for 1, 2, 3, and 4 emplaced laterals.**

In order to test the efficiency of laterals, the base case model was also predicted for ten years as a continuing stripper well. In the base case model, oil production declined gradually, as expected over the ten years prediction. Figure 54 shows the predicted base-case pressure decline, and Figure 55 shows the predicted oil rate and cumulative production for the well. In contrast, the predicted impact of the laterals is shown in Figure 56 for oil rate, and Figure 57 for cumulative production. Table 14 summarizes the results for the four tests compared to the base case, and Figure 57 shows key reservoir properties at the end of the simulation for Layer 4. In each case laterals increased productivity. As more laterals were added improvements occurred in drainage as well.

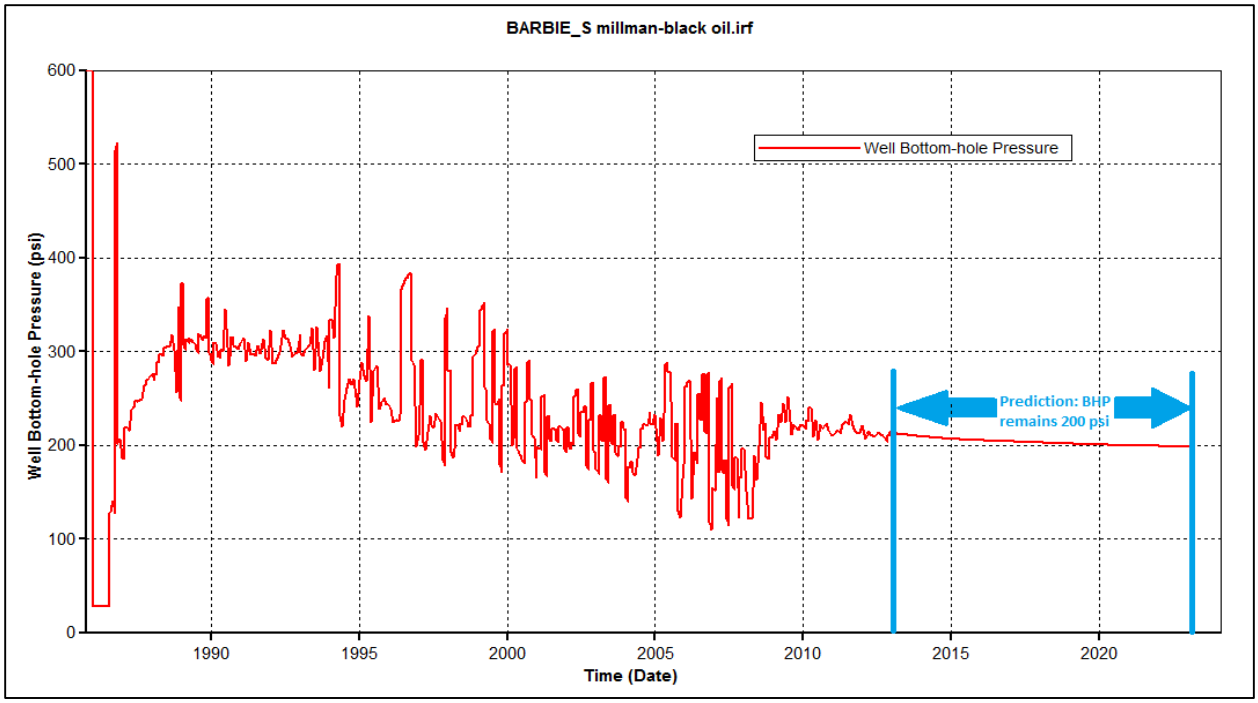


**Figure 54. Predicted bottomhole pressure of Barbie State No. 1.**

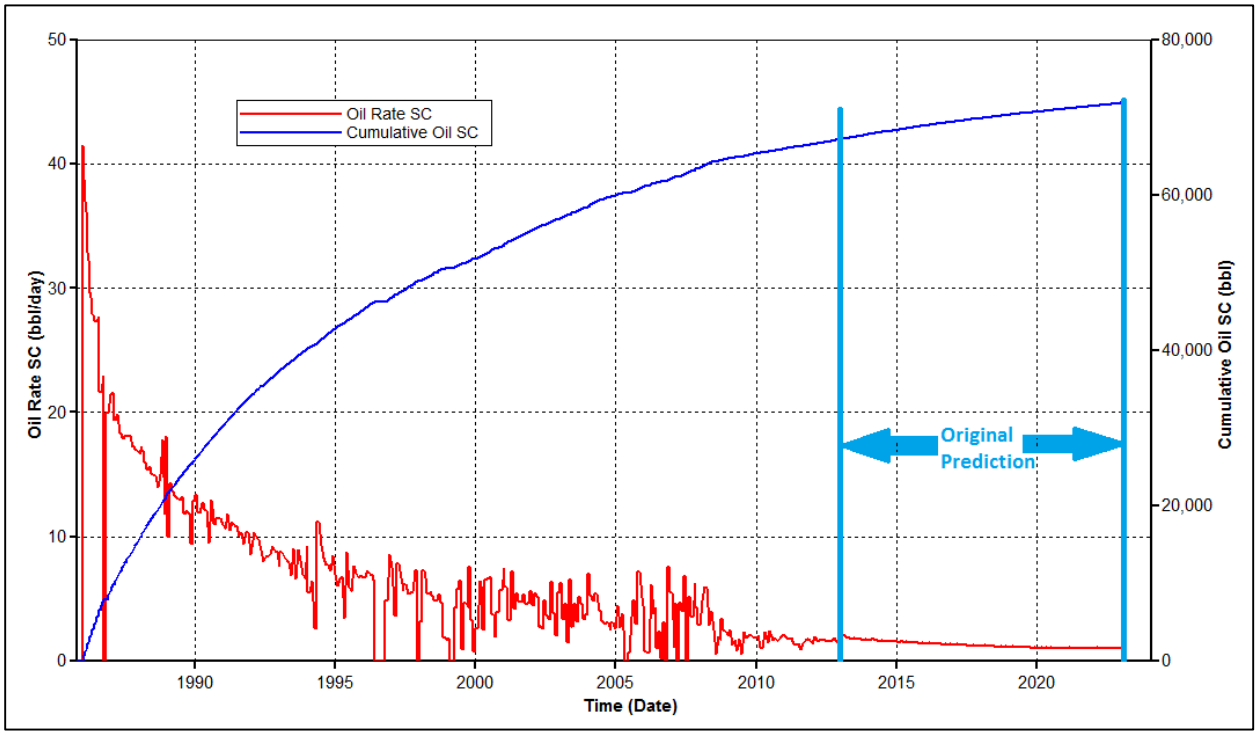


**Figure 55. Predicted oil production rate and cumulatives for the base case (no stimulation).**

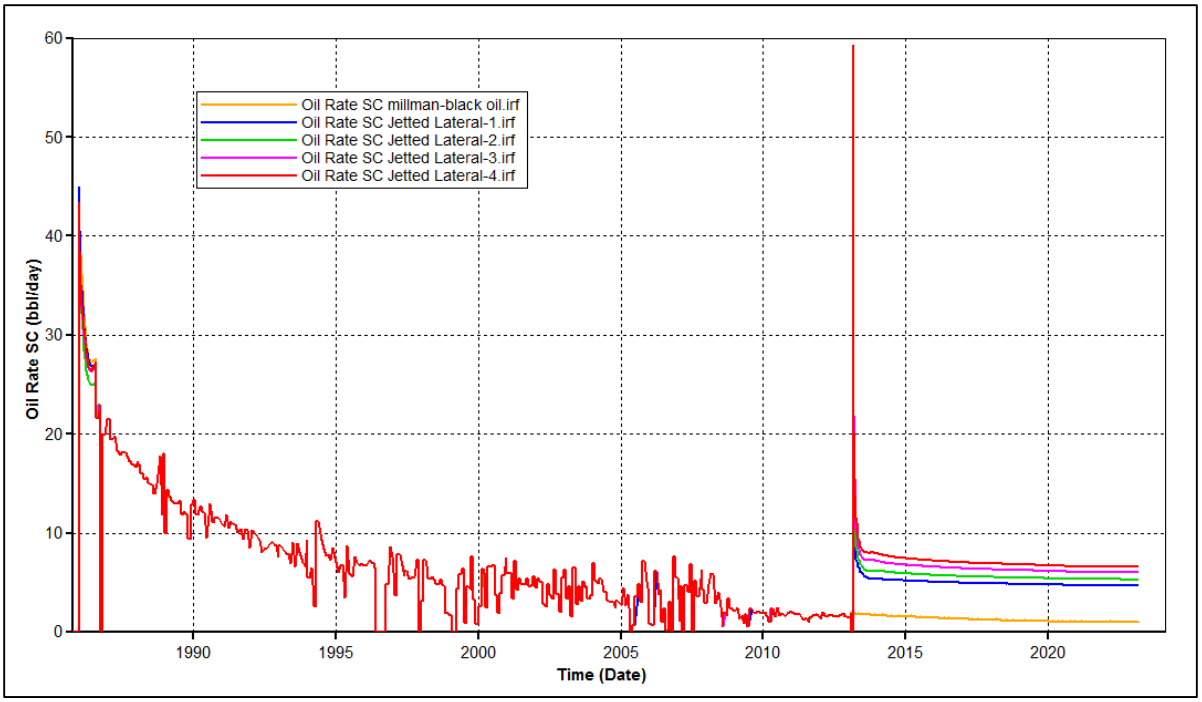


**Figure 56. Comparison of predicted oil production rates using various lateral patterns.**

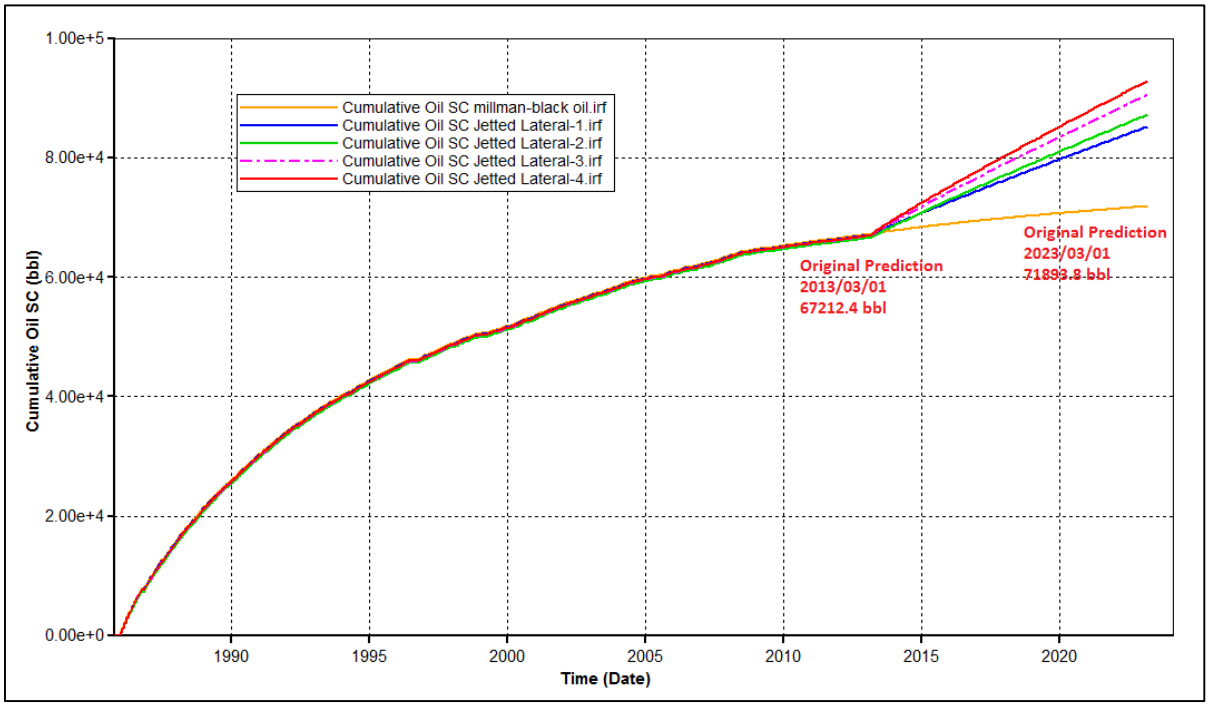


**Figure 57. Comparison of predicted cumulative production using emplaced laterals for prediction.**

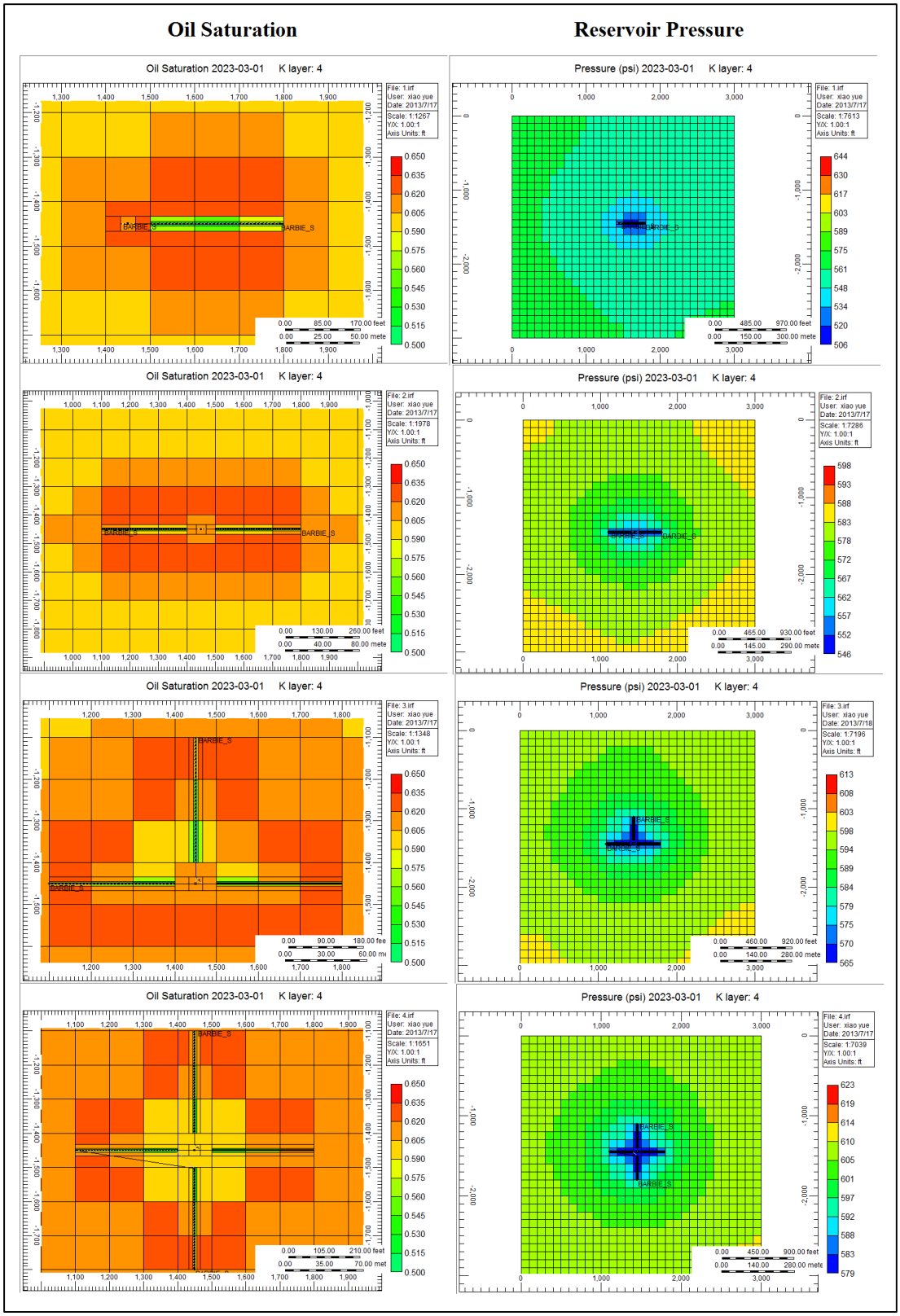


**Figure 58. Oil saturation and pressure distribution of four types of lateral patterns at year 2023.**

**Table 14. Comparisons of Lateral Efficiency in Enhancing Oil Production**

| | Base | 1 Lateral | 2 Laterals | 3 Laterals | 4 Laterals |
|---|---|---|---|---|---|
| **Average Oil Rate (bbl/day)** | 1.28 | 4.86 | 5.44 | 6.39 | 7.04 |
| **Cumulative Oil Production(bbl)** | 71894 | 84953 | 87082 | 90524 | 92905 |
| **Enhanced Oil Production(bbl)** | 4682 | 13059 | 15188 | 18630 | 21011 |
| **Production incremental Percent (%)** | 0.0% | 18.2% | 21.1 | 25.9% | 29.2% |

### 1.1.13 Prediction of Response for a Previously Unstimulated Zone.

A sixth layer was created by duplicating the third layer and using the same reservoir properties (Figure 59). Four laterals was placed in layer 6 at the well location 3/1/2013 and simulation prediction was made until 3/1/3023. Table 15 shows the production response for the previously unperforated layer using four emplaced laterals.

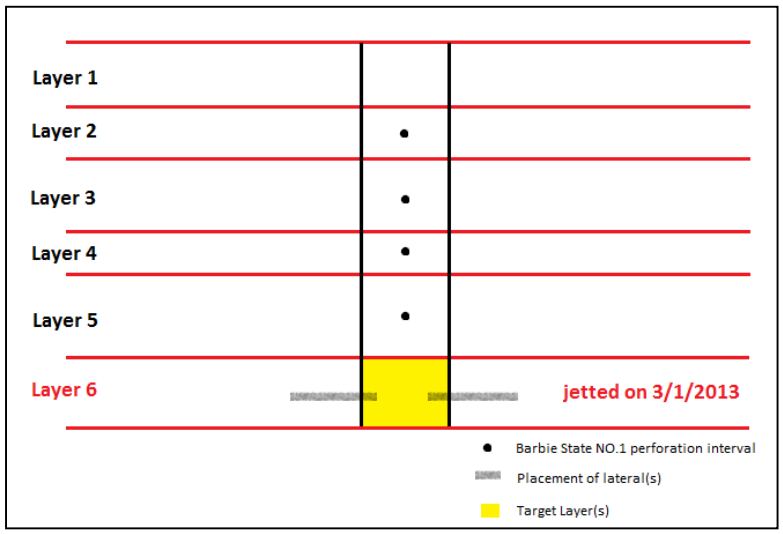


**Figure 59. Laterals emplaced in a duplicated layer. Predicted starting 3/1/2013.**

**Table 15. Comparisons of Lateral Efficiency in Enhancing Oil Production--Duplicated Layer**

| | Original | 4 Lateral in 6$^{th}$ layer |
|---|---|---|
| **Oil Rate (bbl/day)** | 1.39 | 7.48 |
| **Cumulative Oil Production(bbl)** | 78221.5 | 104308 |
| **Enhanced Oil Production(bbl)** | 0 | 26086.5 |
| **Production incremental Percent (%)** | 0.0% | 33.3% |

### 1.1.14 Simulation Summary

Successful characterization of the west Millman field with limited and poor quality data was made with the assistance of well logs and core observation. In this regard the field is a representative example of a small mature field operated by a small producer: relatively low on data, and as stripper wells, a candidate for restimulation to maintain economics. Characterization work flows are summarized as follows:

**Structure**: the west Millman located in Eddy County is terrace shaped with down-dip/up-dip in the west/east direction. **Layers**: The Grayburg sand/dolotones can be divided into five layers based on gamma ray and porosity logs. The results of well log correlation show that the thickness of each layer is quite consistent across the Millman field study area.

**Porosity/Permeability**: porosity and permeability are best on high-energy depositional features, and that the incised cuts into these, which form "noses" in the top structure, have lower porosity and permeability. Analysis of available well log curves, using LESA, was the only technique applied to acquire porosity and permeability information for the simulation.

**Mineralogy**: the study of mineralogy from wireline logs and lithological histogram indicates that the main mineral of the Grayburg formation in west Millman is a combination of sandstone and dolomite.

Once the model was constructed, a 3D-Blackoil full-field simulation model was constructed and validated through history-matching, with limited pressure data. As most wells in the west Millman were fractured and acidized before first production, the entire field can be presented as a low porosity/permeability environment. The results from history-matching show satisfactory outcomes after a few reasonable adjustments were made to better match the model to observed and implied reservoir properties. Furthermore, a single well model was also constructed using the same PVT data and adjusted reservoir properties which lead to a finer management of the prediction stage of the project. While a full-field model was developed, predictions were limited to a single stimulated well, though the full-field model will provide a framework for predicting the impact on other wells in the field if other restimulation candidates are considered after field testing

The prediction of lateral efficiency showed that the four emplaced laterals gave the best overall efficiency for enhancing oil production with 28.5% with a predicted incrimental production increase of 20,588 bbl. If un/under-stimulated zones are identified and stimulated using four laterals, the enhancement is somewhat larger (33.3%) with incrimental oil production of 26,086 barrels.

## 1.2 Lateral Tracking and Sensor Development

The general goal of the DataLogger development is to develop a small, battery-powered device able to record accelerations in X, Y and Z directions during short-radius lateral drilling, offload the data into a computer, and calculate the drilling path after the instrument is returned to the surface. With the general goal in mind, researchers collected as much information as possible related to short-radius lateral drilling parameters from drilling professionals and companies. Based on this information and results from analysis of those data, the general design requirements can be listed in four categories: function, size, power and environment.

1. Function: Measure the acceleration (range is about -2G—+2G) in x, y and z directions, and record them into some kind of storage device.
2. Size: All parts (sensor, microcontroller, storage, battery, wire resistors, capacitors PCB and accessories) must meet the space requirement for fitting into a shell/tube section with dimensions of diameter 0.5 in. × length 1.25 in.
3. Power: Must provide enough power for DataLogger to work more than three hours (Voltage and Capacity).
4. Environment: the DataLogger must survive the harsh environments encountered in the lateral: high temperatures, pressures, chemicals, and hydrocarbons.

The following narrative describes the development process, including development paths that were pursued and determined be impractical or unfeasible.

### 1.2.1 Initial Three-Section Design

According to the design requirements, which allow only a short tool package to navigate a tight turn in an in-casing shoe the DataLogger was initially designed with three sections:

- The power section: provides power for the other two sections.
- The microcontroller and storage section: reads the data from the accelerometer and records it into the storage (flash memory chip).
- The triaxial piezoelectric accelerometer section: measures accelerations during drilling.

The three sections are connected with a flexible coupling and wires in the following order: Battery→microcontroller→ accelerometer. One end of the DataLogger is connected to a jetting hose and the other end is connected to the jet head with a flexible coupling as shown in Figure 60. The battery provides the power needed for microcontroller, flash memory and accelerometer sensor. Due to the limited space, a battery with a necessarily small dimension might provide insufficient power for operation and/or for the duration of the measurement process.

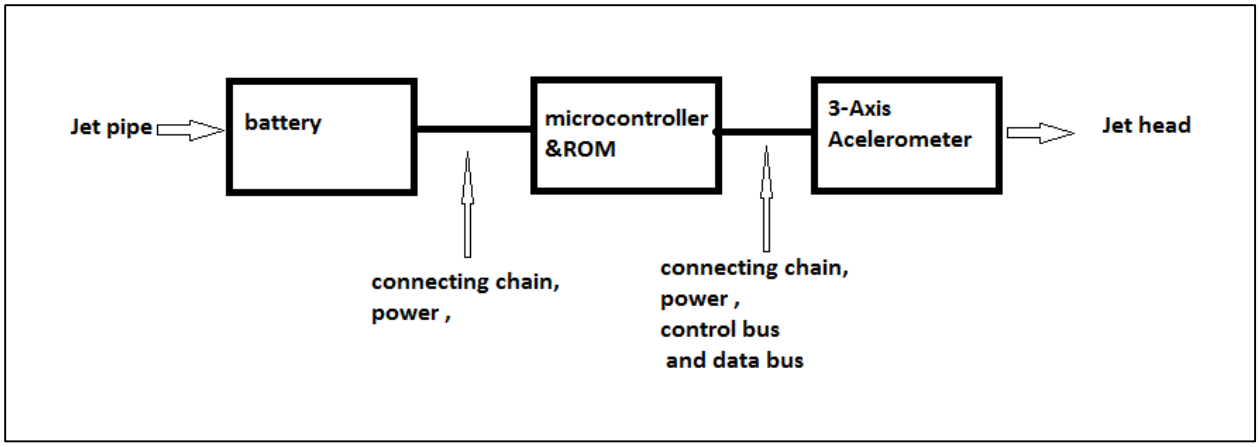


**Figure 60. Initial three-section design.**

The shell of each section is a piece of stainless steel tubing with dimensions of 1.25 in. L × 0.5 in. outer diameter (OD) × 0.049 in. wall × 0.402 in. inner diameter (ID). The inner diameter is 0.43 in. = 10.21mm T-316/316L. Thus the useful space for DataLogger parts is D = 0.43 in. × 1.25 in. L (10.21mm D x 31.75mm L); considering there are two caps needed to seal the two ends of the shell, (10.21mm D × 25 mm L) this still leaves a reasonable space to accommodate the DataLogger. After conducting an extensive search, and after supply companies, a microcontroller and storage (flash memory) was obtained that could meet the requirements.

A few technical problems could not be solved with current technologies and products: The size of the three-axis piezoelectric accelerometer with industrial grade accuracy is larger than the limited space and even if a special order were made from providers, the accelerometer itself might barely fit into the tube. To work properly it still would need the conditioner, specific cable, and 18+ voltage 2–20 mA battery, an amplifier and a 12-bit A/D converter. Each of these components individually was larger than the space of a section, especially complicated by the size of the cable and 18V power supply. The sealed waterproof flexible power and signal linkage between sections also were not easily resolved. Figure 61 shows a typical Piezo accelerometer circuit consisting of accelerometer, amplifier, coaxial cable, constant current source and A/D converter.

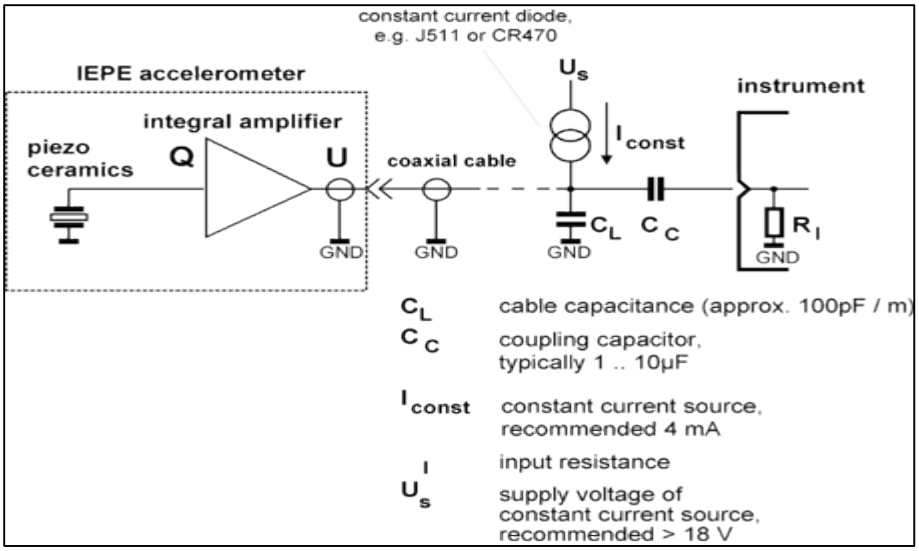


**Figure 61. Typical physical accelerometer circuit.**

### 1.2.2 Digital System Design with a Three-Axis MEMS Accelerometer

To avoid these unsolvable size and power issues with current technologies it was decided to:

- Find a replacement for the three-axis accelerometer with much smaller body, digital output (thus no need for conditioner/amplifier, coaxial cable, constant current source and A/D converter) and lower power consumption (lower operation voltage and lower current).
- Redesign the entire system to fit in one section to prevent issues with finding an appropriately scaled and sealed, waterproof, flexible wire linkage.

After searching and comparing different products it was decided to use a three-axis MEMS (Micro-Electro-Mechanical Systems) accelerometer (LIS331DLH). The LIS331 series products are produced by STMicroelectronics.

The LIS331DLH accelerometer is an ultra low-power, high performance, three-axis linear accelerometer belonging to the "nano" family, with digital I2C/SPI serial interface standard output. The device features ultra low-power operational modes that allow advanced power saving and smart sleep to wake-up functions. LIS331 has a 12-bit sample rate corresponding to 50-1,000 samples per second. The LIS331DLH also has dynamically user-selectable full scales of ±2g/±4g/±8g and it is capable of measuring accelerations with a 12-bit sample rate of 50–1,000

samples per second while utilizing a self-test capability that allows the user to check the functioning of the sensor in the final application. In addition, the device may be configured to generate an interrupt signal by inertial wake-up/free-fall events as well as by the position of the device itself. Finally, thresholds and timing of the interrupt generators are programmable by the end user. The LIS331DLH is available in small thin plastic land grid array packages (LGA 3mm × 3mm × 1mm) and it is guaranteed to operate over an extended temperature range from -40°C to +85°C, which encompasses most oilfield deployments. A sample block diagram for the chip is shown in Figure 62. To summarize the LIS331DLH's main features:

1. Wide supply voltage, 2.16 V to 3.6 V
2. Low voltage compatible IOs, 1.8 V
3. Ultra low-power mode consumption down to 10 µA
4. ±2g/±4g/±8g dynamically selectable full-scale
5. I2C/SPI digital output interface
6. Very small body: 3 mm × 3 mm × 1 mm

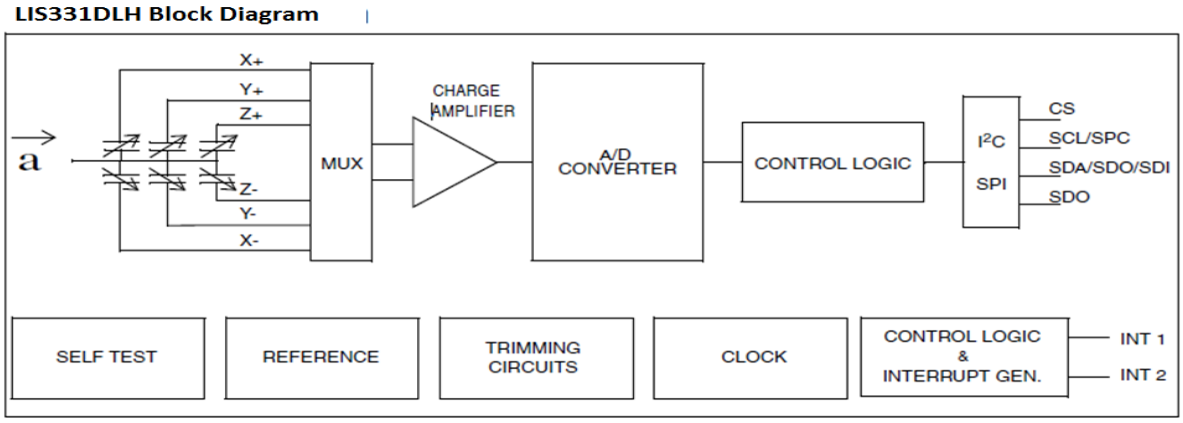


**Figure 62. LIS331DLH block diagram.**

Using the LIS331DLH as the DataLogger sensor does not require an extra amplifier/conditioner, coaxial cable, constant current source or an A/D converter , because all these elements have been integrated into it (Figure 62). The downside is that this product is not industrial-grade, which means it has potential accuracy problems that must be addressed. Since the LIS331DLH was selected, a microcontroller, storage, and a battery were also obtained that met the design requirements and can work with the LIS331DLH.

Fortunately, there is an abundance of microcontroller products from many manufacturers on the market. A few of the popular microcontroller series of microcontrollers are Intel's 8051 series, Microchip's PIC series, Texas Instrument's series and Atmel AVR series. The DataLogger must have a small body and lower power consumption, so a popular and inexpensive 8-bit

microcontroller produced by Microchip was chosen. The PIC12VF1840 controller was selected due to following features:

1. SOIC package (Narrow 3.9 mm body) or DFN package (3 mm x 3 mm x 0.9 mm body)
2. 8-pin
3. I2C/SPI serial communication interface,
4. Ultra low power, 75uA, and low voltage, 1.8v—3.6v
5. 4KB program memory

Additionally, Microchip provides many development tools: IDE, C compiler and Programmer. The Microchip website provides many downloadable datasheets, application notes, sample codes, online technical support and user forums.

There are many kinds of data storage devices: hard drives, DVD/CD, USB, MMC, and secure data cards, but most of these are too big to fit into the shell. Even the smallest secure data cards: from top to bottom Standard SD card, MiniSD card, and MicroSD card, could not fit into the shell (Figure 63).

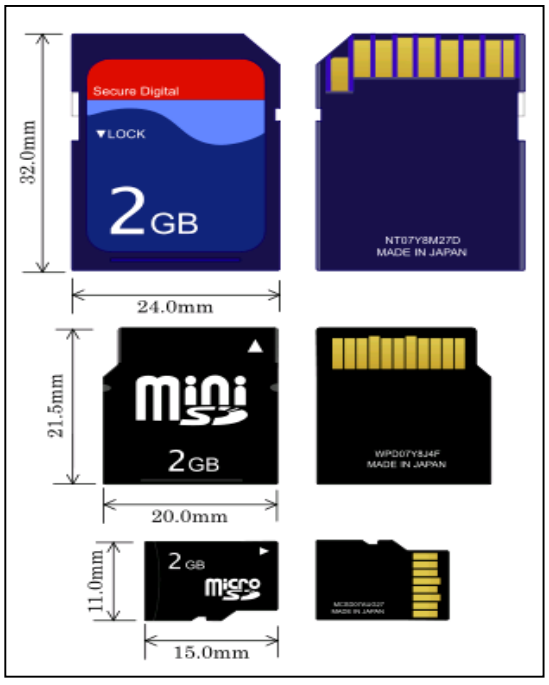


**Figure 63. Secure datacard dimensions.**

Another available option is a flash memory chip with serial data bus. The greatest capacity that could be found to fit the size constraints is a 64 Mbit chip: SST25VF064C, which has the following features:

1. Flash Memory
2. Size: 5mm × 5mm
3. 64 Mbits = 8MBytes
4. SOIC package 8-pin
5. Serial communication interface (SPI/I2C(=IIC))
6. Low power/voltage 2.7v–3.6v
7. 33–80 MHz for High-Speed Read
8. Endurance: 100,000 Cycles (typical)
9. Data Retention: Greater than 100 years
10. Low Power Consumption
    a. Active Read Current: 12 mA (typical @ 80 MHz)
    b. Standby Current: 5 μA (typical)

Assuming the sampling rate of the LIS331HH is set at 100 samples per second, at every second, the DataLogger will generate 100 × 6 bytes = 600 bytes (each sampling data set contains 6 bytes for X,Y and Z directions). Eight MB divided by 600 bytes per second gives 13,333 seconds of capacity, or 3.7 hours, which is sufficient for deployment of coiled tubing in and out of a well.

Several small capacitors and resistors are needed in the connections between the sensor, microcontroller and flash memory chip to make the DataLogger circuit work properly. Surface mount device **(**SMD) resistors and capacitors come in several possible sizes. Each size is described as a four-digit number. The first two digits indicate the length; the last two indicate the width. For example, the three most popular sizes are:

0603: 0.06 in. × 0.03 in., or 60 × 30 mils, or 1.6 × 0.8 mm
0805: 0.08 in. × 0.05 in., or 80 × 50 mils, or 2.0×1.25 mm
1206: 0.12 in. × 0.06 in., or 120 × 60 mils, or 3.2 × 1.6 mm

Thus, the sizes and capacities of capacitors and resistors are not as much of an issue as is the sensor. Figure 64 shows the sizes of capacitors and resistors listed previously. The resistors and capacitors with "1206" size were selected for the DataLogger circuit (SO-8 is the size of PIC12F1840 with SOIC package).

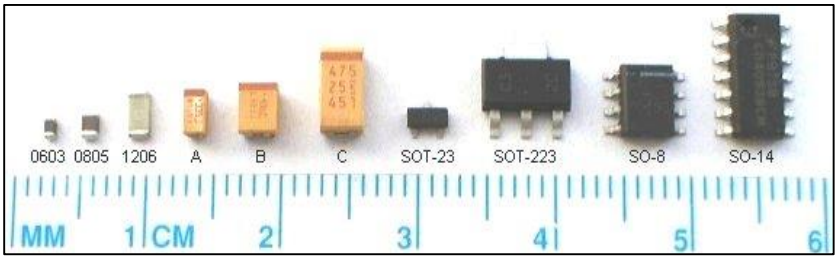


**Figure 64. Capacitor sizing.**

Since the sensor, microcontroller and flash memory chip selected all work at about 3V, to power the DataLogger a 3V battery that meets the size requirements, diameter less than 10.9 mm and height/thickness less than 5 mm, is needed. Due to the size requirement, only coin-shaped cells will fit. Only one option exists among coin-shaped cells: the lithium cell CR1025, the smallest one shown in Figure 65, with 3V voltage 30mAh and dimension 10 mm d. × 2.5mm h.


**Figure 65. Lithium cell batteries. The smallest depicted, CR1025, meets our requirements.**

Lithium batteries have better discharge characteristics than alkaline batteries. Figure 66 shows AA lithium battery and AA alkaline battery discharge characteristics; the voltage of the lithium battery does not drop as rapidly during low drain or high drain before it is exhausted.

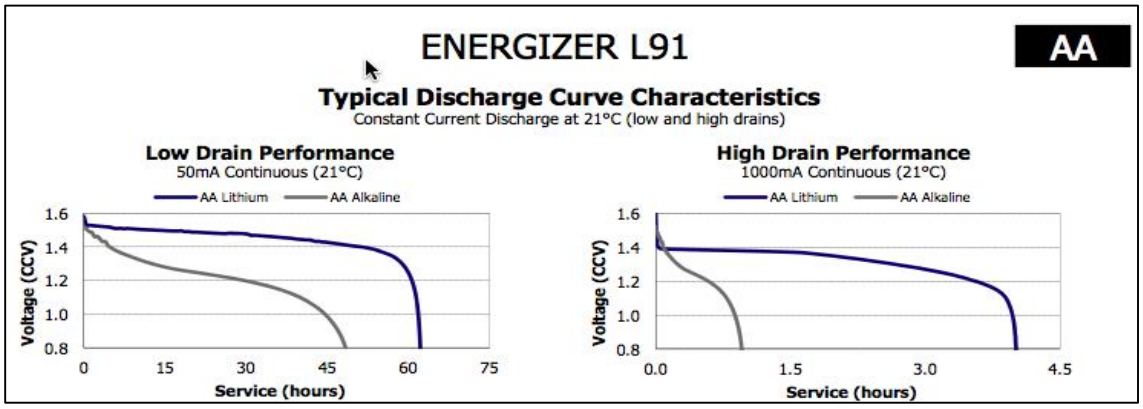


**Figure 66. Lithium battery discharge characteristics are superior to those of alkaline batteries.**

The C-rate is the measure of the rate at which a battery is discharged relative to its maximum capacity. A 1C rate means that the discharge current will discharge the entire battery in 1 hour. For a battery such as the CR1025, with a capacity of 30 mAmp-hrs, this equates to a discharge current of 30 mAmps. Most portable batteries, with the exception of lead acid, are rated at 1C. The same battery discharged at 0.5C provides 15mA for two hours. At 2C, the same battery delivers 60mA for 30 minutes. In order to evaluate the battery for the datalogger, as designed, a breakdown of power usage by component was designed (Table 16).

**Table 16. Size and Power Consumption by Component**

| Name | PIC12LF1840 | LIS331 | SST25VF064C | Battery | Resistor /Capacitor |
|---|---|---|---|---|---|
| Size | 3.9mmx3.9mm(SOIC body) | 3x3x1mm | 5x5mm | 10x2.5mm | 3x2mm |
| Operation Voltage | 1.8—3.6v | 2.16-3.6v | 2.7—3.6v | Lithium 3V | |
| Operation current | 75uA | 250uA | 25mA | 30mAH(?) | |
| Standby/sleep | 500nA | 10uA | 5uA | | |

On this basis, it is possible to evaluate the power consumption: the operation voltages are, respectively: 1.8—3.6V, 2.16—3.6V and 2.7—3.6V so the CR1025 battery fits the requirement. The total maximum operation current is: 75uA+ 250uA + 25mA=25.325mA. Based on the C-rate of lithium batteries, the CR1025 can support 30 / 25.325 = 1.18 hours. However, the SST25VF064C chip is only enabled when being written. Checking the software (C program) and the recorded wave by logic analyzer (Figure 67) shows that the SST25VF064 chip is enabled less than one-third of the time in a cycle of read-write. During the enabled windows, the chip is not always in writing mode; most of its time is spent waiting and communicating with the MCU. Therefore, the CR1025 battery should power the DataLogger for more than 3.3 hours. Bench tests showed that the CR1025 is not exhausted after the DataLogger has run for over 3.5 hours and the memory chip was fully written.

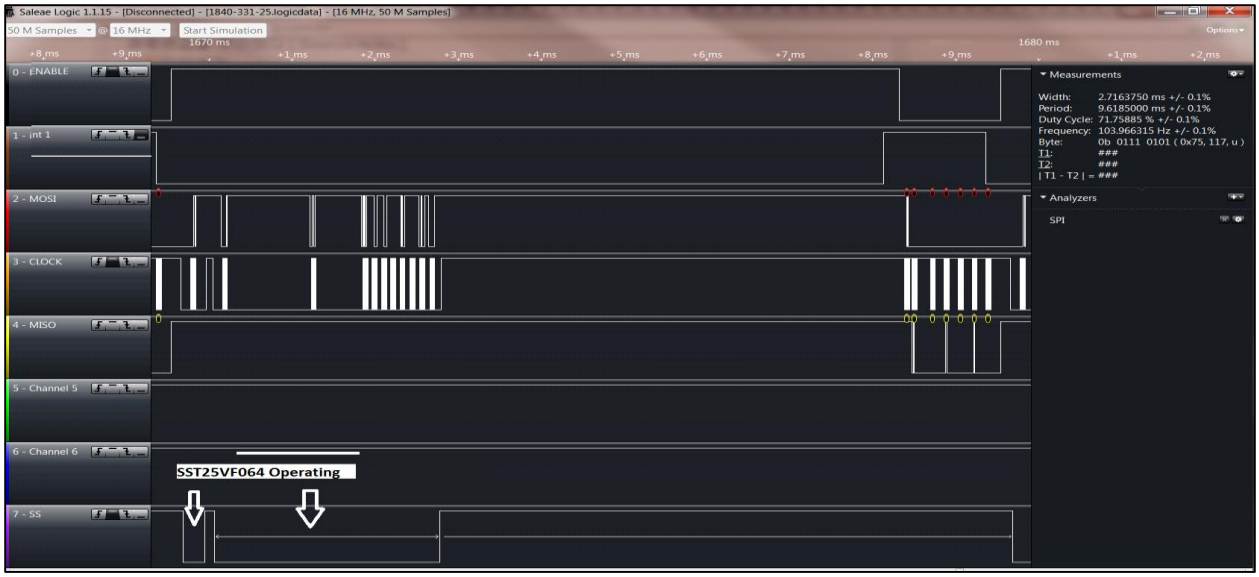


**Figure 67. The SST25VF064 chip is only enabled less than one-third of the time in a cycle of read-write.**

It was concluded that the CR1025 is able to power the DataLogger for 3.5 hours, well after the selected storage chip (the SST25VF064 ) would be full and the DataLogger no longer writing.

### 1.2.3 The Containment Vessel for the Datalogger

Based on the environmental requirements, a stainless steel tube made of T-316/316L, (0.5 in. OD × 0.035 in. WALL × 0.43 in. ID T-316/316L ) was selected for the shell of the DataLogger. The inner diameter of the T-316/316L is 0.43 in. = 10.9 mm. Although its theoretical bursting pressure is 10,500 lb/in$^2$, the ASME Code suggests a safety factor of four; so it is safe to use at 2625 psi bursting pressure based on temperatures between -20° F and 100° F.

Table 16 also shows the sizes of each main component that are used to build the DataLogger. From the second row (Size). The total length of DataLogger should be 2.9+3+5+2.5 =14.4 mm at a minimum with a diameter of at most 10 mm. The PCB dimension should be equal to or less than 10 mm W × 25 mm L. All components should be soldered on either one side or maybe both sides depending on selected PCB and assembly technologies. Figure 68 illustrates shell and inner-shell dimensions.

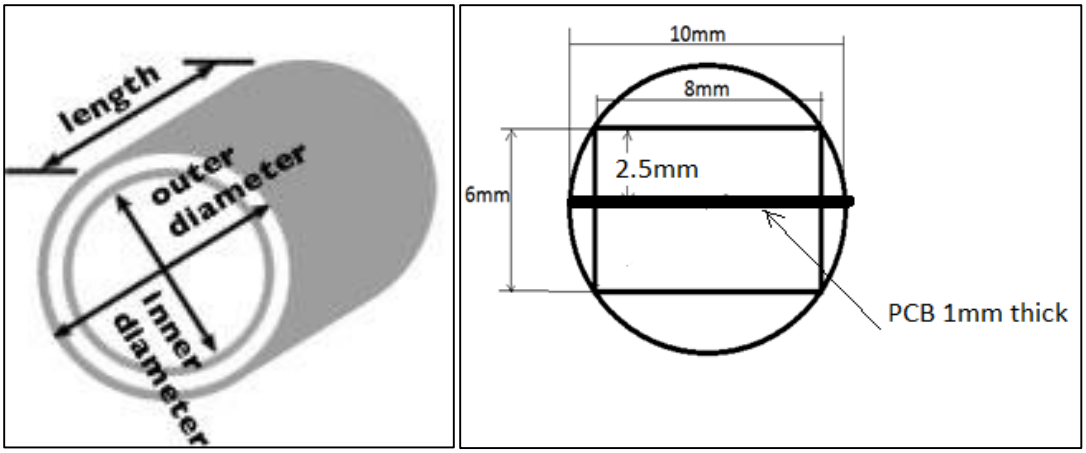


**Figure 68. Shell dimensions (left) and usable space (right).**

Communication among chips is a key part of the DataLogger. Parallel communication is faster but uses more wires/connections so it cannot fit the very small design space. When selecting the components researchers considered the communication issue with the intent that all three chips should have the same serial interface to make the connection simple and communication straightforward. All three main chips selected (Microcontroller PIC12VF1840, 3-Axis Accelerometer LIS331HH and Serial Flash Memory chip SST25VF064C) have an SPI (serial peripheral interface) bus. SPI is an synchronous serial data link, a de facto standard, named by Motorola, that operates in full duplex mode. Devices communicate in master/slave mode where the master device initiates the data frame. Multiple slave devices are allowed with individual slave select lines. SPI bus specifies four logic signals:

1. SCK : Serial Clock (output from master).
2. SDI : Master Data Output/ Slave Data Input (output from master).
3. SDO : Master Data Input/ Slave Data Output (output from slave).
4. CS : Slave Select (active low, output from master).

The MCU (PIOF12VF1840) has eight pins: two pins for power supply (Vcc and Ground) and six pins for IO (Input/Output). Six IO pins are used in the following manner: Three pins (SCK ,SDI and SDO) for the SPI bus, one pin for acceleration data ready (interrupt) and two pins (CS1 and CS2) for slave chip/device selection/enable.

In the DataLogger, the MCU (PIOF12VF1840) is configured as the SPI master, with the LIS331 and the flash memory chip as SPI slaves, and CS1 and CS2 are configured as chip selections respectively for LIS331 and SST25VF064C. Figure 69 shows the datalogger configuration.

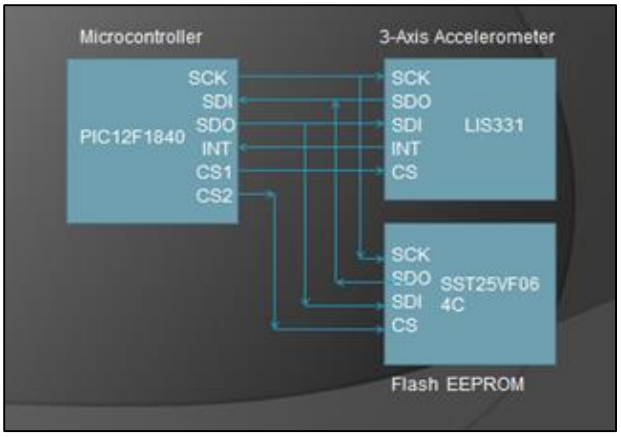


**Figure 69. DataLogger configuration.**

Figure 70 shows the designed circuit schematic of the DataLogger. The DataLogger has been designed and implemented to be as simple and small as possible by choosing small body chips, battery and other components (two capacitors, 10uF and 0.1uF). The final design version contains only three chips, one lithium battery (CR1025), and two capacitors.

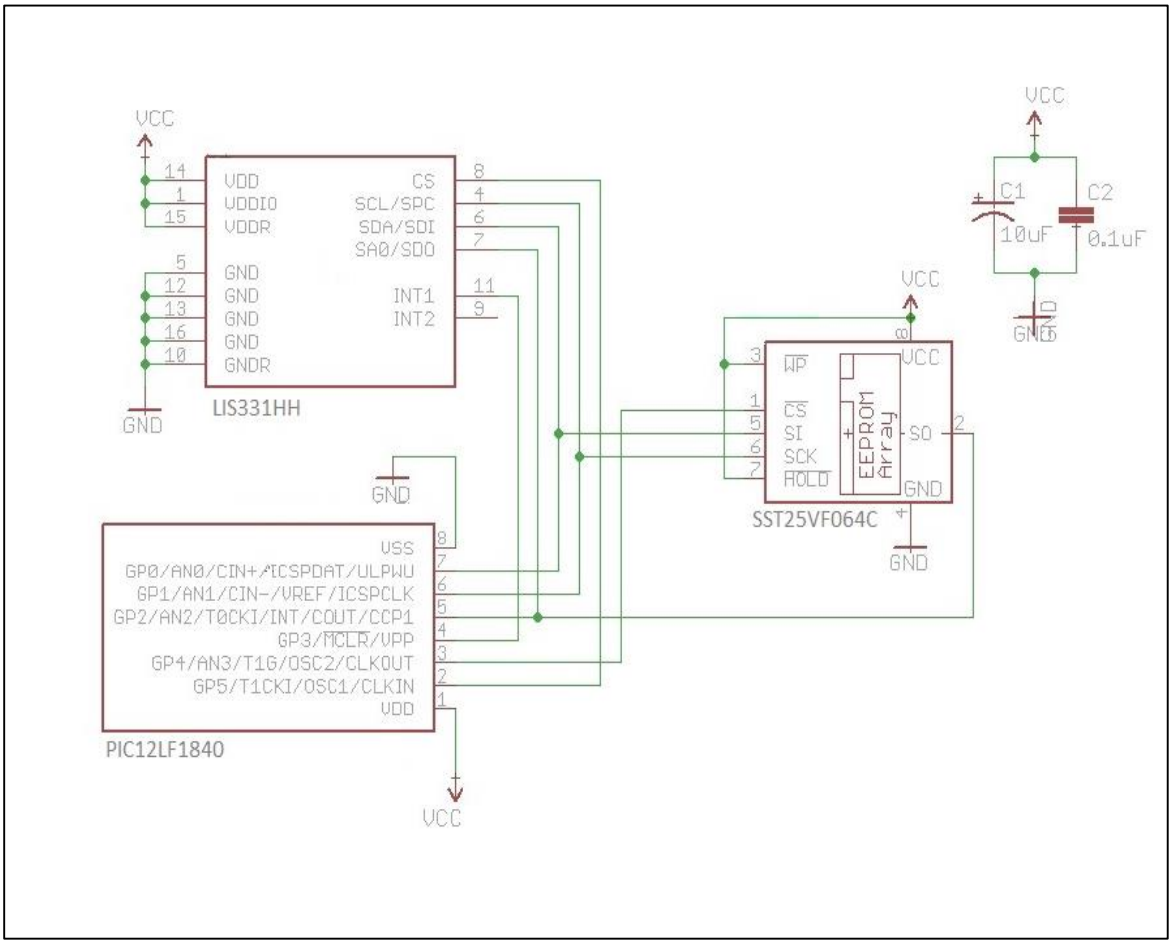


**Figure 70. DataLogger circuit schematic.**

Before fabricating production DataLoggers, it was necessary to test the designed Data-Logger to see if it worked as well expected. A LIS331HH breakout, a PIC12LF1840, SST25VF064C chips and battery, a solder station and tools to build a few prototype DataLoggers by hand soldering were acquired**.** The LIS331HH breakout comes with two capacitors needed by the DataLogger, so the LIS331 and the small two capacitors did not need to be soldered by hand. Figure 71 shows the LIS331 breakout. As its width was greater than 10 mm, researchers used sandpaper to sand off about 1.8 mm on the left and about 1 mm on the right to make it a little narrower than 10 mm.

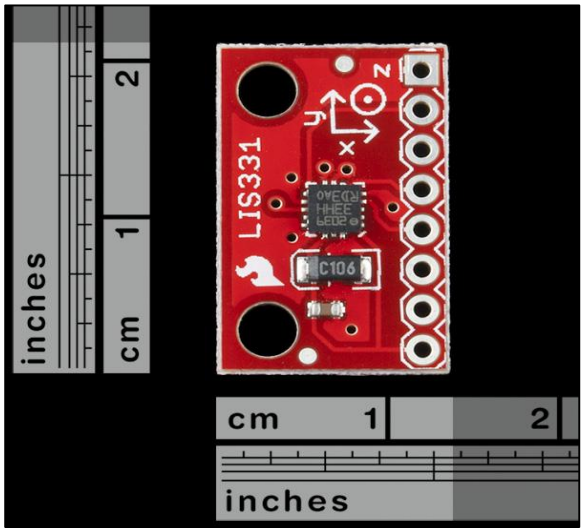


**Figure 71. LIS331 breakout board and dimensions.**

The PIC12LF1840 and SST25VF064C were soldered onto a prototype PCB with dimensions of 20 mm L x 10 mm W and connected it to the LIS331 back to back with connecting wires according to the schematic shown in Figure 70. Figure 72 shows the prototype built with the LIS331HH breakout and PIC12F1840 and the SST25VF64C chips inside a piece of shell with inner diameter 10 mm and length 25 mm.


**Figure 72. The prototype inside a size representative shell (20 mm H x 10 mm D).**

### 1.2.4 Software Development for the DataLogger

After the circuit was designed and built on a prototype PCB board, software was designed and implemented to make it work for the specific application. The software configures the DataLogger, measures and records the acceleration, and analyzes the recorded data, ultimately computing the path or position by twice integrating the recorded accelerations. The software for the DataLogger consists of two parts:

1. Control software: written into program memory inside the MCU of the DataLogger, and runs on the DataLogger to configure the DataLogger, measure, and record accelerations until the SST25VF064C is full or powered off.
2. Data processing software: runs on a workstation or laptop PC to process recorded data and compute the path/position by integrating the recorded accelerations.

The software development platform consisted of:

1. DELL T7500 Work Station with Windows 7 Professional
2. Microchip's MPLAB X IDE for writing and editing C program
3. MPLAB XC compiler for compiling the C program into binary codes of PIC12F1840
4. Microchip's Real ICE for programing the binary codes into the program memory of PIC12F1840
5. Saleae Logic analyzer for recording, viewing, and measuring digital signals.
6. Java Development Kit for developing data processing codes
7. SF600 SPI flash IC programmer and DediProg software for reading the data from the flash memory chip SST25VF064C.

Items 2–7 were installed on or connected to a DELL T7500 Work with Window 7 Professional as illustrated in Figure 73.

MPLAB® X IDE is a software program that runs on a PC to develop applications for Microchip microcontrollers and digital signal controllers. It is called an integrated development environment (IDE), because it provides a single integrated environment to develop code for embedded microcontrollers. The C programming language was chosen to develop the program for the PIC12F1840 instead of Assembly because C is a higher level language than Assembly. Both languages need to know details of the microcontroller, sensor and SST25VF64C chips, but C can handle pages and math operations easily; in addition, C codes are easy to read and maintain by humans. C code's efficiency is adequate for this project.

MPLAB XC (C language for Microchip MCUs ) allows users to code and control Microchip's MCUs and provides a comprehensive solution for a project's development software needs. The MPLAB® XC compiler supports all 8-, 16- and 32- bit PIC MCUs and dsPIC® DSCs, integrating with MPLAB® X IDE to provide a full graphical user interface.
Figure 74 shows a GUI of MPLAB X IDE integrated with XC8.

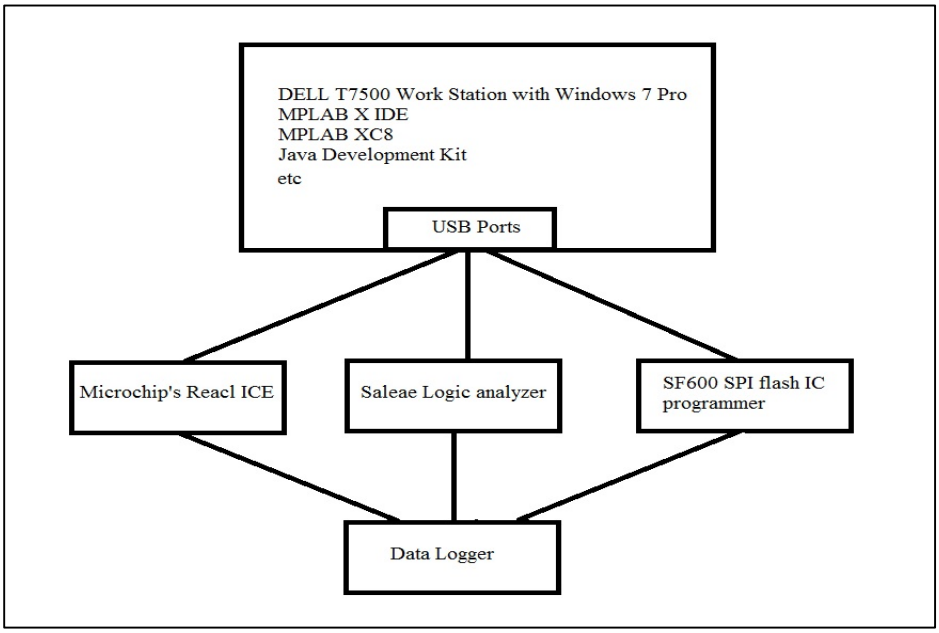


**Figure 73. DataLogger development platform.**

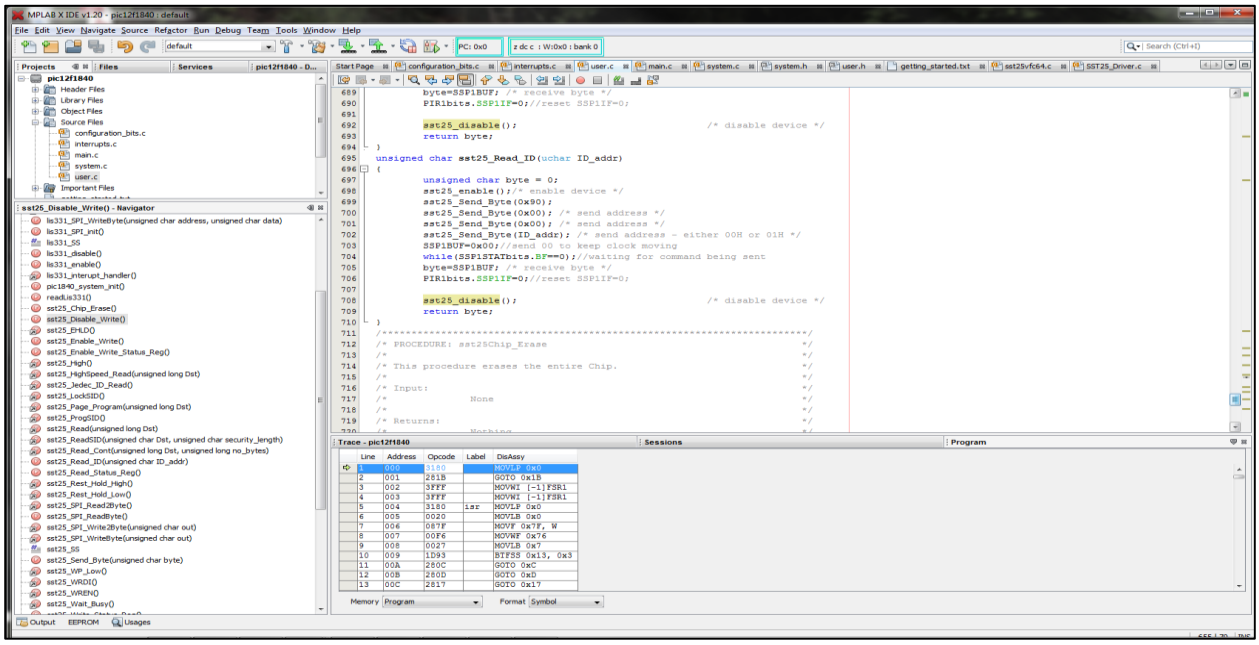

**Figure 74. GUI image of MPLAB X IDE integrated with SC8.**

Microchip's Real ICE is a modern emulator that supports hardware and software development for selected Microchip PIC® microcontrollers (MCUs) with programming and debug functions. Real ICE must connect to a computer that runs MPLAB® X IDE to work properly. Figure 75 shows Microchip's Real ICE logic analyzer and test breadboard.

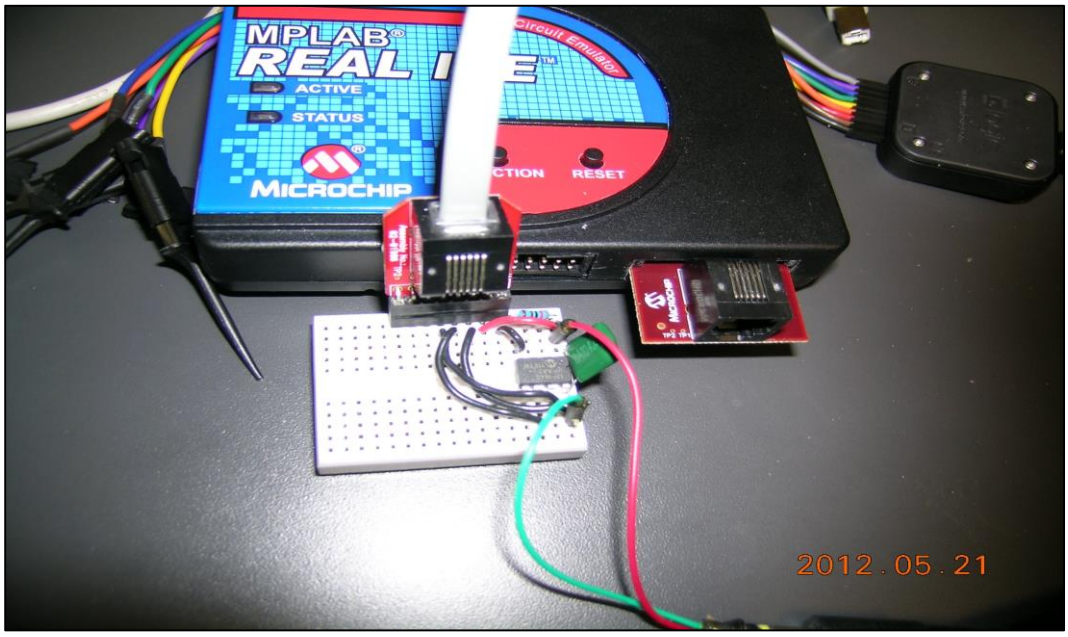


**Figure 75. Microchip's Real ICE, logic analyzer (right) and test breadboard.**

The C program can be written and edited directly in the MPLAB IDE window, compiled, and programmed into the programmable memory of a configured and connected Microchip's MCU. For this project, PIC12F1840 was used through Real ICE.

A Saleae Logic8 logic analyzer is used to record, view, and measure digital signals. Logic8 also currently has 17 different protocol analyzers including serial, I2C, SPI, CAN and many more. Logic8 can sample each of its eight channels at speeds up to 24MHz and can record up to 10 billion samples.

The SF600 is a high speed "in System Programming" programmer for updating the SPI Flash soldered on board (in-circuit programming) or in the socket adaptor (offline programming). The programmer is easily controlled by the computer's DediProg Software through the USB bus, which offers friendly interface and powerful features to users. In this project, it is used to read the data out from the SST25VF064C chip (SPI flash memory) on the DataLogger (Figure 76).


**Figure 76. SF600 serial flash memory programmer.**

The Java Development Kit (JDK) is a free Oracle product that can be downloaded from the Oracle website, and was used for this project to develop the data processing software. The Dell T7500 workstation has two Intel E5606 processors, 12GB memory and a 2TB hard drive. There are two USB ports on the front panel, and six on the back panel. (three USB ports were required during development) The workstation ran Windows 7 64-bit professional.

The control software was developed with Microchip XC then compiled with Microchip's XC compiler into executable codes for PIC12F1840 and programmed into MCU ( PIC12F1840) chip's program memory using REAL ICE device. The control software development followed the outline below:

1. Write and/or edit C program in MPLAB X IDE window
2. Compile C program into binary codes
3. Send binary codes to REAL ICE and burn them into program memory of MCU
4. Plug/solder MCU into prototype and power on
5. Logic analyzer record and display the all 6-pin signals
6. See if the DataLogger function properly or not based on the displayed signals
7. If yes go to next; else go back to 1.
8. Stop

The required software functions of the software for PIC12LF1840 are:

1. Configure the PIC12F1840's SPI bus at pin 5,6 and 7, interrupt function at pin 4, SPI slave selection pin: pin 1 for LIS331HH and pin 2 for SST25VF64C and set the clock rate at 500kHZ;
2. Configure LIS331HH scale rang as {-6g, 6g}, sampling rate as 100/S and data ready signal output at "int1" pin;
3. Enable SST25VF64C page program/write;
4. Wait for the data ready signal from LIS331HH;.
5. If the data are ready, PIC12LF1840 will respond and start reading 6-byte acceleration data from the LIS331HH;
6. Write data into the SST25VF64C and return to 4).

Figure 77 shows the entire flowchart for software operations at the chip level.

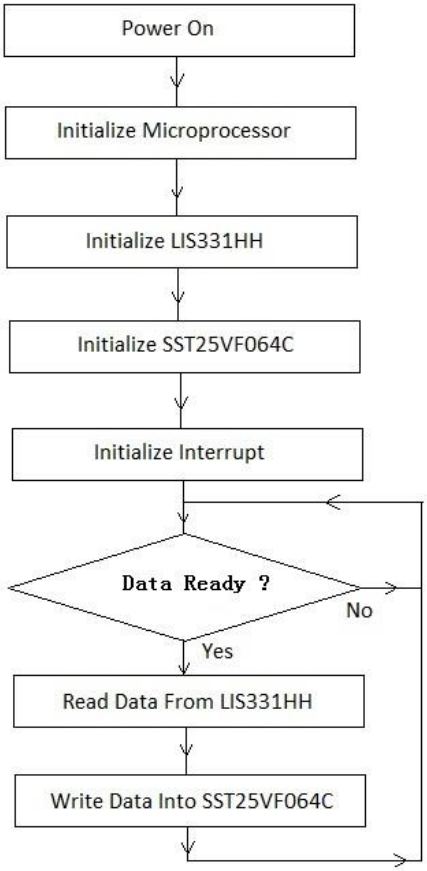


**Figure 77. Software flowchart.**

Power consumption is an important issue since a battery cell powers the DataLogger. The PIC12LF1840 8-bit microcontroller uses active currents of less than *50 μA/MHz*, which means that the lower the clock rate is set, the less power is consumed. To save power and make sure the DataLogger works properly with enough power during the required time period, the clock rate was set as low as possible. The clock rate of PIC12F1840 was set to 0.5MHZ and the SPI clock rate was set to 125KHz, so the SPI bandwidth is 125K bits/8→ about 10.5K bytes.
The following analysis shows the clock rate is sufficient for DataLogger to work properly.

The sampling rate of LIS331HH is set as 100 samples per second; each time step, 6 bytes of data are generated (two bytes for each axis), fewer than 10 ms are available for the interrupt service routine to read, write data and return. In total, 600 bytes data must be read from LIS331 and written into flash memory per second, which means a total of 1200 bytes on the SPI bus for read and write operations during one second. 1200 Bytes is significantly less than 10.5k, even when doubled overhead plus other delays caused by other operations is considered, so the 10.5kB bandwidth is adequate. Thus, 10 ms is more than enough for the MCU to read and write data.

Bench tests showed that the interrupt service routine takes about 4 ms in total to complete its task after a data ready signal/interrupt appears, and then it waits about 6 ms for next data ready signal/interrupt. Recorded data in the memory chip (SST25VF064C) is read out using a serial flash memory programmer SF600, which connects to a PC with USB cable and reads and saves data in binary format on the PC for further data processing.

Based upon the foregoing discussion, 600 bytes per second (64Mb/8)/600→13333 seconds →3.7 hours of data can be stored in the SST25VF64C. In fact, the SST25VF064C is divided into 256-byte pages and the continuous writing is limited to one page, which means the interrupt service routine must write 6 bytes on one page and not break the boundary to the next page every 10 ms. Dividing 256 by 6 gives 42; the remainder 4 bytes are left unchanged for convenient coding and quick operation. In the interrupt service routine, if the page address is 252 then it will add 4 and force it to jump to the beginning (0) of next page.

The PIC12LF1840 has a MSSP model with configurable SPI/I2C bus. The MSSP module can operate in one of two modes:

- Serial Peripheral Interface (SPI)
- Inter-Integrated Circuit (I2C™)

First it is necessary to configure the MSSP to work as a SPI. Then the SPI modes for LIS331 and for SST25VF64C must be configured because the SPI has four work modes (mode 0–mode 4) based on the combinations of polarity and phases of SPI clock and data signals. The LIS331 is designed to work with SPI mode 3 and the SST25VF064C is designed to work with

SPI mode 0, respectively, by their manufacturers. To be able to communicate with a slave chip properly, the MCU must first configure or set its SPI to work at the same mode as the slave chip.

In the DataLogger the code first configures the SPI work in mode 3 to communicate with LIS331 and then switch to mode 0 when needing to communicate with the SST25VF64C, then switch back to mode 3 for the next LIS331 operation. More details can be found in the following C functions:

**PIC12F1840 initiation function:**

```
    void pic1840_system_init(){
   ANSELA=0x00; //all pins set as Digital  I/O pins
   SSP1IE=0;//forbid interrupt
   PIR1bits.SSP1IF=0;//PIR1 bit,  SSP1IE=0;
   INTCON=0;//all 0 then setup one by one
  INTCONbits.GIE=0;// Global interrupt disabled first, will set after system init
   SSP1CON1bits.SSPEN=1;//Enable SPI
   SSP1CON1bits.SSPM=0b0000;//clock =Fosc/4
   SSP1STAT=0x00;
     //SST25 need SPI  mode 0 and LIS331 needs SPI  mode 3,first set SPI mode 3 for  LIS331HH
//switching to SPI mode 0 and back in SST25 codes
 SSP1CON1bits.CKP=1;
 SSP1STATbits.CKE=0;
 SSP1STATbits.SMP=0;//sampling at middle
   //bit5--bit0  -->TRISA5---TRISA0
 TRISA=0b00001100;// SDO/RA0 and SPC/SCK/RA1,RA4 and RA5 are outputs all others as inputs
WPUA = 1; //All RAx are weak pull up }
void interrupt_init(void){
   //set RA3 as Lis331's interrupt input pin
 IOCAP3 = 1; //allow positive edge interrupt
  INTCONbits.IOCIE = 1; //enable the Interrupt On Change
  INTCONbits.PEIE = 1; //enable peripheral  device interrupt
  INTCONbits.GIE = 1; // global interrupt enabled
  IOCAF3 = 0; //clear corresponding interrupt flag;
  RA3=0;}
```

The LIS331 has internal low–and high-pass filters. The low-pass filter is fixed with the sampling rate configured on fly. Offset can be eliminated by enabling the built-in high pass filter. To avoid gravity drift, researchers configured the LIS331 sampling rate as 100Hz with default low–pass filter cut-off frequency 74Hz (non-configurable) and the configured high-pass filter cut-off frequency as 2Hz. Therefore, the bandwidth is 2Hz—74Hz. The final bandwidth will be decided based on data analysis from the field-testing.

### 1.2.5 Software Testing

After the components were hand-soldered together and the software was developed, the compiled codes were programed into MCU(PIC12F1840) with Real ICE. The DataLogger was initiated by attaching a CR1025 battery on its Vcc and ground. A Saleae Logic analyzer was

used to record and display the signals. Figure 78 demonstrates that the DataLogger ran very well, which means the software development was successful, as is the DataLogger hardware. From top to bottom, the signals in Figure 78 are:

1. LIS331HH enable,
2. LIS331HH data ready (interrupt signal),
3. PIC12F1840 SPI data output,
4. PIC12F1840 SPI clock,
5. PIC12F1840 SPI data input,
6. SST25VF64C SPI serial flash memory chip selection.

The sampling rate is 100 times/S, i.e. every 0.01s the LIS331 generates a "data ready" signal and the PIC12F1840 responds to the interrupt and enters the interrupt service subroutine: read data and write into memory. The interrupt signal will reset after reading the 6 bytes acceleration data and set again once the next data are ready (in 0.01s).

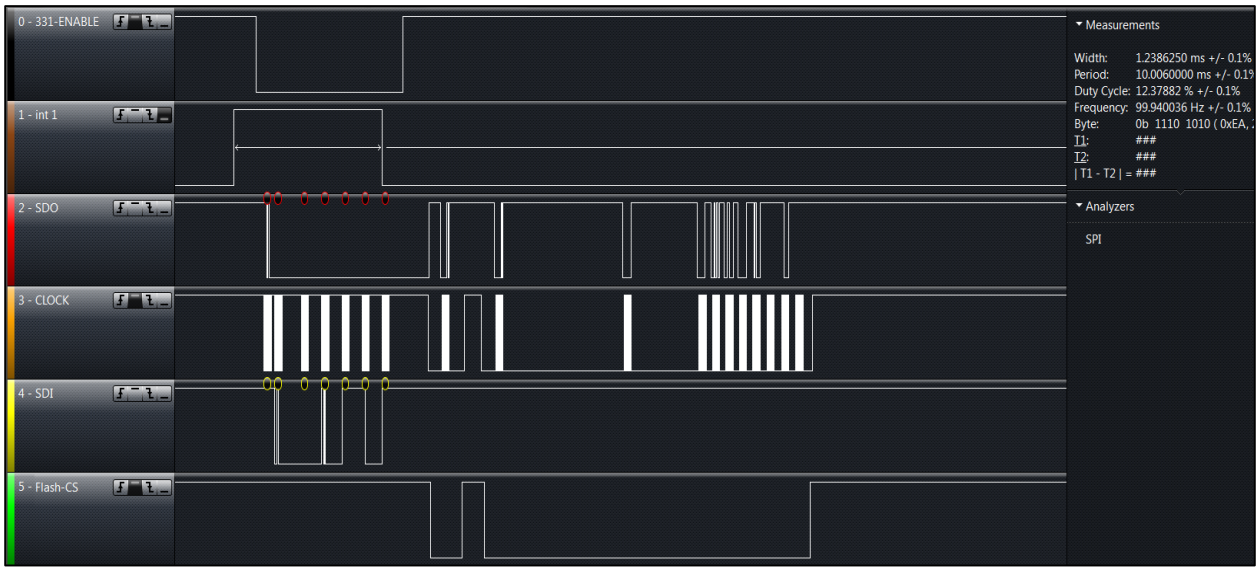


**Figure 78. DataLogger waveform analysis. All waveforms reported as predicted.**

### 1.2.6 Data Processing Software

The data processing software was developed using Java, which transfers the binary data file into a text file on the PC and then the data are calibrated, filtered and integrated twice to get the position in X, Y and Z directions. The path that the DataLogger travels can be visualized on the screen of a PC. Recorded raw data in SPI serial memory are in gravity units, which are read

out using a SF600 SPI memory programmer with clip and stored into a binary file on a PC compatible computer. After comparing many calibration methods and filters, it was found that the following data method generated better results for this application:

1. Transform the recoded raw data from binary to decimal.
2. Transfer data from gravity unit to acceleration ($m/s^2$)
3. Calibrate the bias.
4. Filter the data (Moving-Average –Filter and Low-Pass Filter)
5. Integrate twice to compute velocity and then position.

Java was used to develop the data processing software, which implemented the outlined method and is used to process test data. Before starting each test each DataLogger rested for about one minute, recording 3600 samples (60 seconds × 100 samples/second). The rest period data was averaged and used to compute the bias in the Xb, Yb and Zb axes subtracting Xb, Yb,and Zb respectively, from all the samples. The next step was to filter out the noise and finally to compute velocity and distance in X, Y and Z directions. Figure 79 shows the data processing procedure.

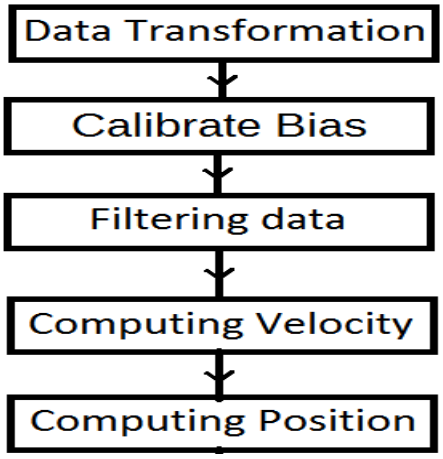


**Figure 79. Data processing flowchart.**

Each 256-byte page of SSt25VF064 only used 252 bytes, so the last 4 bytes have nothing written to them. When reading binary file, if the page address is 252 then it will add 4 to it and force it to jump to the beginning (0) of next page to read. Each time it reads 6 bytes and merges them into three 16-bit accelerations for the X, Y and Z axes respectively. The configured scale of LIS331HH in the DataLogger is {-6G, 6G}. The LIS331HH provides 16-bit data output, i.e. the raw data is assigned a 16-bit integer in the gravity unit, the lowest 4 bits of the data are 0 × 0000. First, the raw data must be scaled into the configured range {-6g,+6g }. 16-bit data has 65536 values (though the lowest 4 bits are always zero), so the scale should be 6-(-6)/65536 = 0.00018310546875.; i.e., one LSB = 0.00018310546875g. Because, on average, g = 9.81$m/s^2$,

we have one LSB=0.00018310546875 × 9.81= 0.0017962646484375 m/s$^2$. Raw data (assigned an integer in G units) can be transferred to an assigned decimal float in m/s$^2$ units with the following formula:

**m/s$^2$ = Gravity* 12/(2$^{16}$) *Raw = 0.0017962646484375 *Raw**

where "Raw" is raw acceleration data in the 16-bit assigned binary integer. The C code is presented below:

```
"Gravity" is 9.81 m/s^2 .
Below are codes for reading, merging sacling  and
For (int  i=0,j=0;i<Raw_Data_Length-6;i=i+6,j++){
//convert raw data to "signed short" and
//store into double array in double format which is easier for later processing
//merge two bytes into a test value(2'complement in short format)
 // identify if there is no data written into it then stop converting data!
  //normally the first byte's (Xl byte ) lower digits  of each sampled data(6 bytes Xl Xh Yl
Yh Zl Zh) must be zero (0000)
        //if it is F (1111) that means no valid data!
        if((aInput[i]& 0x0f)==0x0f){break;}
        totalData++;
           //X --acceleration
       leftByte=aInput[i]& 0xff;
        rightByte=aInput[i+1] & 0xff;
        value=(short)(rightByte<<8 | leftByte<<0);
          //value=value-
         xyzresult[j][0]= ((double) value)*MeterSecond2_6G;
         xyzshort[j][0]= value;
        //Y --Acceleration
         leftByte=aInput[i+2]& 0xff;
        rightByte=aInput[i+3] & 0xff;
        value=(short)(rightByte<<8 | leftByte<<0);
         xyzresult[j][1]= ((double) value)*MeterSecond2_6G;
        xyzshort[j][1]= value;
       //Z --Acceleration
        leftByte=aInput[i+4]& 0xff;
        rightByte=aInput[i+5] & 0xff;
        value=(short)(rightByte<<8 | leftByte<<0);
           xyzresult[j][2]= ((double) value)*MeterSecond2_6G;
           xyzshort[j][2]= value;
    }
```

Any bias in the accelerometer output will cause a shift in the measured accelerations from its true values. Biases are differences between an accelerometer's expected output and its measured output, which show up consistently every time a new measurement is taken. Any of these errors that are repeatable can be calculated during calibration, so that during actual end-use the measurements made by the sensor can be compensated in real-time to digitally remove any errors. Calibration can enhance performance by improving the overall accuracy of the underlying

accelerometers. Most low-cost MEMS sensors available on the market fall into a performance category known as *automotive* grade sensors. The use of the term *automotive* grade in this context does not necessarily imply that the sensor meets specific performance standards specific to the automotive industry. The origin of the term *automotive* grade when discussing MEMS sensor performance likely has to do with the fact that the automotive industry was one of the first to utilize MEMS inertial sensors in large volume. This performance grade is also sometimes referred to as *consumer* grade. LIS331 is one of *automotive/consumer* grade sensors. Acceleration bias-caused error in horizontal position can be calculated by:

**HPe = 0.5*Bias*T*T**

Table 17 shows the difference between the errors caused specifically by accelerometer bias after calibration for both industrial and automotive grade sensors.

**Table 17. Error Differences for Sensors**

| | Accelerometer Bias Error | Horizontal Position Error | | | |
|---|---|---|---|---|---|
| Grade | [mg] | 1 sec | 5 sec | 10 sec | 20 sec |
| Industrial | 3 | 15 mm | 370 mm | 1.5 m | 5.9 m |
| Automotive | 125 | 700 mm | 18 m | 70 m | 280 m |

According to the datasheet of the LIS331, its bias (TyOff—Typical zero-g level offset accuracy) error is about +/- 75 mg/s typically [page 9], which means its horizontal position error in one seconds and three seconds would be:

- If T = 1 then HPe = 0.5*70mg*1*1=0.5*0.070*9.8=0.343 meter
- If T = 3 then HPe = 0.353*3*3=3.087 meter

Lab tests showed the LIS331's output is in the range of {-70mg, 70mg} when the DataLogger is at rest; that means the output shows the at-rest DataLogger is moving. The errors caused mainly by bias are:

1. TyOff ( Typical zero-*g* level offset accuracy ±70 m*g)*
2. TCOff (Zero-*g* level change vs Temperature ±0.4 m*g*/°C).

To achieve better performance it was necessary to remove the bias from output before integrating to get velocity/position.

The calibration process is as follows:

1. Power on DataLogger,
2. Leave it at rest for about a minute,
3. Power off DataLogger,

4. Offload data into workstation,
5. Calculate the average of all data for each axis,
6. Store these values as bias and let real acceleration = (rawdata-bias)

For one DataLogger prototype, the prototype's battery was turned on and left at rest for about 50 minutes; the raw data were then transferred to the workstation (Figures 80–81).

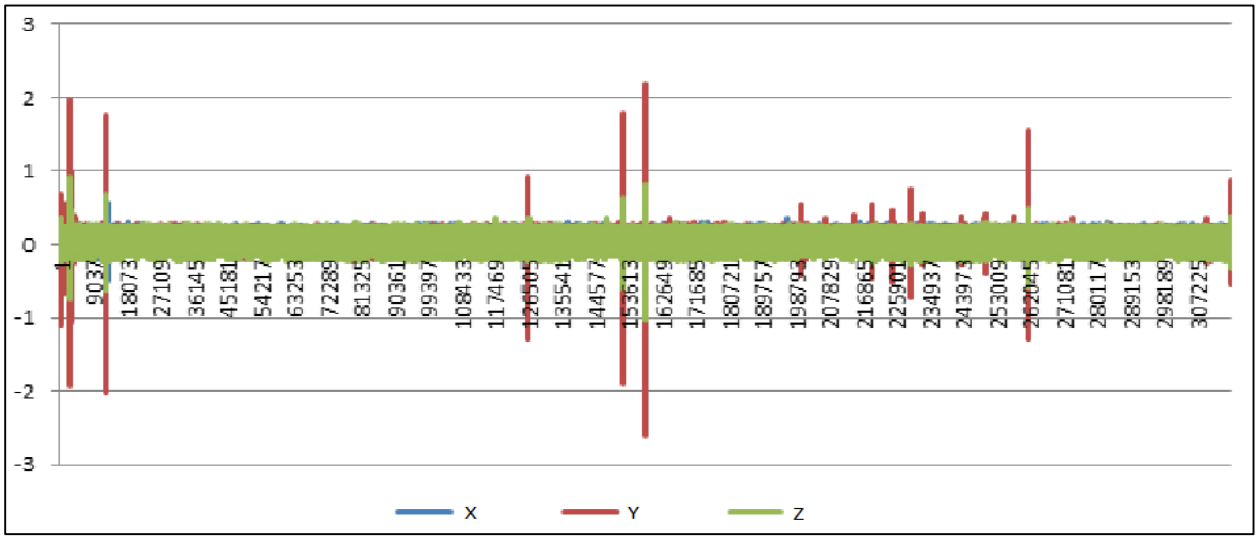


**Figure 80. Raw data (x-y-z) when the accelerometer is at rest.**

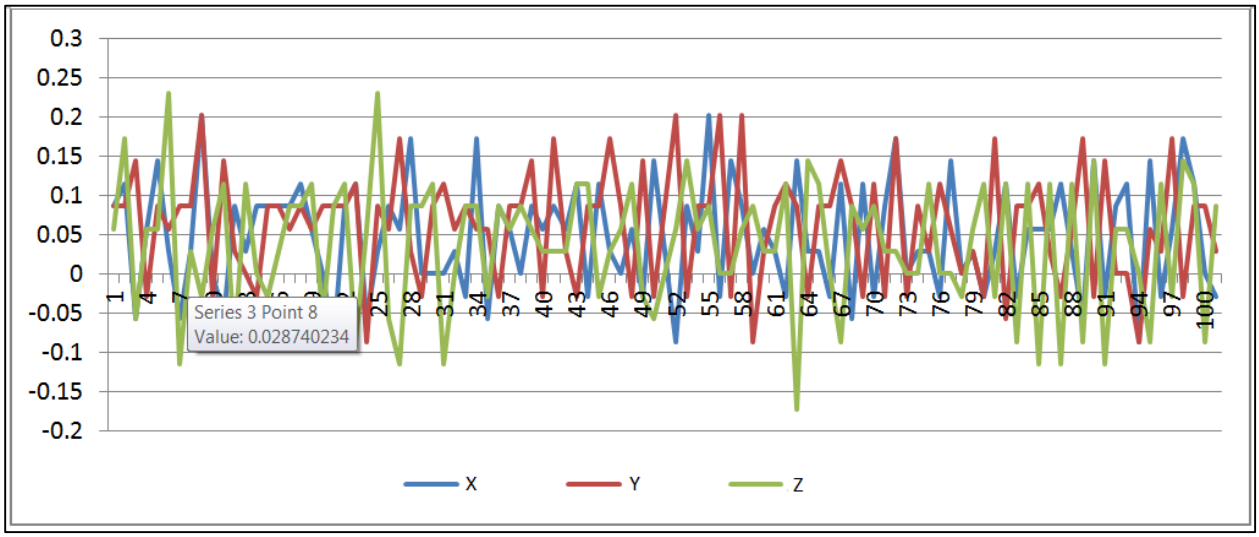


**Figure 81. Zoomed view of raw data when LIS331 is at rest.**

The accelerations in x, y and z directions are between -0.15 mg –+0.25 mg biased and can be calibrated using the formula :

**Bias X = (RawX(1)+…..+RawX (N))/N**

The same process is also applied for Y and Z axes:

BiasX = 0.04506964516908977 = 45.0 mm/second^2
BiasY = 0.05384817218743698 = 53.8mm/second^2
BiasZ = 0.03965850777160196 = 39.7mm/second^2

These biases can then be used to calibrate the data using the following relationship:

**CalibratedData= raw data-bias**

The mean of the calibrated data is the raw data shift from the Bias to 0.0. Figure 82 shows the calibration results from the X axis. Its mean average is reduced from 45 to 0. But as Figure 82 shows, the noise, while reduced, is still there.

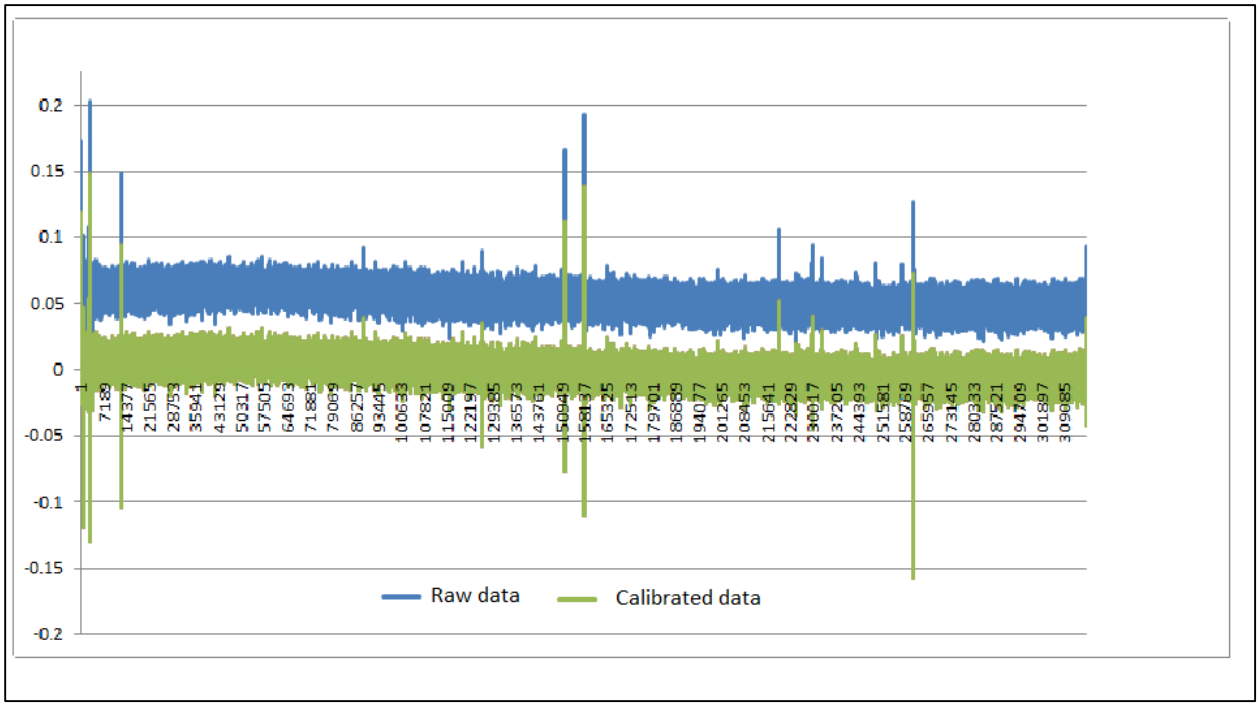


**Figure 82. Raw data and bias-calibrated data in the X axis.**

Temperature can also impact the readings. TCOff (Zero-*g* level change vs temperature) = (Max delta from 25 °C) = ±0.4 m*g*/°C . If the test environment temperature is 65°C, that will be 8 mg compensating for the errors caused by temperature, which usually requires a thermal sensor. Due to the limited space it is impossible to add a heat sink.

To minimize the effects of temperature change, the DataLogger is instead rested for 30 seconds and data is recorded just after powering on and prior to placing it into the test environment. The 30 seconds data at rest is used to calibrate LIS331 and reduce the bias, which includes TyOff and TCOff .

### 1.2.6 Data Filtering

As shown in Figure 82, though the filter inside LIS331 was enabled and biases were calibrated, the data still contained noise, so further steps were undertaken to reduce the noise. To get rid of noise, filters must be applied to the data. There are many kinds of filters, from simple ones to complicated ones. Two filters that improved results:

1. Moving average filter:

$$\bar{x}_k = \frac{1}{n}\sum_{i=k-n+1}^{k} x_i$$

2.Low-pass filter

$$\bar{x}_k = \alpha \bar{x}_{k-1} + (1-\alpha)x_k$$

Both the moving average filter and the first–order low-pass filter were applied to the calibrated data one after another for better effects. Figures 83–84 show raw data, calibrated data and filtered data. After calibration and filtering, the data became smooth and the noise values fell in a range of {-5mg/s$^{\wedge 2}$ , +10mg/s$^{\wedge 2}$}, which is much smaller than in the raw data.

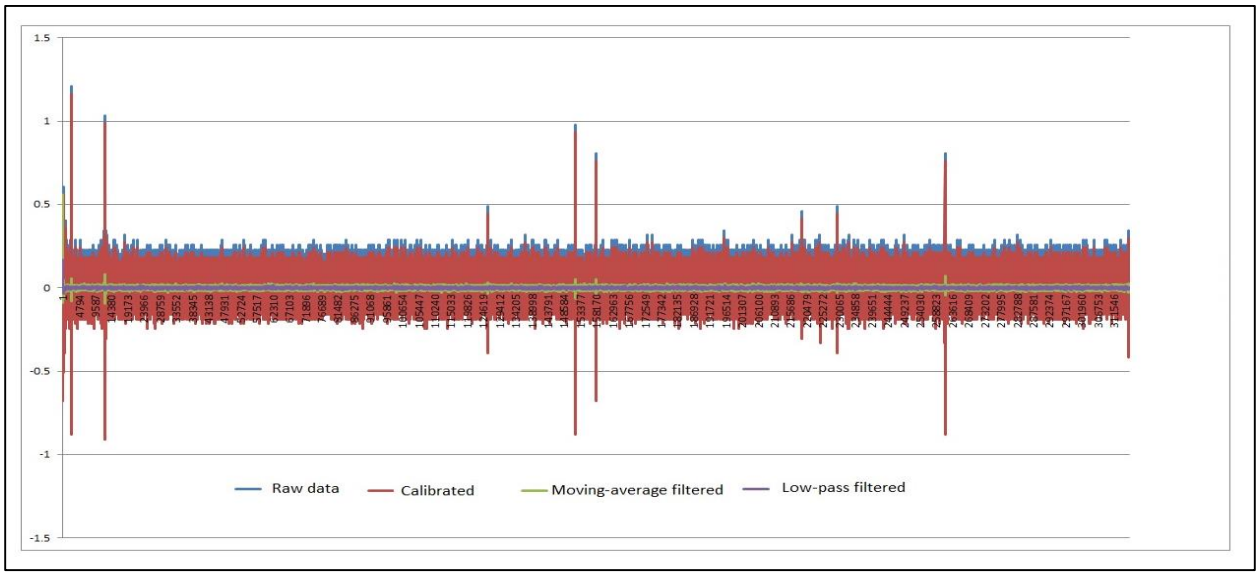


**Figure 83. Raw data, calibration, moving-average filter, low-pass filter.**

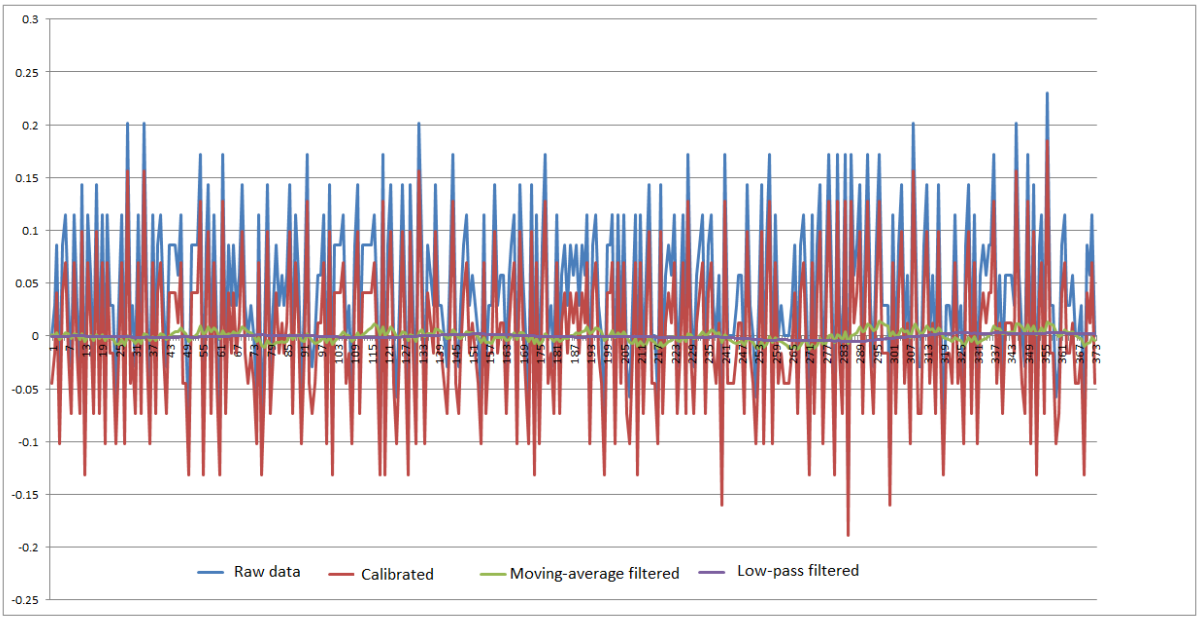


**Figure 84. Zoomed view of raw data, calibrated data, and filtered data from Figure 83.**

After the transformation and calibration, a low-pass/Kalman filter was applied to the transferred data, then the filtered acceleration data was integrated once to get velocity and again to get the distance (path/position). The Java code used is as follows:

```
for(i=0;i<Filtered_Data_Length-1;i++)
{//First integration---->computing
//Velocity: 0 1 2 indicate x  y  z axis
  //delta t=1/100 = 0.01 second
V[i+1][0]=V[i][0]+(A[i][0]+A[i+1][0])  0.5*Delta_T;
V[i+1][1]=V[i][1]+(A[i][1]+A[i+1][1]) *0.5*Delta_T;
V[i+1][2]=V[i][2]+(A[i][2]+A[i+1][2]) *0.5*Delta_T;
    //Second  integration---->computing //position: 0 1 2 indicate x  y  z axis
P[i+1][0]=P[i][0]+(V[i][0]+V[i+1][0])  *0.5*Delta_T;
P[i+1][1]=P[i][1]+(V[i][1]+V[i+1][1])  *0.5*Delta_T;
P[i+1][2]=P[i][2]+(V[i][2]+V[i+1][2])*0.5*Delta_T; }
```

### 1.2.7 Bench Scale Lab Tests

To validate and improve the design of the DataLogger and the data processing methods, 22 laboratory tests were performed. Early on the velocity and distance drifted too much, due to the bias of the sensor itself. The data analysis showed that the shorter the time that the data recorded, the less the velocity and distance drift. One way to reduce bias effects is to record data only when the actual test starts (the DataLogger enter the horizontal portion of the lateral). Recording data in this way can also save flash memory. But, due to the limited program memory, the size of the MCU and the difficulty in identifying the true start point in real time, researchers

chose another method. By offloading the recorded data into the work station (PC) transforming and filtering them, then using Excel's plot function to plot the wave, it is possible to identify the start point and end point by time and acceleration change. Then the appropriate section of data can be copied and saved into a text file. Finally, integration can be used to compute the velocities and distances (Figure 85).

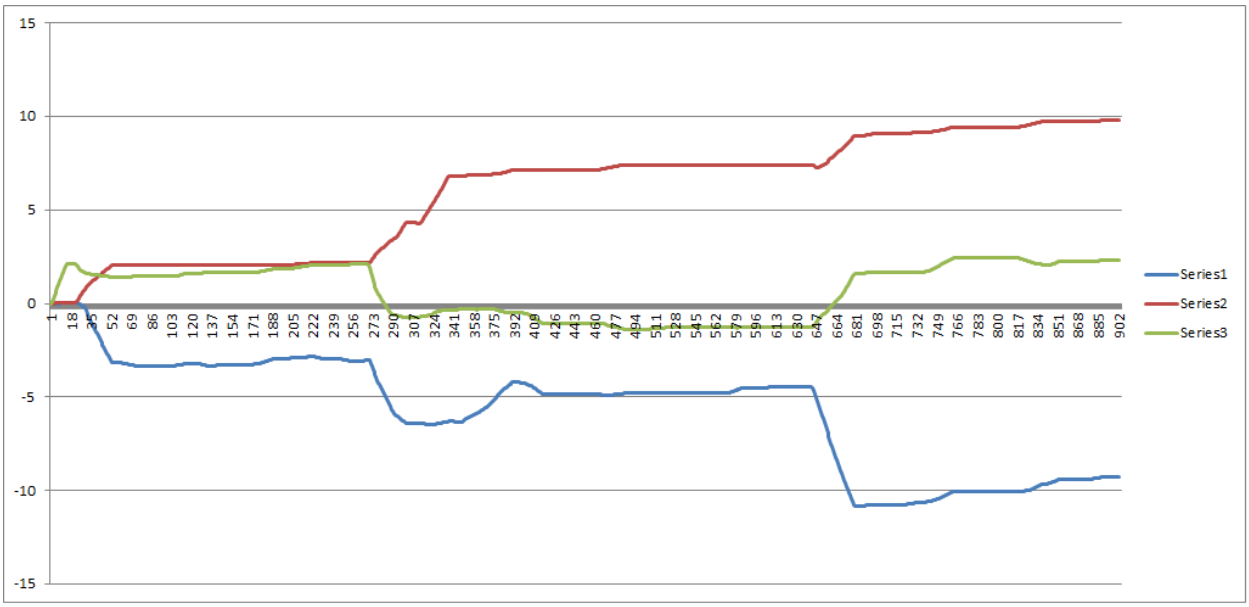


**Figure 85. Computed distance by axis for a successful bench scale test.**

### 1.2.8 Datalogger Development Summary

After successful bench scale development the sensors were ready for field-testing and refinements of the methodology and measurement and subsequent calculation of the emplaced short-radius laterals.

## 1.3 Drilling Technology

This project, as originally envisioned, was to field test radial drilling, and the original drilling partner was Well Enhancement Services. After the project was funded, Well Enhancement Services was acquired by Radial Drilling Services Inc. After approximately one year of work it became apparent that an agreement could not be made and the project sought a new drilling partner. Jet Drill approached the project at a RPSEA Onshore Production meeting and offered a new technology. Jet Drill had tested four different jetting heads and concluded that the technology had some systemic issues. They had then sought a purely mechanical alternative and that technology, the Viper Drill, was ready for field-testing. The project reconfigured with Jet

Drill as the new drilling partner, using their new system. This section describes both jet drilling and Viper Drill technologies.

### 1.3.1 History of Short Radius Lateral Drilling

The effort to mechanically drill out at literally 90° to the wellbore dates back nearly 100 years—basically to the dawn of the modern oil and gas industry. In fact, in the mid-twentieth century, one person who attempted the task declared it "not possible in actual practice". Given the difficulty of mechanically drilling out at right angles to wellbores, starting in the mid-90s, a wave of entrepreneurs proposed to create radial boreholes into the pay zone by means of a hose and jetting nozzle. These jetting systems were typically deployed by small coiled tubing units. Most of these systems employed some sort of downhole whipstock secured on the end of production tubing. The whipstock directs the tools toward the casing and formation and usually stays in place for the duration of the procedure. The attractiveness of the jetting systems stems from the fact that hoses are inherently flexible and should be able to easily transition around the tight radius of the whipstock. Many jetting companies advertised lateral distance of up to 300 ft and targeted well recompletion and infill replacement (Figure 86).

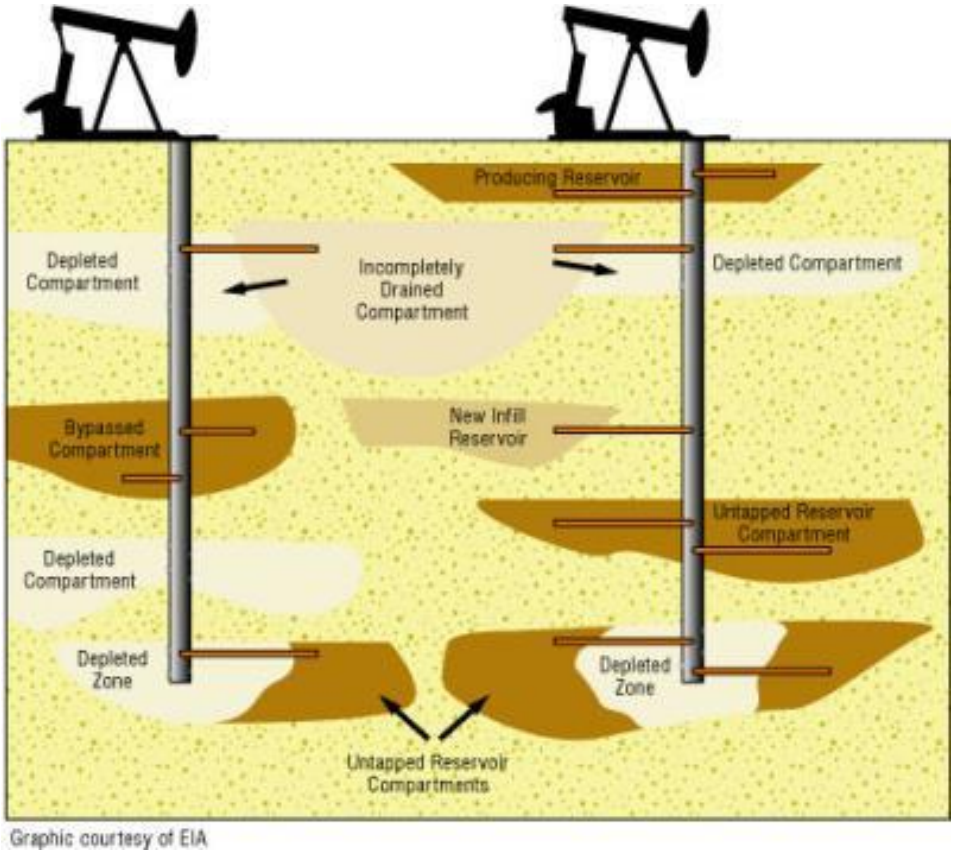


**Figure 86. Impact of short-radius laterals: target bypassed pay, infill compartments, and untapped portions of the reservoir.**

### 1.3.2 Jet Drilling technology

Jet drilling utilizes a casing drill and water jet deployed through a 1 in. coiled tubing unit. Water is pumped through the coiled tubing and is then pushed under pressure through micro jets on a cutting head. The jet tip and water supply hose are 0.5 in. in diameter; cutting jets on tip eat away at carbonate rock or carbonate cemented sandstones. Drive jets push the jet tip and pull the hose up to 300 ft away from the wellbore, helping to flush rock residue from the lateral. When the technology works, a jagged ~1-in. jetted lateral results in increased drainage. Since jetting systems are incapable of forming a hole through the metal casing, the first step typically involves running casing milling tools around the radius of the whipstock. These casing cutting tools are then retracted from the well and the jetting tools are affixed to the end of a hose and run down-hole. The nozzles used on these systems are typically adapted from the sewer cleaning industries, and some are stationary, while more advanced implementations rotate or create a swirling spray pattern. High-pressure fluid (typically weak acid, or fresh water + kcl) used in jetting systems is then pumped through the nozzle in an attempt to erode the rock.

Jetting systems have been prone to a number of shortcomings, however, and hence developed a spotty track-record with industry. For example:

1. Some vendors could not reliably cut a hole in the casing
2. Some systems allowed the jetting hose to collapse or fold over in the wellbore (Figure 87)
3. The flexible hose, ideal for transitioning around the whipstock, could potentially drift
4. In most systems, there was uncertainty of whether and how far the nozzle had actually jetted out.
5. The power available to forward-facing orifices was limited by the fact that most of the power supplied to the nozzle had to be directed to rear-facing jets in order to bias the nozzle forward (Newton's Third law)
6. Jetting systems had difficulty cutting moderate and harder formations, let alone chert and clasts.

Jet Drill had extensively tested jet drilling technology at bench and field scales and had been able, under ideal circumstances, to drill shallow wells with short tubing, high porosity sandstones, with no large clasts, and after attempting four different jet drill head technologies, were able to drill at most a 14 foot lateral, under ideal circumstances, and usually much shorter. In order to drill any formation at any depth they began development of the Viper Drill.

**Figure 87. Some jetting systems allowed the hose to become balled up above the whipstock, which can lead to a false sense of drilling rate and penetration.**

### 1.3.3 Viper Drill Technology

Viper Drill is a purely mechanical drilling system that uses a proprietary patented system of interlocking toothed segments that when combined create a flexible drilling string able to make a right turn in a specialized shoe installed in a wellbore (Figures 88–89). Viper Drill can be deployed on cased or open-hole completed wells, and uses a casing milling bit to form a hole in the casing; then the tubing is pulled and the viper drill is attached. The Viper Drill can drill out at 90° from 5.5 in. or larger casing, and at higher angles from smaller casing. This puts into play the majority of mature stripper wells in the USA. The Viper Drill then creates a hole in the pay zone by utilizing a rotating, mechanical drill bit on the end of the Viper Drill string (Figure 90). The drilling bit is either carbide or PDC, so it can cut very hard zones, including chert/clasts. The conduit used to provide lubricating fluid to the cutting head encased in a type of metal exo-skeleton whose metal cladding accomplishes several purposes including: protection of the stain-less steel hose from abrasion; assistance in assuring the cutting head drills straight, and transferal of weight on bit (WOB) to the drill head to cut the formation.

The Viper Drill can meet most of the claims of jet drilling, most importantly: improved communication between the payzone and wellbore; by-pass of near-wellbore damage, and provi-sion of a conduit to push chemicals/treatments into the zone. Additional potential applications include mitigation of water-coning, treatment of carbonate zones with HCL to create wormholes, orientation of laterals to preferentially intersect fracture planes, and in lieu of or as a precursor (e.g. to prevent screen-out) to certain frac jobs or where fraccing is under a moratorium. Figure 91 shows the potential of the Viper Drill system compared to traditional perfs.

**Figure 88. Viper Drill string being prepared for deployment. Flexibility is demonstrated by natural droop of the string under gravity.**

**Figure 89. Left, casing shoe; right, casing shoe open, showing casing cutter.**


**Figure 90. Left, Viper Drill cutting head. Right, resulting hole in a Berea sandstone core.**

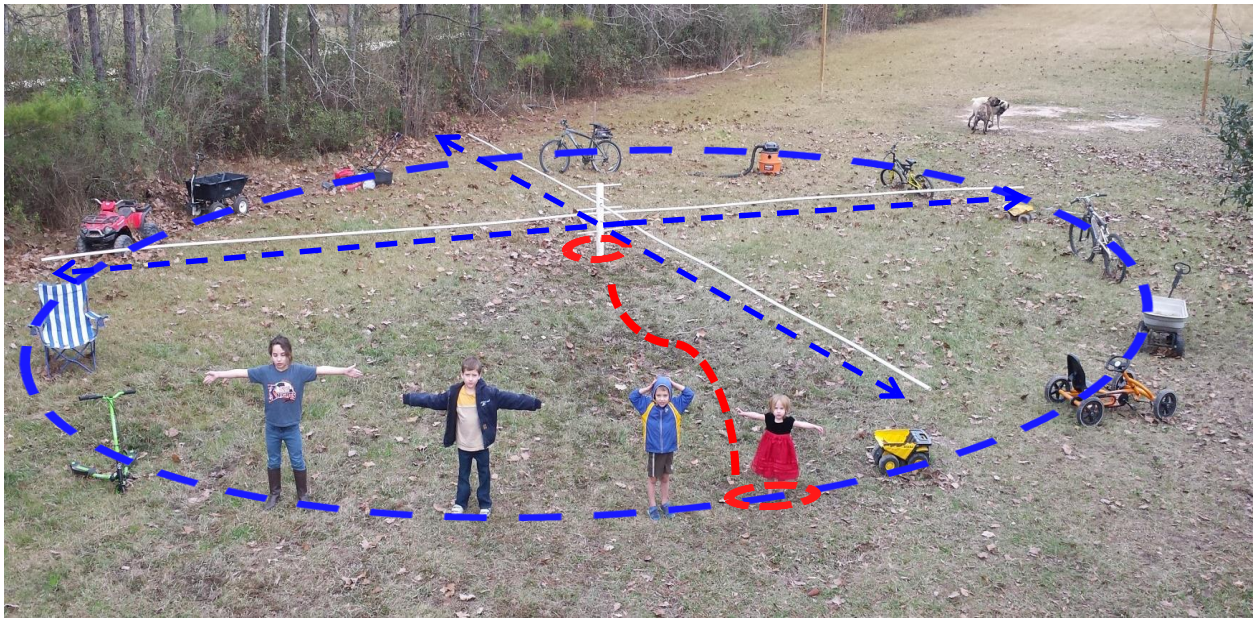

**Figure 91. Effective radius of perforations vs Viper Drill laterals. Red circles are 2–3 ft radius of impact from perforations and blue circle = Viper Drill penetration of 30 ft.**

# *2.0 Results and Discussion*

## 2.1 Field Testing

Field validation testing began in May 2014 after significant delays from attempting to arrange a contract with Radial Drilling, forming a new contractual relationship with Viper Drill, and waiting for the Viper Drill technology to become mature enough for field-testing.

Well testing occurred at two wells, The Barbie #3 and the Federal 00 #3, with testing at the Barbie #3 during May and June 2015, and at the Federal 00 #3 between July and October 2015. Field testing had the purpose of testing the Viper Drill as a drilling system, testing the sensors for measuring the emplaced laterals, and measuring the response of the wells to the stimulation. Testing was cyclical and resulted in refinements to both the Viper Drill system, and to the sensors and sensor testing system.

### 2.1.1 Barbie #3 Test

Located in the NW edge of the Permian Basin in Eddy County, NM, Barbie #3 is a shallow stripper well. A multi-zone completion oil well with comingled production, Barbie #3 has varying lithology ranging from tight dolomites to fine-grained sandstone to poorly consolidated shaley sandstone. Drilled in the mid 1980s, this stripper oil well was selected for the Viper Drill ultra-short radius lateral drilling procedure. A second aspect to this project involved the deployment of a novel sensor made up of small X-Y-Z axis accelerometers. The purpose of the sensor was to independently verify the distances drilled and, if possible, to determine the trajectory of each of the laterals. In this well, 12 laterals were drilled in three different zones, resulting in a total distance of just over 120 ft. Short drilling strings were used in initial testing to work out bugs in the system. Longer strings were used for later tests. Three zones were tested: Zones 1–2 were recompletions of previously stimulated intervals, and Zone 3 was a stimulation of a new interval.

**Zone 1: Lower Sandstone**

The deepest target zone was a sandstone pay located between 1731 and 1736 ft measured depth. The laterals drilled into this zone ranged from about 5.5 to 7.75 ft. The cumulative distance of the three laterals drilled into this zone was 20.75 ft. Drilling rates into this fine-grained zone were less than expected, averaging about 1 ft/h. The pumped fluid totaled approximately 315 bbl, equating to slightly over 100 bbl per lateral. The well began circulating on the last of the three laterals drilled into this zone, at which point the circulated fluid was used for drilling.

**Zone 2: Upper Dolomite**

Located a short way uphole, between approximately 1715 and 1717 ft measured depth, this target was a thin dolomitic pay. Three laterals drilled were drilled into this zone. The shortest

was drilled to 5.5 ft while the second and third were drilled 7.25 and 7.5 ft, respectively. The total distance of the laterals drilled into this pay was 20.25 ft. A fine-grained sedimentary zone, drilling rates averaged about 1 ft/h.

The first lateral drilled into this zone presented a unique challenge, as the drilling head of the Viper Drill system disengaged from the drill string in the lateral. This was caused by a series of stick-slips, subsequently addressed with a simple set-screw. The more interesting point is that the drilling operator was able to successfully re-engage the drilling head and then drill three additional feet into the zone.

After the third lateral was drilled into this thin zone, another was attempted. A clear hole was cut through the casing, but when drilling through the cement a series of unusual stalls was encountered. Upon its return to surface the bit was examined and it appeared to have been cutting a metallic object beyond the casing—possibly a casing centralizer. The Viper Drill EOR™ formation drill-string was lowered into the well and made a short distance before indicators suggested this lateral had intersected one of the nearby laterals (i.e. the drill-string met minimal resistance when pushed deeper). Efforts to drill further were aborted for fear of complications of the dogleg where the laterals intersected. This was not counted as a distinct lateral.

Typically, circulation was returned after about 5–10 bbl of fluid had been pumped in. The total fluid pumped for these laterals was 400 bbl, the majority of which was recirculated.

**Zone 3: Penrose Sand**

The third and final zone targeted was a shaley sandstone, locally known as the Penrose. The drilling logs on this zone described it as unconsolidated sand. The original logs indicated a high ROP through the zone. When lateral drilling in this zone, however, spots of slow/very hard drilling were sporadically encountered. This suggested hard inclusions or chert. Indeed, not expecting anything hard in this unconsolidatedzone, the drilling operator incorrectly suspected a tool-string issue and prematurely stopped drilling at 3 ft out into the first lateral in this zone. Further corroboration for the hard inclusions theory came in the form of distinct wear marks on a carbide drill bit. In fact, in one of the laterals drilled into the Penrose, the PDC inserts on the drilling head were lost out at 4 ft., in a spot where it appeared to the operator that the drill-string was chipping on something very hard. Fortunately, this was the only time that PDC inserts had broken off a drill-head. When not drilling thru hard inclusions the drilling rate through the Penrose averaged about 2.5 to 3.5 ft/h, with a peak ROP of about 5.5 ft/h. Aside from the first lateral in the Penrose (the sixth overall lateral) where the operator prematurely stopped at 3 ft and the third lateral into this zone (the eighth overall lateral) when the operator lost the PDC inserts (negating further drilling of that lateral), all of the laterals were drilled to 14.5 ft past the casing. Besides the depth indicators on the surface unit, these distance figures were confirmed by tell-tale signs on the drill-strings when it landed out on the top of the whipstock. Total fluid pumped to

drill the six Penrose laterals was about 850 bbl, or about 140 bbl per lateral, all of which was being recirculated.

Table 18 summarizes the 12 laterals drilled into the three zones. The indicated total distance of the laterals was just over 120 ft  lateral zone lateral distance (ft).

**Table 18. Summary of the 12 Laterals Drilled**

| Lateral | Zone | Lateral Distance (ft) |
|---|---|---|
| 1 | 2-Dolomite | 5 ½ |
| 2 | 1-Sandstone | 5 ½ |
| 3 | 1-Sandstone | 7 ½ |
| 4 | 1-Sandstone | 7 ¾ |
| 5 | 2-Dolomite | 7 ¼ |
| 6 | 3-Dolomite | 3 |
| 7 | 3 – Penrose Sand | 14 ½ |
| 8 | 3 – Penrose Sand | 4 |
| 9 | 3 – Penrose Sand | 14 ½ |
| 10 | 3 – Penrose Sand | 14 ½ |
| 11 | 3 – Penrose Sand | 14 ½ |
| 12 | 3 – Penrose Sand | 14 ½ |

Generally, as time progressed and as the operators gained greater familiarity with the zones and their drilling response, greater distances were attained; the exceptions being the sixth and eighth laterals, explained previously. All laterals but the sixth and eighth were tested with the Datalogger sensor.

Untreated fresh water was used for the majority of the procedure, as the operator had indicated that the risk of swellable clays or formation damage was negligible. Toward the end, a surfactant was added to increase lubricity for the mud motor. Circulation was attained at approximately 275 bbl and then these fluids were used for the remainder of the drilling. In total, approximately 850 bbl were pumped during this workover.

**Challenges Encountered**

Typical of fielding new technologies, a number of unforeseen issues were encountered. Some of these pertained to the surface equipment and some to the downhole tools. While the workover efforts started out with some technical issues, they finished out much more smoothly.

## Equipment Challenges

Early in the workover of the well, problems with the surface equipment arose. These related to some easily fixed hydraulic leaks (basic maintenance) and to some faulty bearings on the injector head. The bearing failure was more involved, requiring replacement, and correspondingly delayed the project. While the casing and cement string performed flawlessly, some unexpected issues arose with the formation drilling-string and probe tool-strings. For example, on the first run of the formation drilling tool the drilling head was lost in the lateral due to stick-slips. This was a problem not previously encountered. Unclear weight indications were mitigated by incorporating sinker bars above the downhole tools; meanwhile, insufficient flow to the cutting head was addressed by fixing the defective hose crimps. The project also experienced problems with the initial probe that conveyed the sensor (Figure 92). The probe was designed to use a jet hose and while the probe had been successfully tested at the shop, in the field, the crew had problems getting it to transition through the tight "J-path" of the downhole whipstock. A new, "short, stocky" sensor probe (Figure 93) designed to deploy on the end of the Viper Drill string was built, surface tested and subsequently run successfully on all subsequent downhole probe runs.

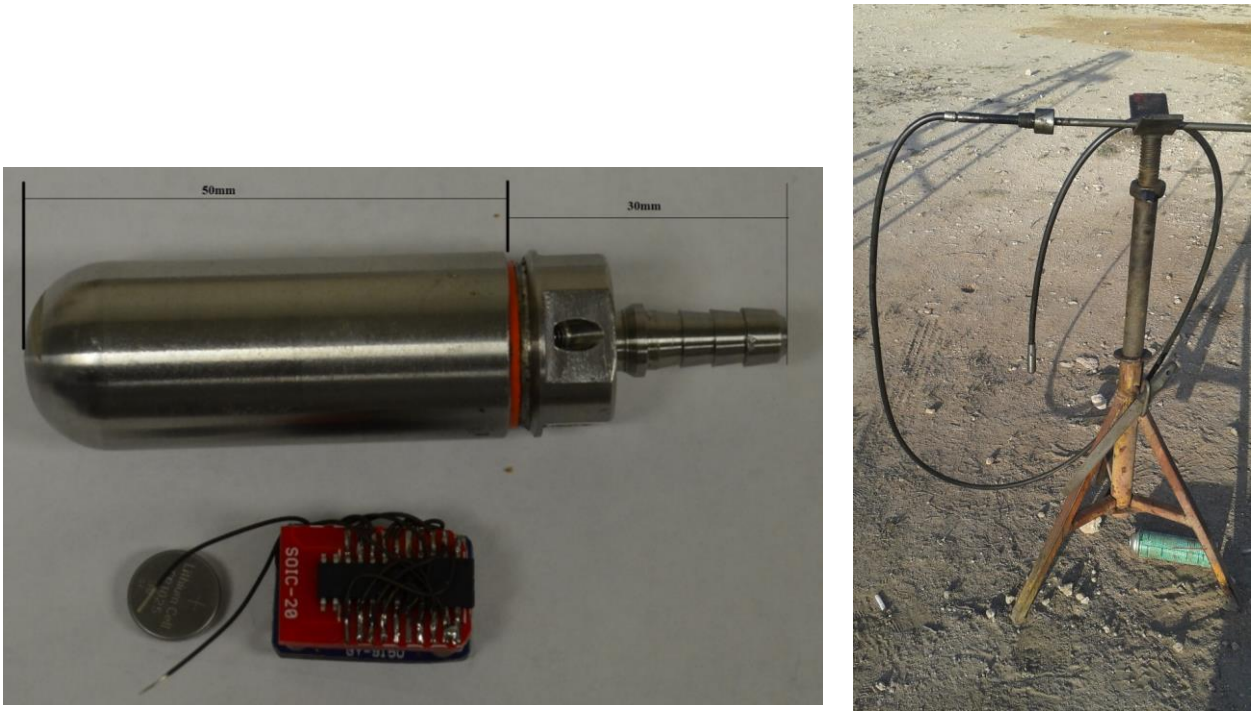


**Figure 92. Left, initial sensor package sized to fit the sensor and fit through the shoe. Right, sensor package deployed on the end of a rubber jet hose.**

**Figure 93. New sensor package designed to deploy on end of Viper Drill.**

### Sensor Probe Challenges

For the sensor, faster acceleration is preferable. When tested in lab conditions—e.g. when accelerating the sensor at the rate of gravity—the sensor yields highly accurate data. To accomplish high rates of acceleration in the field, however, presents some formidable challenges. One must not only develop a sensor tool-string and probe that can be quickly stripped out the lateral and thru the whipstock "J", but they must also quickly attain the requisite high speeds. Run on a coiled tubing unit, the workhorse used to accomplish this is the injector head. The Viper Drill injector, like industry standard injector heads, however, is only rated for 175 ft/m—or about 3 ft/sec notably, such speeds are maximum speeds and are only typically attained after CTU operators accelerate to such levels—something that normally occurs over the distance of several hundred ft. By contrast, for this project, high rates of speed—or, more specifically acceleration—are needed in a matter of several yards. Moreover, while the injector head does the work of stripping the tubing out of the well—and hence the attached probe string out of the lateral—it must also be synchronized with the reel onto which the tubing is spooled. The weight of the reel and tubing, however, present thousands of pounds of inertia that must also be correspondingly accelerated. What all of this means is that the raw data retrieved from the downhole probe runs were not as clean as desired, due to the lower acceleration values. Thus, while multiple runs were made in the field to measure each lateral—with longer laterals yielding better data, the data still required additional processing. Sensor results will be discussed in Section 2.1.3.

### 2.1.2 Federal 00 #3 Test

Located in the NW edge of the Permian Basin in Eddy County, NM, Federal OO-#003 is a shallow well producing from a single set of perfs in the Cedar Hill / Bone Spring at a depth of approximately 5,016 to 5,038 ft. The operator selected a single previously unstimulated target in this second test well for the Viper Drill EOR™ procedure, an ultra-short radius lateral drilling procedure. A second aspect to this project involved the deployment of a novel sensor made up of

small X-Y-Z axis accelerometers. The purpose of the sensor was to independently verify the distances drilled and, if possible, to determine the trajectory of each of the laterals.

**Lateral Drilling Summary**

The Viper Drill EOR™ procedure entails drilling holes through the casing, cement and formation. Unlike conventional horizontal drilling technologies, this technology produces laterals that literally radiate outward at 90 degrees from the wellbore. The Viper Drill system employs a mechanical cutting head to drill an approximately 1.25 in. diameter hole through the formation rock. Typically, multiple laterals are drilled into each target zone to form a sort of wagon wheel of drainage tunnels.

**Well Work-Over Summary**

The following narrative summarizes the radial drilling work directed at the thin target. A total of 14 laterals were drilled into this stratum, excluding an attempted lateral on 8/3 that was abandoned at 2 ft after the anchor that locks in the whipstock slipped, preventing further drilling. Going forward, a different style anchor was procured and employed without further incident.

**Target Zone / Summary**

The lateral drainage boreholes on this well targeted a portion of the Delaware formation. Located at the edge of the field, this particular stratum had not been previously produced, but the well operator believed this to be a worthwhile target. This stratum was aggressively drilled with laterals spaced at about every 6 in. vertically and radiating outward at azimuths spacing of approximately 120º. The 12 laterals were emplaced at a depth ranging from 2,727.5 ft to 2,734 ft—a space of about 6.5 ft.

**ROP and Fluid Usage**

The ROP of laterals drilled into this zone averaged above 5.5 ft/hr, with a high of 10 ft/hr. The total fluid pumped was slightly over 1,000 bbl, for an equivalent of about 85 bbl per lateral. As this was a cased hole completed well, some of the total fluid pumped was associated with milling a hole in the case to access the formation. If one excludes this fluid, the equivalent fluid to drill each lateral averaged closer to 70 bbl. For purposes of drilling fluid, untreated fresh water was used for the majority of the procedure as the operator believed that the risk of swellable clays or formation damage was negligible. A surfactant was added to the drilling fluid, however, to increase the lubricity for the mud motor.

## Laterals Overview

Table 19 gives the details of the 15 laterals drilled into the Delaware zone. The longest laterals totaled 32 ft with the majority of them being 30 ft or more. The lateral drilled on 10/1 was shorter than 30 feet for field demonstration.

**Table 19. Details of 15 Laterals Drilled Into the Delaware Zone**

| FEDERAL 003 | | |
|---|---|---|
| **LATERAL #** | DEPTH | LATERAL LENGTH |
| **1** | 2833 | 32 FT |
| **2** | 2832 | 32 FT |
| **3** | 2834 | 32 FT |
| **4** | 2833.5 | 31.5 FT |
| **5** | 2833 | 16 FT |
| **6** | 2832.5 | 12 FT |
| **7** | 2832 | 15.5 FT |
| **8** | 2831.5 | 2 FT |
| **9** | 2830.5 | 30 FT |
| **10** | 2830 | 20.5 FT |
| **11** | 2829.5 | 30 FT |
| **12** | 2829 | 30 FT |
| **13** | 2828.5 | 30 FT |
| **14** | 2828 | 30 FT |
| **15** | 2827.5 | 30 FT |

## Premature Coiled Tubing Failure

A particularly frustrating aspect of the work on this well pertained to the coiled tubing--more specifically, a new roll of coiled tubing that was used on this well. While fatigue to coiled tubing is a well-known and closely monitored phenomena, this roll of new coiled tubing developed a failure at approximately 1,500 ft, even though the usage on the tubing was only about one-third of the running feet where such failures are common. Fortunately, additional tubing had been spooled onto the drum and so this portion of tubing was cut off and the job progressed.

## Discussion and Analysis

A noticeable improvement in drilling rates was observed between the first and second well, with average ROPs on the Federal #OO-003 being more than double those on Barbie #003. In addition, both the average and the maximum drilling distance were more than doubled compared to Barbie #003. Part of the difference in ROP stems, no doubt, from the fact that different zones were being targeted on the two wells (which are located 13 miles apart). While this makes

exact comparisons tricky, Viper Drill made a number of adjustments to their downhole tools and to part of the bottomhole assembly (BHA) that sits above the whipstock. These improvements resulted in the drill string being better constrained during the formation drilling procedures, resulting in reduced torque losses and improved transference of weight to the drill head. The net result was a roughly 2× improvement in rate of penetration (ROP)**.**

A further improvement on this second well pertained to more accurate sensor probe runs/results. While some variability was still evident in the results, the reported values much more closely matched the depths drilled by the Viper drill-string. For example, in one particular instance, a single lateral was surveyed a total of four times (at roughly two different pull back speeds). Results for the four runs varied from the known distance (31.5 ft) by an average of 11%, with the highest variance being 16.5% and the lowest being less than 1%. Independent of the sensor probe, the depth of penetration (lateral length) is indicated on surface instrumentation and confirmed via tell-tales on the drill-string. These tell-tales can only be confirmed once the drill string has been returned to the surface and inspected. The results of the sensor show that the drill-string exits the casing at 90° and drills into the formation. As the project progressed and models were fine-tuned, significantly improved surveying of the laterals was attained.

### 2.1.3 Results of Testing the Datalogger in the Field

During field testing at the Barbie #3 it was determined that additional efforts would be required to get a sufficient pull rate from the equipment and additional processing to the data would be required to extract the path from the raw data. This section discusses results of improvements to the datalogger, improvements to the software and processing algorithm, and results of field tests using the improved system

**Improvements to the DataLogger**

During testing at the Barbie #3 it was determined that the original sensor package deployed on a jet hose would not be reliable and that a new package deployed on the Viper Drill would instead be used (Figures 93–94). This required some adjustments to the configuration of the sensor. Also, based on test results and slower pull speeds than expected, additional corrections to the data were required. Incremental changes and improvements to the sensor were also made. These changes are catalogued in this section. In particular:

1. The dimension of the new shell changed from 10 mm diameter × 25 mm height to 20 mm diameter × 15 mm height.
2. The recording time would need to be longer, at least two hours, due to deeper emplacement of laterals in the Federal 00 #3. This also requires more data storage and a larger capacity battery.

3. The MPU-9150 breakout dimension is larger than the house dimension of new shell, and power consumption is a little larger, so a smaller implementation with lower power consumption was needed.

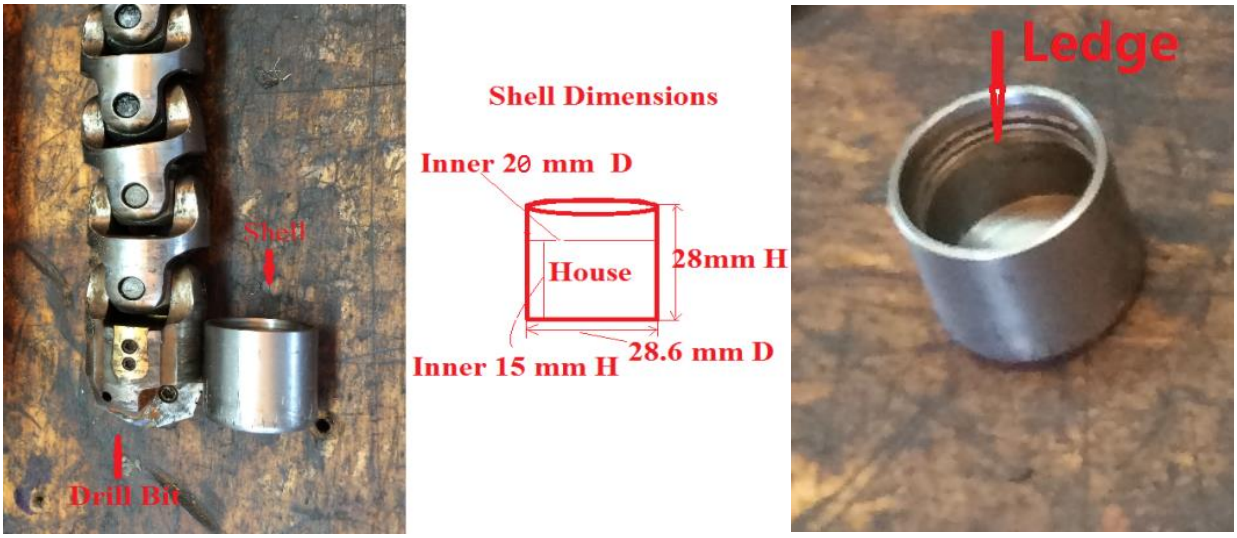


**Figure 94. New shell, its dimensions and the ledge that defines the usable interior space. Note that the cutting head is shown on the end of the casing cutting string and not the ViperDrill string.**

Based on the new issues and requirements, researchers identified a tiny MPU-9250 breakout and IS25LP128 Serial Flash Memory Chip, which met the new requirements. Fortunately the shell with a larger house dimension accommodated a larger CR1635 lithium coin battery.

### Tiny MPU-9250 Breakout

The MPU-9250 is a second generation, 9-axis motion tracking device for smartphones, tablets, wearable sensors, and other consumer markets. The MPU-9250, delivered in a 3 × 3 × 1 mm QFN package, is the world's smallest 9-axis MotionTracking device and incorporates design innovations enabling dramatically reduced chip size and power consumption, while at the same time improving performance and reducing cost.

The MPU-9250 MotionTracking device sets a new benchmark for 9-axis performance with power consumption only 9.3µA and a size that is 44% smaller than the company's first-generation device. Gyro noise performance is three times better, and compass full scale range is over four times better than competitive offerings. The MPU-9250 is a System in Package (SiP) that combines two chips: the MPU-6500, which contains a 3-axis gyroscope, a 3-axis accelerometer,

and an onboard Digital Motion Processor™ (DMP™) capable of processing complex algorithms; and the AK8963, the market-leading 3-axis digital compass. Improvements include supporting the accelerometer low power mode with as little as 6.4µA and improved compass data resolution of 16-bits (0.15 µT per LSB). The full-scale measurement range of ±4800µT helps alleviate compass placement challenges on complex PCBs. Figure 95 shows the tiny MPU-9250 breakout. Its dimension is only15 mm × 15 mm × 4 mm (CJMCU 10DOF 9 Axis MPU9250 + BMP180 Sensor Module). This tiny MPU-9250 breakout consists of MPU-9250 chip + high-precision pressure-sensing BMP180 chips. The BMP180 sensor has been removed to save power and space, since its function is not needed in the DataLogger.

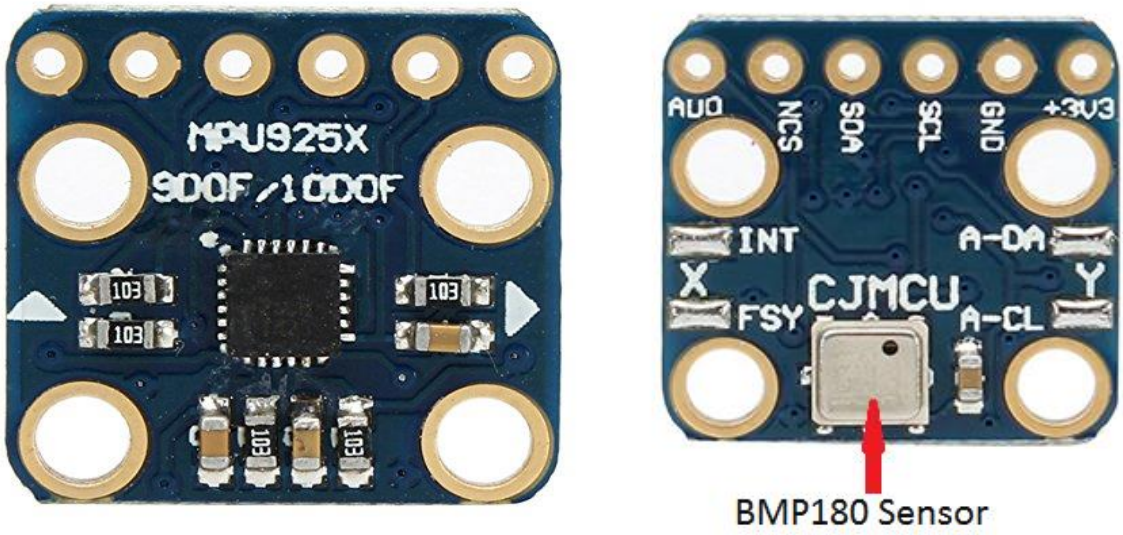


**Figure 95. MPU-9250 breakout. Left, top; Right, bottom with BMP180 removed to save energy and space**

Main features of the breakout:

1. Compatible with MPU-9150, but smaller and adds an SPI interface
2. Operation Voltage range: 2.16-3.6v
3. Communication: SPI / IIC
4. Dimensions: 15 mm × 15 mm × 4 mm(MPU-9150 breakout: 20 mm ×15 mm × 4 mm )

Figure 96 shows a schematic of the MPU-9250 breakout, and Figure 97 shows the axes of the MPU-9250 where the Z-axis points to the center of the earth, so that Gravity Z is ~1G when the DataLogger sits level to the surface of the earth. Figure 98 shows the SPI and I2C interfaces of the MPU-9250.

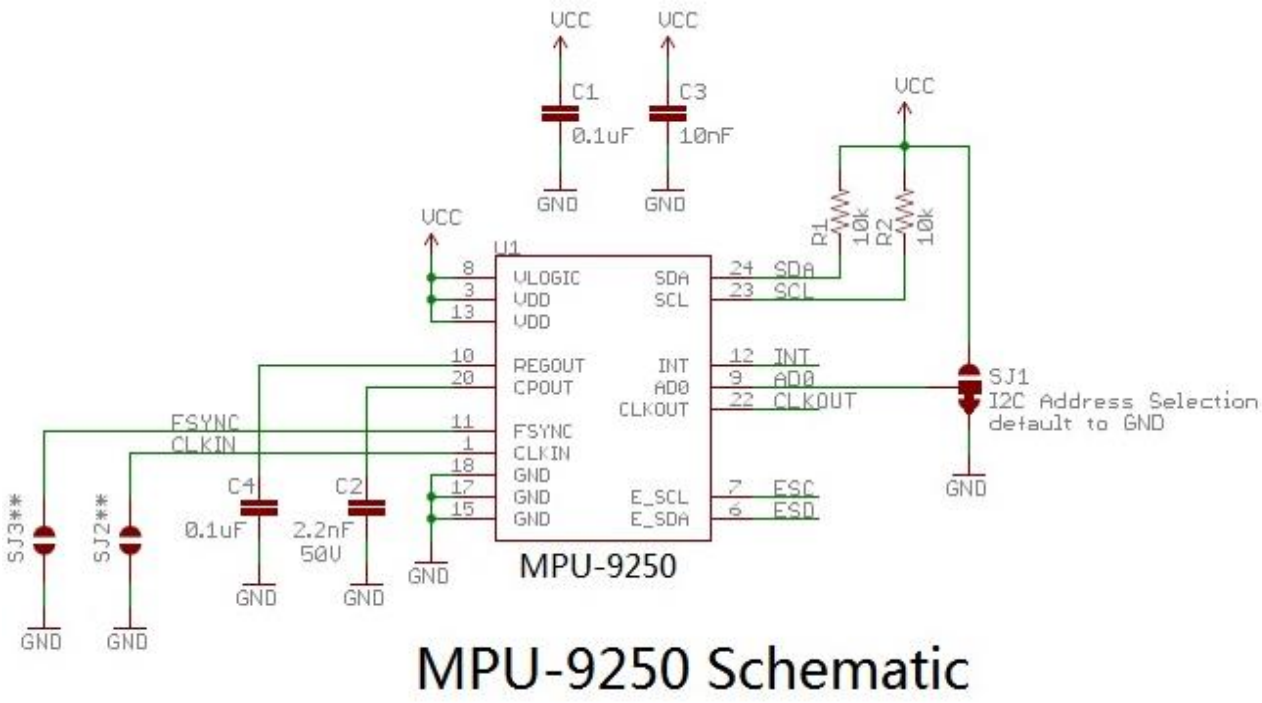


**Figure 96. Schematic of the tiny MPU-9250 breakout.**

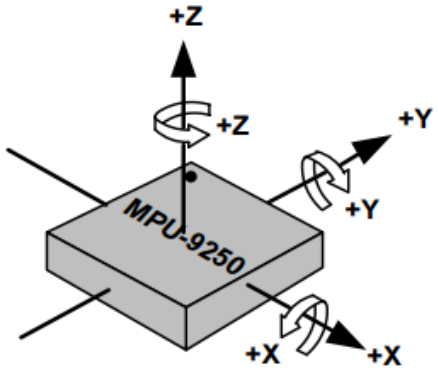


**Figure 97. The axes of the MPU-9250. The Z direction is vertical to the center of the earth.**

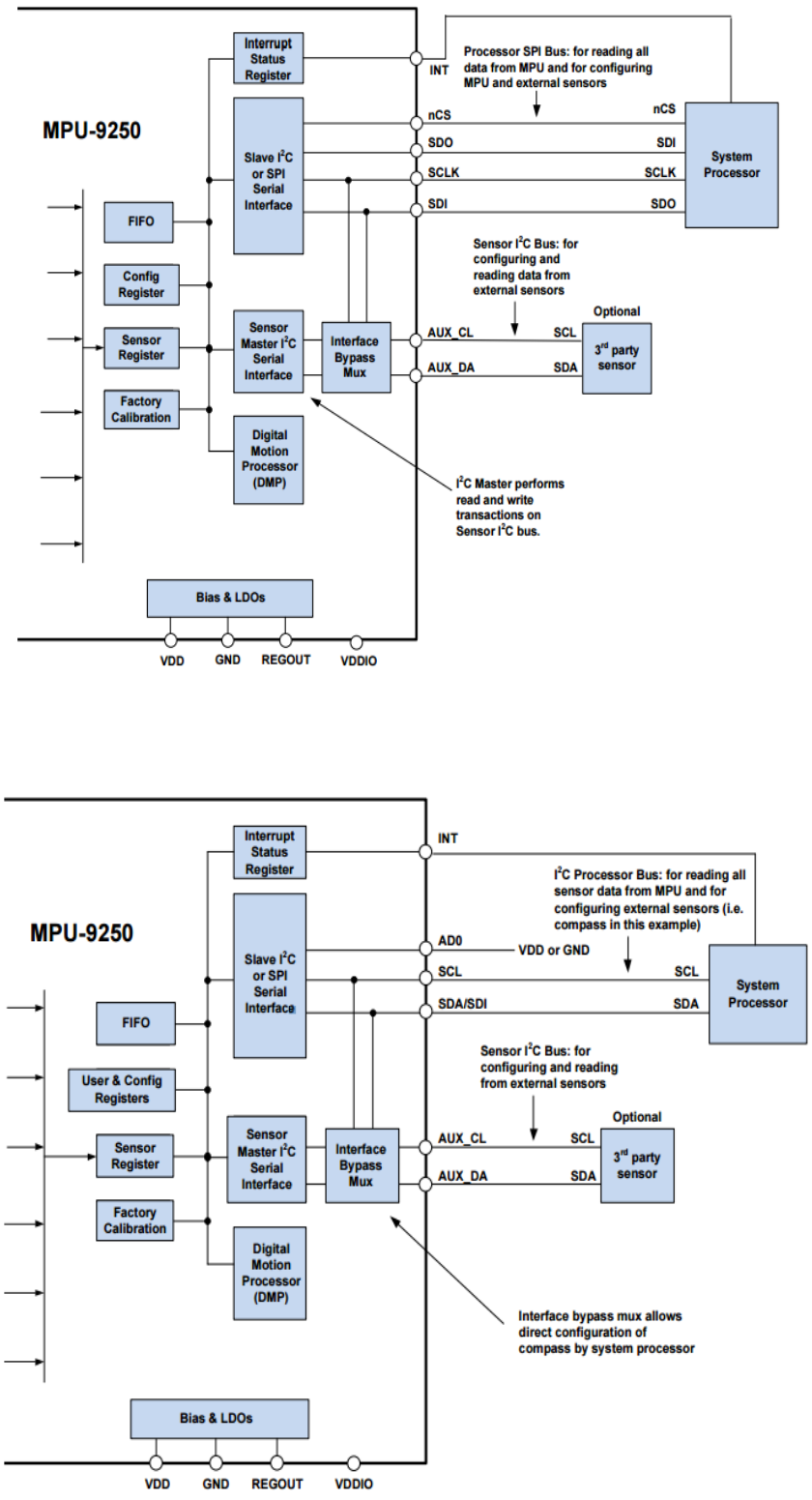


**Figure 98. MPU-9250 SPI Interface (top) and MPU-9250 I2C interface (bottom).**

Due to the tight schedule between running field tests, data access to the sensor with I2C interface was unchanged. Though the SPI may run at higher speed, it needs four lines while the I2C needs only two lines. Staying with I2C reduced firmware changes already burned into the MCU and schematic circuits. The improved DataLogger still reads data from the MPU-9250 through I2C bus/interface, as it did with the MPU-9150. Replacement of the MPU-9150 breakout with the tiny MPU-9250 breakout allows the DataLogger to fit in the new data package while reducing power requirements.

**IS25LP128 Serial Flash Memory Chip**

The flash memory chip SST25VF064C (8MB) of the prototype version can only record about one hour of data, and new implementation's require two hours. The IS25LP128 (Figure 99) is manufactured by Integrated Silicon Solution, Inc. and is a new product with the following features:

- 128M-bit/16M-bytes
- Industry Standard Serial Interface
- 256 bytes per Programmable Page
- Supports standard SPI
- 8-pin SOIC 208mil
- Low Power:
  - Single 2.3V to 3.6V Voltage Supply
  - 10 mA Active Read Current
  - 10 µA Standby Current
- Wide Temp. Ranges:
  - -Extended: -40°C to +105°C
  - -V Grade: -40°C to +125°C
  - -Auto Grade: up to +125°C

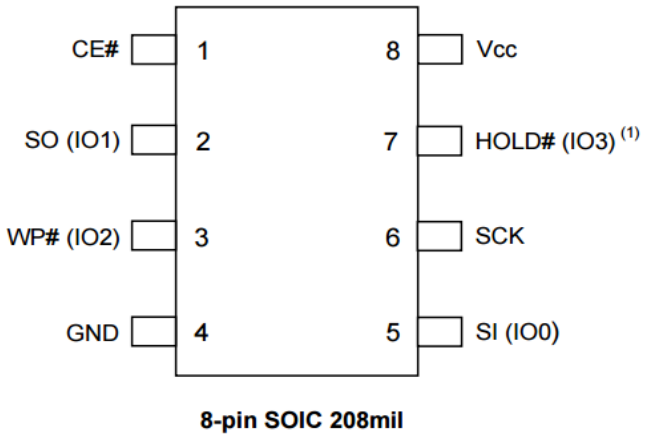


**Figure 99. 8-pin SOIC package of the IS25LP128 Serial Flash Memory Chip.**

Compared to the previously used SS25VF064 chip, the IS25LP128 has two improved features:

- Single 2.3V to 3.6V voltage supply (2.3v is required for the DataLogger to run for 2+ hours powered by a coin battery)
- 16MB capacity

In addition, the IS25LP128 is compatible with the SS25VF064, which means no changes were needed on the PCB board and the only change needed in the firmware was to set a memory constant from 8MB to 16 MB to let the processor adress the 16MB's of memory.

**Power Supply - Lithium Coin Battery**

In lab tests, AAA batteries were used to save on expensive coin batteries, when testing at bench scale it was found that the CR1025 battery could not power the entire DataLogger as calculated and expected. After a few more tests and analysis, it was found that after powering on the DataLogger for only 20 minutes, some batteries' voltage could drop to under 2.7V, at which point the collected data would not be written into the SST25VF064C SPI flash memory chip though other parts of DataLogger would still work, because both MPU-9150s use a lower operational voltage range.

It was necessary to determine why the voltage dropped too fast. After testing, researchers found that one of reasons is the interval heavy drain (writing data into SST25VF064C), a large load for the CR1025 coin battery, which has a 30mAh capacity. This caused the voltage to quickly drop under 2.7V, though the battery can still provide enough current. Another reason may be two pull-up resistors ( "472" →4.7K ohm) on the MPU-9150 breakout. Another issue is the two pull-up resistors needed by the I2C bus to work properly with MPU-9150/MPU-9250, each of which takes 1+ mA constantly during data-reading operations. Fortunately the new larger diameter data package (20 mm D) allows use of a larger battery, the CR1632(140mAh), which is 4+ times larger than the CR1025 in capacity.

**Improved DataLogger**

With the MPU-9250, IS25LP128 and CR1632, 20 second generation DataLoggers were made for the Federal 00 #3 test, which were designed to work and record data for two or more hours. Before field-testing, and to make sure that the DataLogger could function, all DataLoggers were tested with one CR1632 respectively. About half (9/20) worked properly and recorded data for two hours and ten minutes. The other half (11/20), those that did not record data for two hours and ten minutes, were rejected for field use. It was concluded that main reasons for failure were parameter variations in the pull-up resistors. Figure 100 shows the schematic of the new DataLogger designed with the MPU-9250, PICLF1825 and IS25LP128.

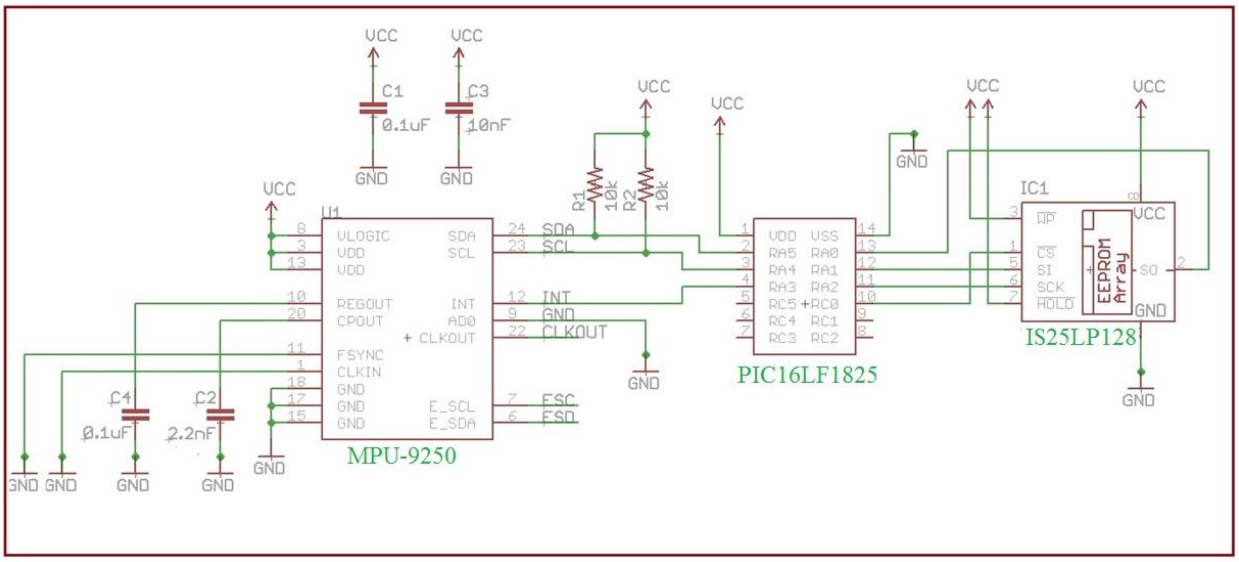


**Figure 100. Schematic of the improved DataLogger with the MPU-9250, PIC16F1825, and IS25LP128.**

The new DataLogger has three layers:

1. Battery(CR1632 140mAh)
2. MPU-9250 Breakout
3. MCU and IS25LP128 on a small PCB

The system is constructed in the lab, with the exception of the battery, which is soldered on immediately before deployment. Figure 101 shows images of a DataLogger used in the field tests.

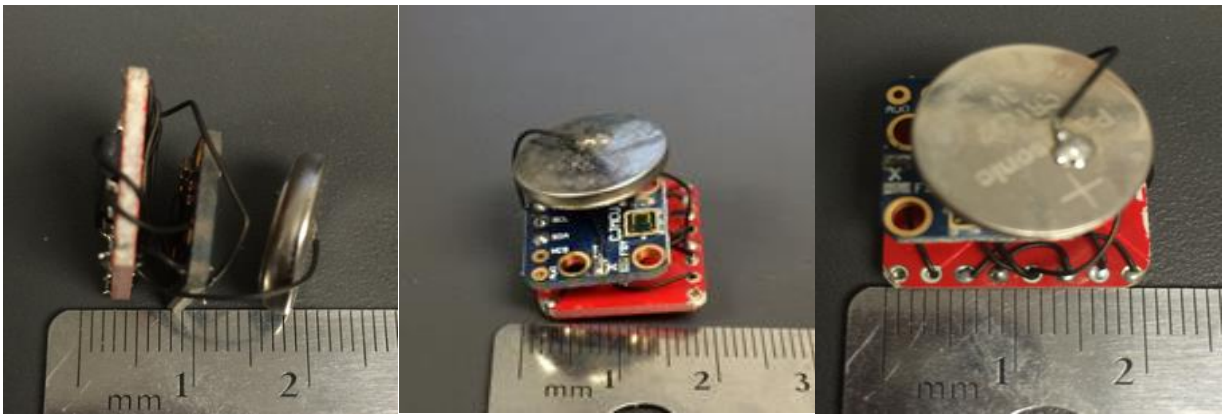

**Figure 101. DataLogger with MPU-9250 breakout and CR1632 battery.**

## Improvements to Software/Algorithms

The interfaces and functions of data processing software were changed and improved throughout the course of the project and in response to early field tests, by adding algorithms and analysis tool such as FFT, filters, 3D/2D charts and graphics that allowed quick checks of results and visuals to aid in troubleshooting. Figure 102 shows the main interface of the new data processing software with raw data in hexadecimal format displayed. Figure 103 shows a chart panel that displays signal curves for each processing step and allows the results of algorithms and parameters to be quickly viewed in the field. Figure 104 shows a recorded 3-axis gravity curve set. Primary diagnostics from this view are used to identify the DataLogger status: moving, resting, rotating and turning.

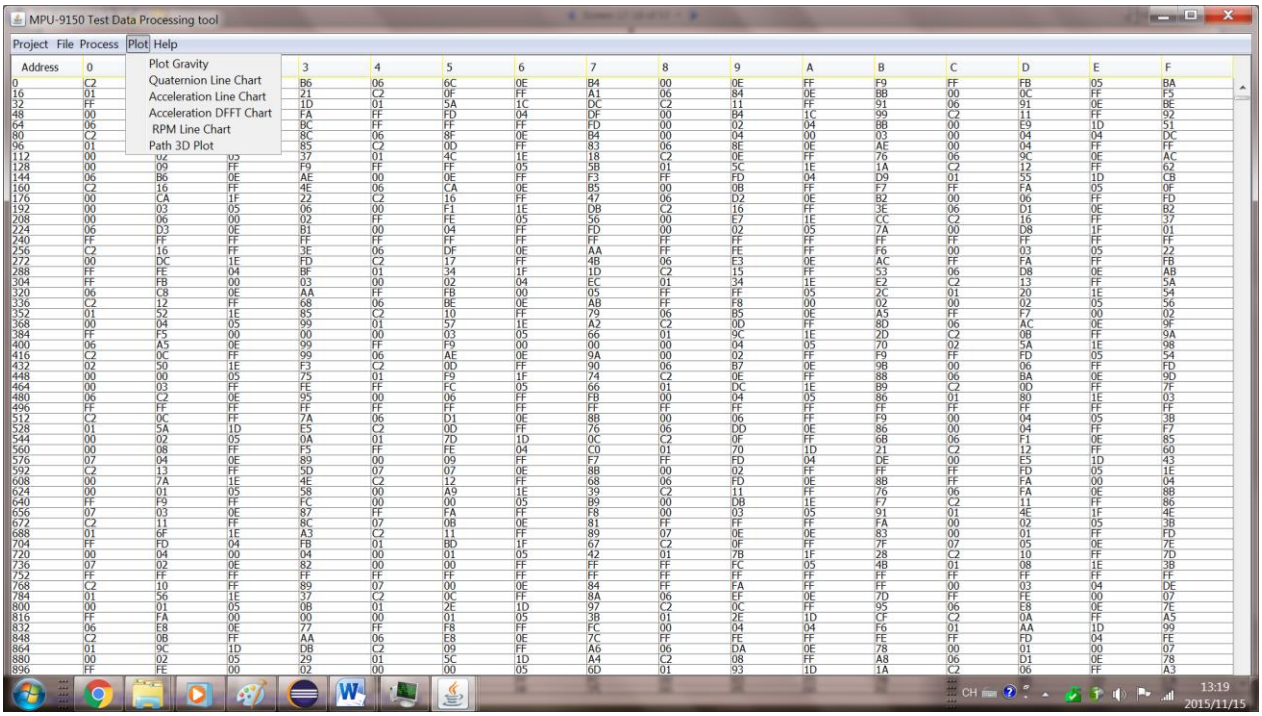


**Figure 102. Main interface of data processing tool with raw data displayed.**

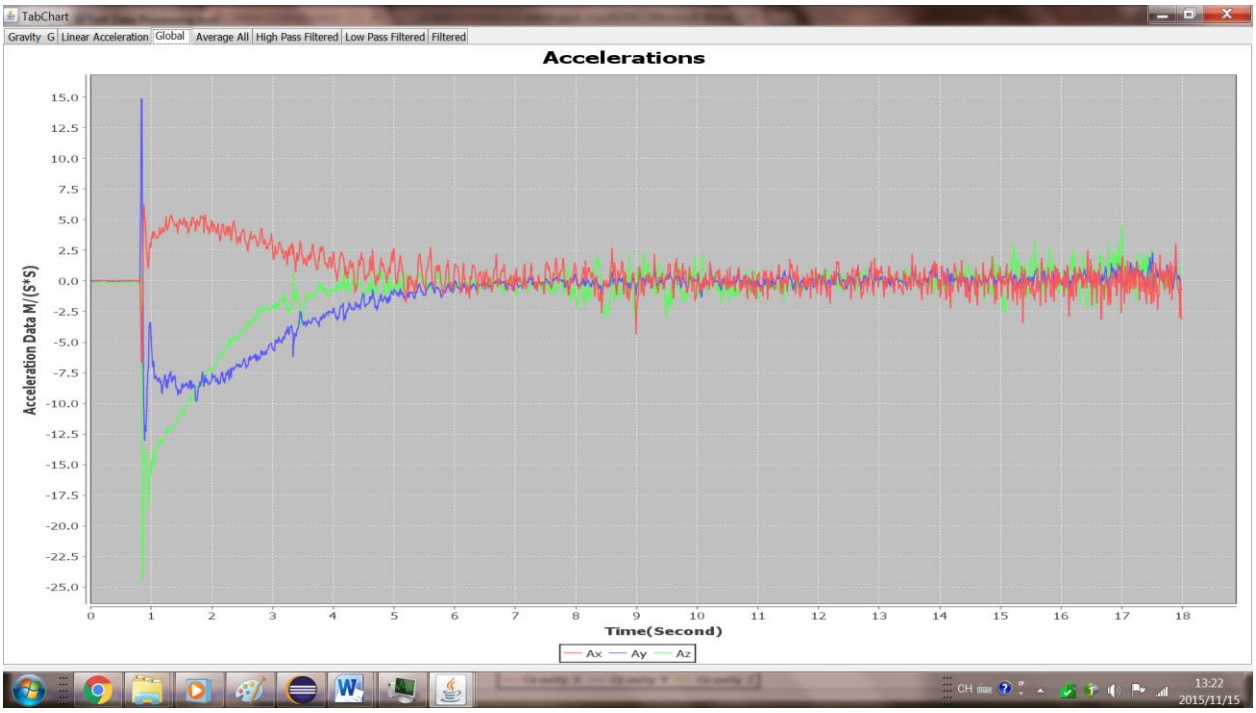


**Figure 103. Chart panel used to display the signal curves. This display shows a sample of x-y-z axis data.**

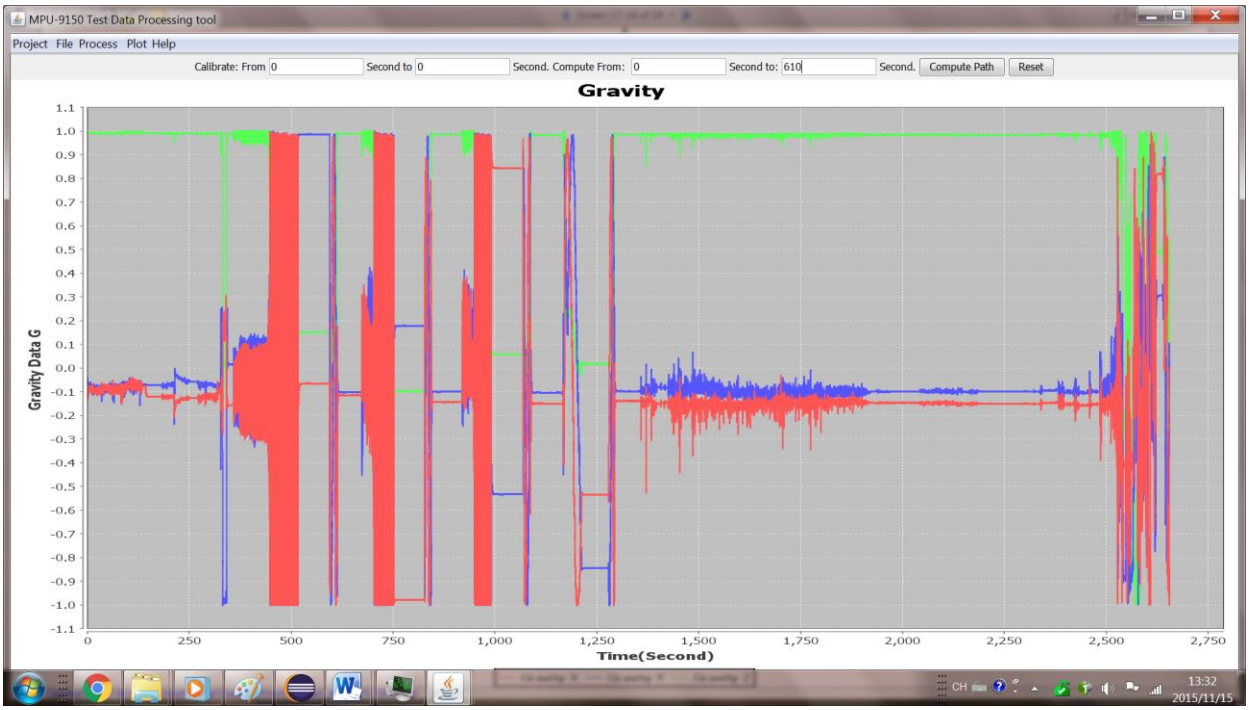


**Figure 104. Displayed gravity curves for a sample DataLogger record.**

**Data Processing Procedure**

To use the current Data Processing Tool to process recorded data, the following steps must be followed:

1. Create a project (for data sets)
2. Open recorded data file with suffix ".bin" to load recorded data
3. Comput gravity by clicking "start computing"
4. Display calculated gravity curves by click "Plot"→ "Plot Gravity Curves"
5. Identify pulling out part of a test run by zooming in on the curve (See Figure 105)
6. Select the start point/time and end point/time of the DataLogger traveling in a lateral
7. Input the times in **From** and **To** text fields, then click compute
8. Click Plot→Path 3D Plot to check the travel path of the DataLogger in the lateral (Figure 106)
9. Values of path length will be output to a text window.

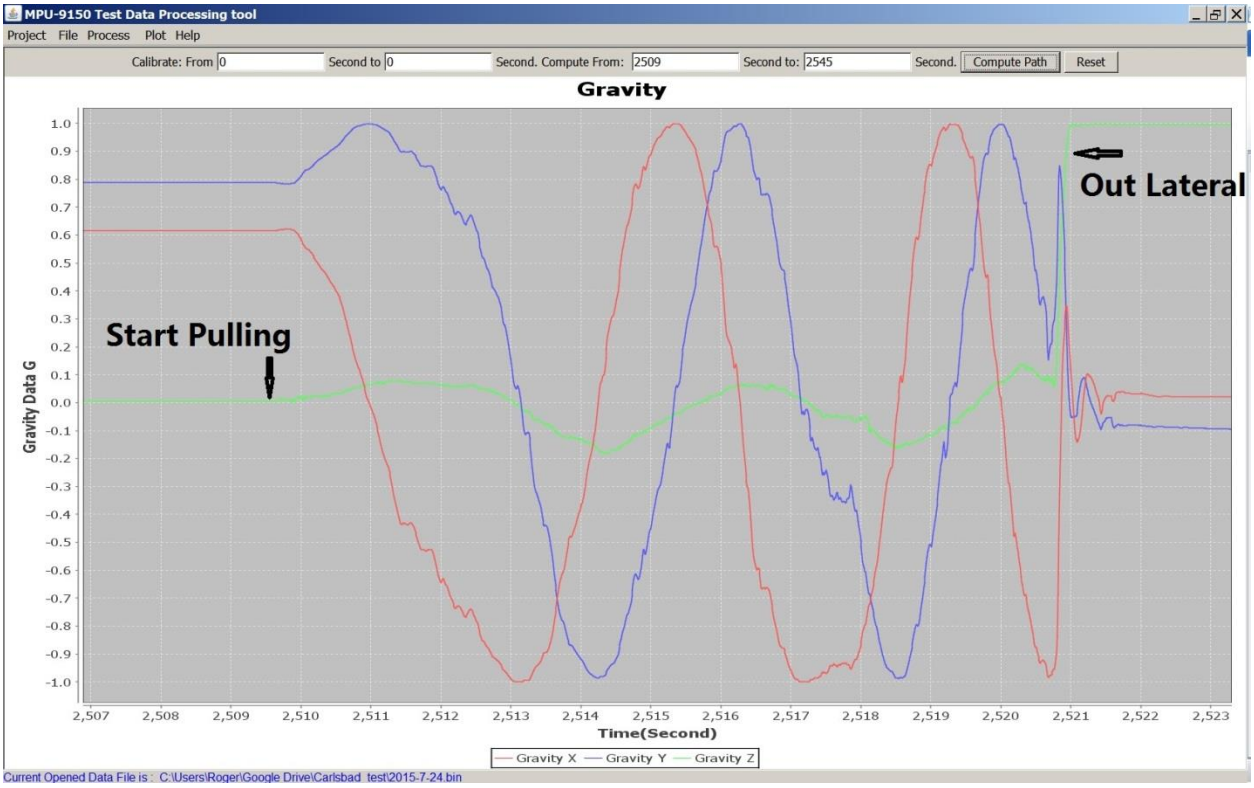


**Figure 105. Graph used to identify the start and end times of DataLogger travel in the lateral using a zoomed view in the chart window.**

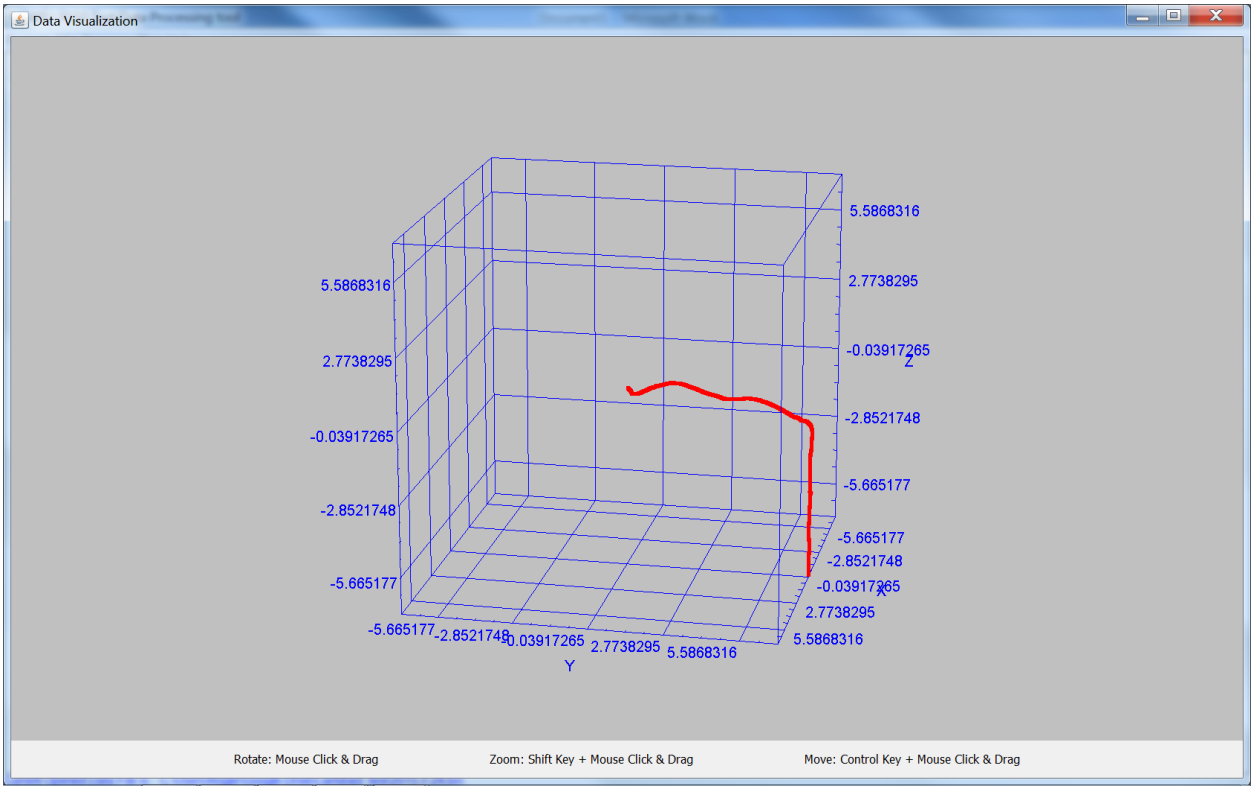


**Figure 106. Calculated path of the DataLogger traveling in the lateral.**

In order to realize the image in Figure 106, the selected DataLogger recording must be processed using the following steps:

1. Calibrate raw accelerations data (if selected)
2. Filter raw data
3. Calculate Gravity (two methods: Filters or Quaternion )
4. Remove gravity and compute linear accelerations
5. Transform from body frame coordinates to global coordinates
6. Calculate speed/distance by integrating accelerations once/twice.

## Field tests, Data Processing Results, and Analysis

All field data were processed by the Data Processing Tool with different algorithms and parameters, and analyzed to identify lateral paths and to improve the algorithms and optimize parameters for future use. A total of 20 data sets were collected, with 11 from Barbie #3 and nine from the Federal 00 #3. The particulars of the acquisition parameters and number of runs per lateral are tabulated in Tables 20 and 21 for the Barbie #3, and the Federal 00, respectively.

**Table 20. Acquisition Parameters and Runs per Lateral for Barbie #3**
Drilled Laterals: 15
Tested Laterals: 8
Collected data sets: 11

| Lateral number | Drilled Date | Length (feet) | Tested with datalogger? | # of tests |
|---|---|---|---|---|
| 1 | 4/17 | 5.50 | No | |
| 2 | 4/22 | 5.50 | No | |
| 3 | 5/11 | 7.50 | Yes (tested 4 times) | 4 |
| 4 | 5/14 | 7.75 | Yes | 1 |
| 5 | 5/15 | 7.25 | Yes | 1 |
| 6 | 5/18 | 3.00 | No | |
| 7 | 5/19 | 14.50 | Yes | 1 |
| 8 | 5/21 | 4.00 | No | |
| 9 | 5/24 | 14.50 | Yes (shell leaks, repeated) | 1 |
| 10 | 5/27 | 14.50 | No | |
| 11 | 5/29 | 14.50 | Yes | 1 |
| 12 | 6/1 | 14.50 | Yes | 1 |
| 13 | 6/3 | 14.58 | Yes | 1 |
| 14 | 10/30 | 20.00 | No | |
| 15 | 11/2 | 11.00 | No | |

**Table 21. Parameters and Runs for Federal 00**
Drilled Laterals: 15
Tested Laterals: 8
Collected data sets: 9

| Lateral number | Drilled Date | Length (feet) | Tested with datalogger | # of tests |
|---|---|---|---|---|
| 1 | 7/6 | 32.00 | Yes | 1 |
| 2 | 7/10 | 32.00 | No | 0 |
| 3 | 7/21 | 32.00 | No | 0 |
| 4 | 7/24 | 31.50 | Yes | 1 |
| 5 | 7/27 | 16.00 | No | 0 |
| 6 | 7/29 | 12.00 | No | 0 |
| 7 | 7/31 | 15.50 | No | 0 |
| 8 | 8/3 | 2.00 | No | 0 |
| 9 | 9/28 | 30.00 | No | 0 |
| 10 | 10/1 | 20.50 | Yes | 1 |
| 11 | 10/5 | 30.00 | Yes (one line dropped due to shaking, re-peated) | 1 |
| 12 | 10/8 &10/9 | 30.00 | Yes (tested three times ) | 3 |
| 13 | 10/12 | 30.00 | Yes | 1 |
| 14 | 10/16 | 30.00 | Yes | 1 |

| | | | | |
|---|---|---|---|---|
| 15 | 10/19 | 30.00 | Yes (lost with broken chain) | 0 |

The collected data sets are listed below:

1. 2015-5-10.bin
2. 2015-5-11.bin
3. 2015-5-12.bin
4. 2015-5-13.bin
5. 2015-5-16.bin
6. 2015-5-19.bin
7. 2015-5-24.bin
8. 2015-5-29.bin
9. 2015-6-1.bin
10. 2015-6-3.bin
11. 2015-6-4.bin
12. 2015-7-6.bin
13. 2015-7-24.bin
14. 2015-10-1.bin
15. 2015-10-6.bin
16. 2015-10-8.bin
17. 2015-10-8-2.bin(repeat test for 2015-10-8.bin )
18. 2015-10-9.bin (repeat test for 2015-10-8.bin )
19. 2015-10-12.bin
20. 2015-10-16.bin

**Selection of Qualified/Good Data Sets**

There were 20 data sets total, but not all data sets were usable, qualified for further analysis or contained the information needed to improve the algorithm and software. Some test runs were not used based on initial calculations and analysis, due to:

1) High rotation rate on pullout.
2) Pump not shut down or not enough rest enough time to allow tension to release before pulling the sensor from laterals.
3) Too low pull speed: pulling out laterals at a speed lower than 0.5 feet per second.

Figure 107 shows gravity curves of test runs with too many rotations caused by slow pulling speed. Figure 108 shows a test run with too many rotations during traveling in the lateral between starts and end points.

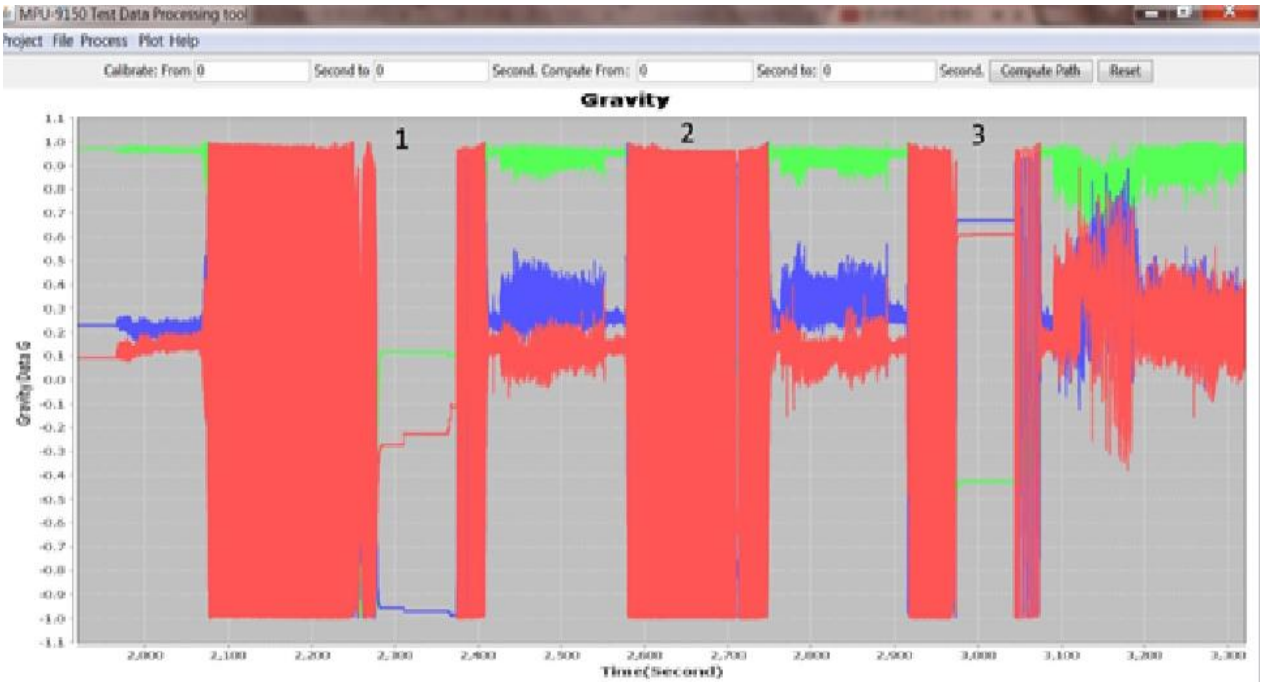


**Figure 107. 3-Axis gravity plot of a DataLogger test run pulled at slow speed.**

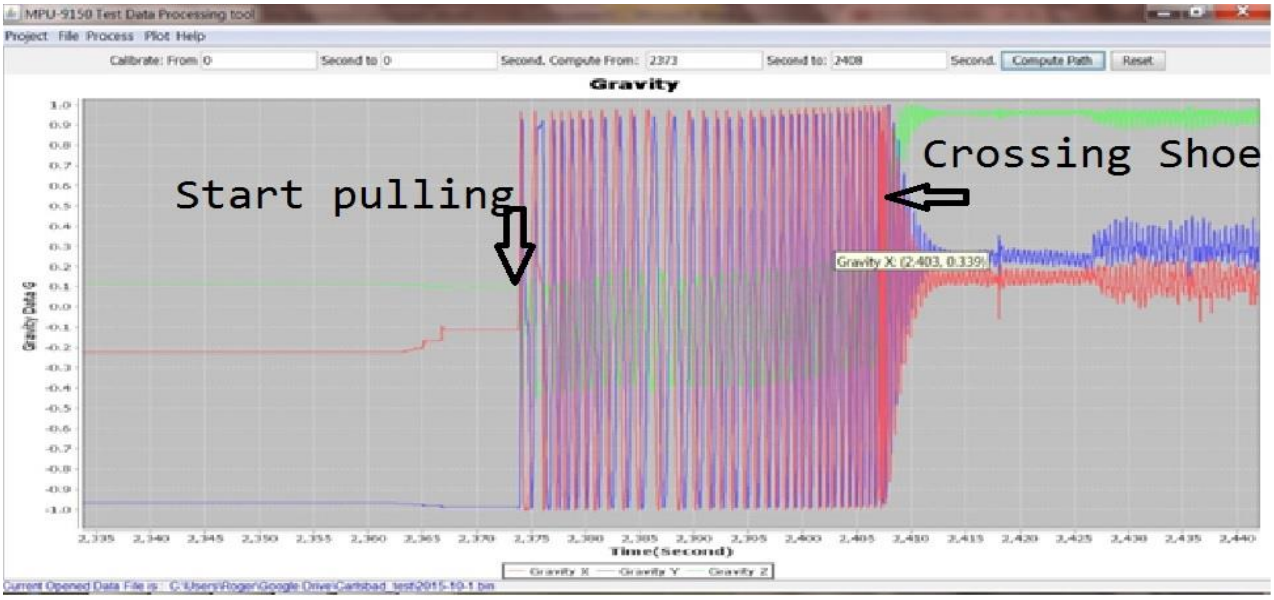


**Figure 108. Gravity curves with too many rotations in a test run.**

During data processing each data set is read in by the Data Processing Tool, transformed, computed and presented as output gravity, distance and lateral path in chart view, text, 2D curves and 3D curves for easy review. Ultimately researchers were unable to compute paths for a number of tests due to pull speeds lower than 0.5 ft/s or from records with excessive rotations.

All data sets recorded before 5/18 meet one of these criteria, but the data contributed to employing faster pull speeds in subsequent tests. In total, five data sets recorded from 14+ ft long laterals drilled in May and June, with pull speeds between 0.5 and 1.0 ft /s, were processed for further analysis (Table 22). These records at the Barbie #3 allowed for refinement of the software and hardware prior to the tests at the Federal 00.

**Table 22. Five Usable Data Sets from 14-ft Laterals in the Barbie #3**

| Number | Test Date | Length (ft)/m | Qualified Test Runs |
|---|---|---|---|
| 1 | 5/19 | 14.50/4.42 | 2 |
| 2 | 5/24 | 14.50.4.42 | 3 |
| 3 | 5/29 | 14.50/4.42 | 4 |
| 4 | 6/1 | 14.50/4.42 | 3 |
| 5 | 6/3 | 14.58/4.44 | 1 |

After improving drilling tools and operational abilities, the next set of tests at the Federal 00 #3 between July and October allowed longer laterals that could reach 30+ feet and pulling speeds faster than 1.0 ft/s, which, while still much slower than the initial design, was able to provide better results than the shorter slower laterals from earlier tests. After initial processing and analysis, an additional five data sets, that include "qualified test data" recorded at speed of 1+ft/s, without rotation driven by the pump motor, and collected from laterals equal to or longer than 30 feet, were used to calibrate the algorithms for this project. Table 23 shows the five data sets and the number of qualified test runs for each data set for tests at the Federal 00.

**Table 23. Good Data Sets from 30+ ft Laterals in the Federal 00**

| Number | Test Date | Length (ft)/m | Qualified Test Runs |
|---|---|---|---|
| 1 | 7/24 | 31.50/9.60 | 4 |
| 2 | 10/8 | 30.00/9.14 | 3 |
| 3 | 10/9 | 30.00/9.14 | 3 |
| 4 | 10/12 | 30.00/9.14 | 3 |
| 5 | 10/16 | 30.00/9.14 | 3 |

**Computing the Length of the Emplaced Laterals**

In order to compute the length of a lateral, it must first be known when the DataLogger enters the shoe, when it turns into the lateral, when reaches the end of the lateral and each path component as it is pulled back out. To easily identify the each position, a test procedure was established based on early tests and was in use for tests July, 2015 at the Federal 00. This procedure is illustrated on a recording of raw gravity curves in Figure 109. Figure 110 shows a zoomed in version of the data in Figure 109. The entire data acquisition process is outlined below:

1. Power on with 30 minutes delay before recording;
2. Trip down well, sensor start to record at 30 minutes;
3. Stop at 30 feet above the shoe for 2 minutes;
4. Enter shoe and reach the end of lateral;
5. Stop and wait 2 minutes;
6. Pull out through lateral and cross shoe;
7. Stop at 30 feet above shoe for 2 minutes;
8. Repeat process if multiple records are desired, or;
9. Pull DataLogger out of the well and shell;
10. Power off and unload recorded data into a laptop;
11. Check if data is recorded properly, if not, repeat test.

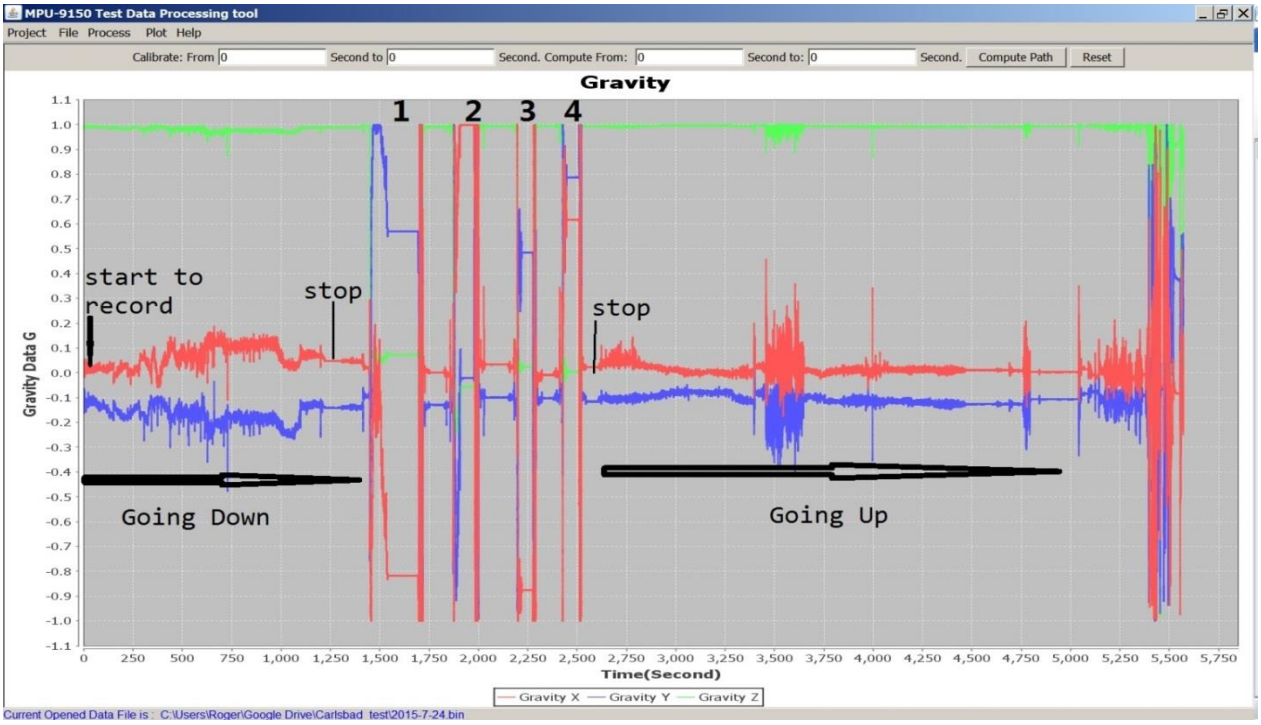


**Figure 109. Total recorded gravity curve of 2015-7-24.bin.**

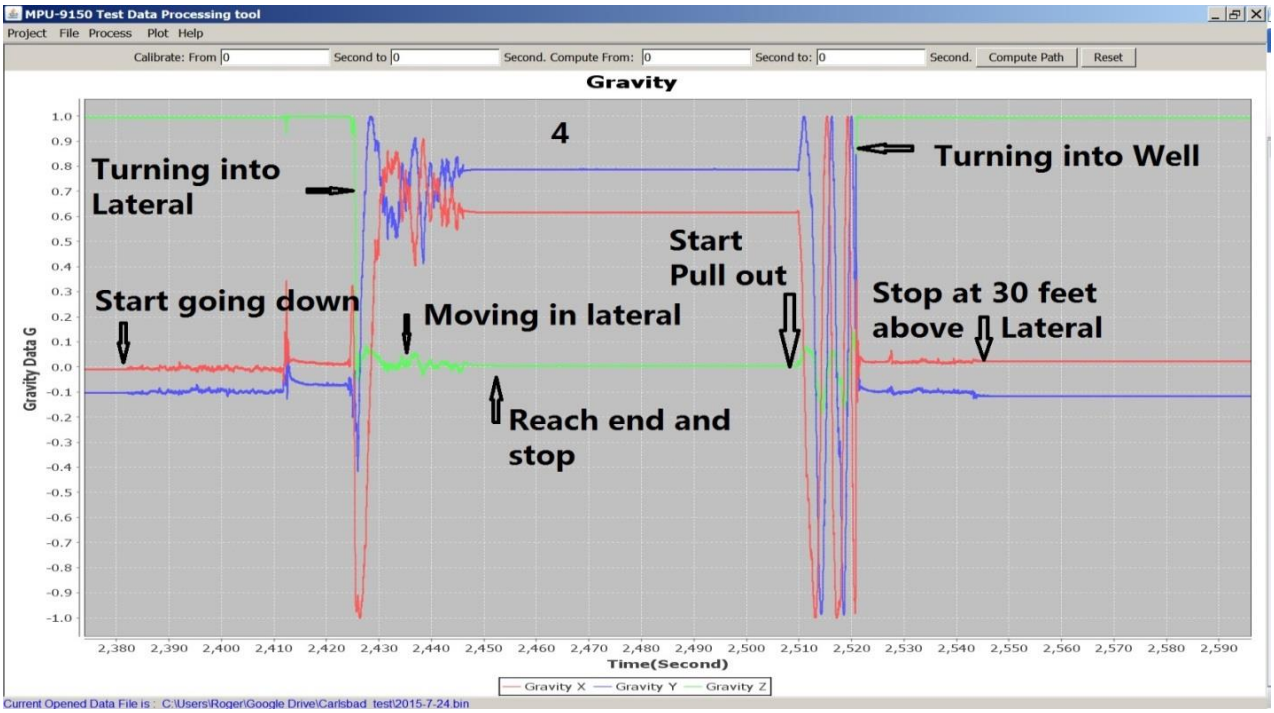


**Figure 110. Gravity curve of fourth test run shown in Figure 109.**

Since the accelerometer's Z axis is pointed to the earth's center, several features may be discerned from Figure 110:

1. When the Z measurement is near 1, the DataLogger is vertical
2. When the DataLogger is about zero that it is horizontal
3. A gravity change from 1 to 0 means turning into shoe, from 0 to 1 means getting out shoe;
4. Variable G in X,Y and Z Axis means the DataLogger is moving;
5. Constant G means the DataLogger is at rest.

Figure 111 shows a portion of the record in Figure 110 that corresponds to the 12 seconds of time it took to pull the sensor back from the end of the lateral.

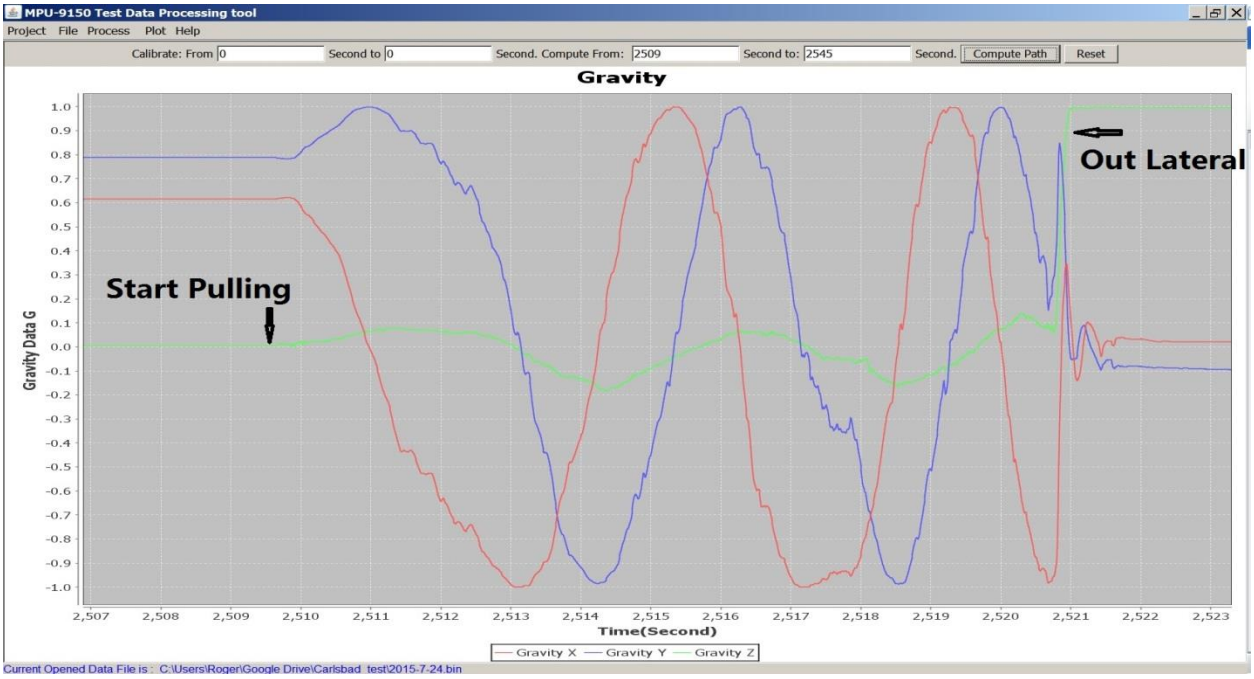


**Figure 111. Zoomed view on the 12 seconds of pulling in the fourth test run shown in Figure 110.**

In total for the fourth test run, from time: 2509.0 seconds to 2545.0 seconds, 26 seconds were recorded during the time the DataLogger traveled through the lateral: pulling out horizontally (31.5 ft) then turning into shoe, pulling out vertically and stopping at 30 ft above lateral. The track of the mapped lateral is shown in Figure 112. Tabulated data for Barbie #3 tests, and Federal 00 #3 tests are shown in Tables 24 and 25. The best results were from test runs recorded with a pull speed of about 0.8 -0.9 ft/s for the shorter Barbie #3 laterals, and between 1.29 and 1.33 for longer laterals in the Federal 00 #3. Best results were towards the end of the fieldwork, in part due to adjustments to software and testing protocols as information was acquired, processed, and optimized throughout the test period to make incremental improvements.

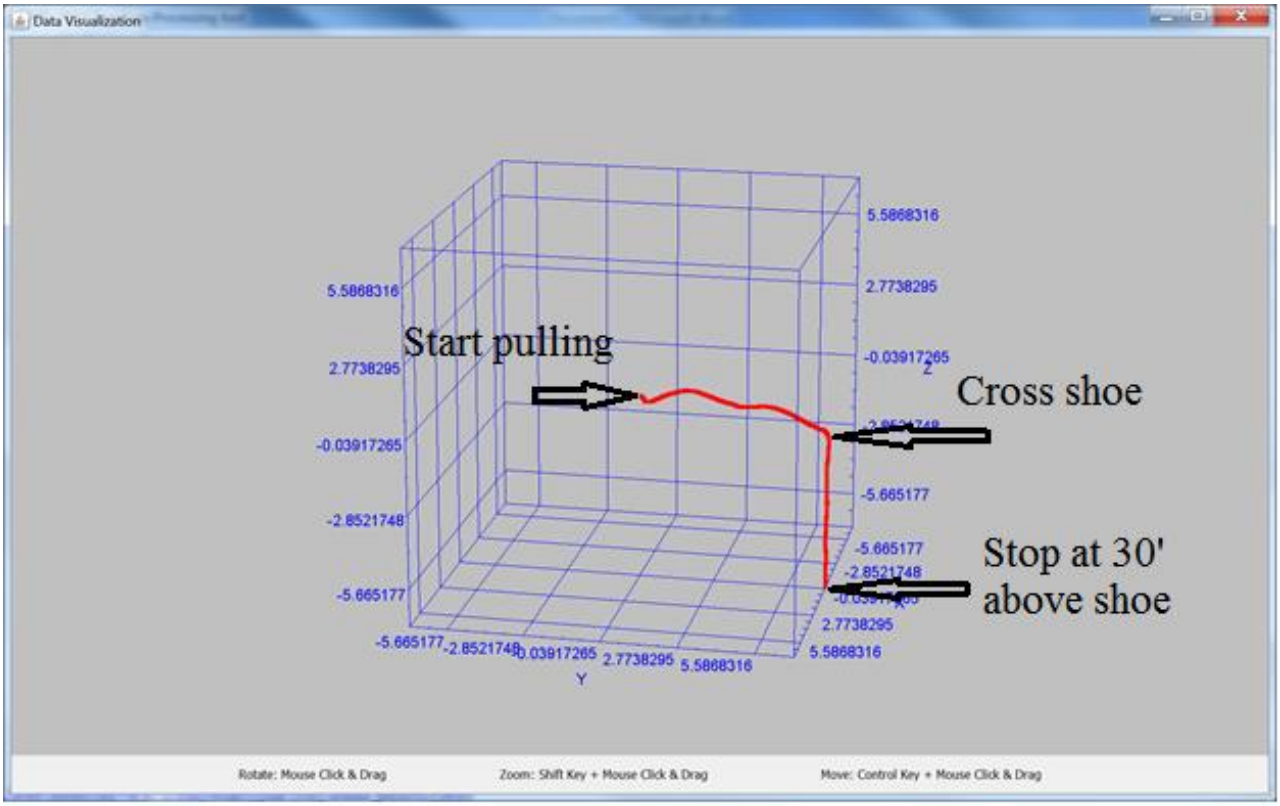


**Figure 112. Computed track of fourth test run using data shown in Figure 112.**

**Table 24. Calculated Lengths and Speeds for the Five Laterals Tested in May-June, 2015 at the Barbie #3**

| Test Date (M/d) | Length (ft) | Test 1 (Length (ft) /Speed (ft/s)) | Test 2 (Length (ft) /Speed (ft/s)) | Test 3 (Length (ft) /Speed (ft/s)) | Test 4 (Length (ft) /Speed (ft/s)) |
|---|---|---|---|---|---|
| 5/19 | 14.50 | 16.47 / 0.71 | 15.03 / 0.88 | | |
| 5/24 | 14.50 | 9.83 / 0.66 | 6.93 / 0.90 | 9.83 / 1.0 | |
| 5/29 | 14.50 | 12.37 /0.81 | 11.77 / 0.88 | 11.67 / 0.66 | 9.13 / 0.97 |
| 6/1 | 14.50 | 15.1 / 0.81 | 12.33 / 1.00 | 19.1 / 0.92 | |
| 6/3 | 14.50 | 7.43 / 1.23 | | | |

**Table 25. Calculated Lengths and Speeds for the Five Laterals Tested July–October, 2015 in the Federal 00#3**

| Test Date (M/d) | Length (ft)/m | Test 1 (Length (ft) /Speed (ft/s)) | Test 2 (Length (ft) /Speed (ft/s)) | Test 3 (Length (ft) /Speed (ft/s)) | Test 4 (Length (ft) /Speed (ft/s)) |
|---|---|---|---|---|---|
| 7/24 | 31.50 | 37.40 / 1.19 | 31.90 / 1.33 | 21.43 / 2.1 | 23.43 / 2.62 |
| 10/8 | 30.00 | 32.47 / 1.20 | 31.67 / 1.18 | 25.60 / 1.13 | |
| 10/9 | 30.00 | 28.83 / 1.29 | 32.73 / 1.09 | 26.80 / 1.20 | |
| 10/12 | 30.00 | 32.17 / 1.29 | 30.40 / 1.27 | 33.40 / 1.27 | |
| 10/16 | 30.00 | 30.60/1.18 | 33.53/1.25 | 33.43/1.25 | |

## 2.2 Economic Evaluation

The first field test was in the Barbie #3, a shallow Grayburg well. Multiple laterals were drilled in the existing productive Grayburg section that included both sandstone and dolomite lithology and then into an upper Penrose sand section that had not been previously completed. The Barbie #3 well is a stripper well thta was producing ~ one barrel of oil per day. Multiple laterals were drilled in the existing productive Grayburg section that included both sandstone and dolomite lithology and then into an upper Penrose sand section that had not been completed. As it was the first test well for the ViperDrill system many of the laterals were short and ongoing revisions of the drilling parameters and operational procedures led to improvements in the lateral drill time and longer laterals toward the end of the Barbie #3 tests. Nevertheless, after the well was put back on production, an estimated production increase of 40% was seen.

After making some revisions to the tool string, including adding drill collars to accommodate 32’ of drill string, ViperDrill rigged up on the Federal “00” #3 well to drill laterals in an untested Delaware sand section that had very good looking log shows with 18 to 22% porosity but also appeared to be sitting on top of a potential water zone with equally high porosity. In total 15 laterals were drilled into this previously unstimulated zone with a total length of 373.5 ft. After the well was put back on line, the overall liquid volume increased and after a period of de-watering the production has increased from 7.5 BO, 19 BW and 8 MCF to 11 BO, 24 BW and 9 MCF, a 47% increase in oil production.

ViperDrill has calculated their cost to drill a 32 ft lateral at about $ 7,500, excluding mobilization costs, and to do a more typical completion in a previously undrained interval with 4 laterals would then cost about $30,000. This compares favorably to other completion/recompletion technologies such as perfing and hydraulic fracturing, especially when additional reservoir communication and the ability to access otherwise difficult to complete thin horizons can make the technology a viable alternative.

## *3.0 Impact to Small Producers*

The objective of this research was to field-demonstrate a newly developed short-radius drilling technology for production enhancement from low-permeability reserves. To prove lateral emplacement, diagnostic techniques were developed and field-tested for monitoring lateral placement and potentially direction. The following questions were answered by this work: (1) How to control and diagnosis the placement and direction of laterals during a short radius lateral enhancement; (2) What are the economics of these emplaced laterals; (3) How reservoir simulation and field testing were used to determine optimal lateral placement strategies.

Well stimulation by radial jet enhancement is an attractive technology for enhanced oil recovery from both existing and new field developments. By using the most advanced coil-tubing technologies, lateral holes with different geometries can penetrate to compartmentalized formations that are left behind or bypassed during conventional waterflooding or within the less permeable oil zones that cannot be sufficiently drained by conventional processes. Quite substantial amounts of residual oil are left in low permeability reserves, such as low permeability zones or low permeability reservoirs, when production becomes uneconomical. The key element to enhance production is to increase the drainage volume by creating connections between a tight formation and the wellbore. Application of the short-radius drilling technology tested in this project will allow for more economical recompletions of these reservoirs, increasing the communication between untapped compartments, thin, not fracturable zones, and previously bypassed pay in mature wells, by creating lateral holes through the casing and drilling out 30+ ft into the reservoir. Thus, additional reserves will be added by recovering previously unavailable oil with an existing well completion structure and operational life can be extended due to an increase in productivity.

The producer (Jeff Harvard of HLCC) was very happy with the results of the test of the drilling system and the sensors and stated:

***"I am fully convinced that this very short radius drilling design works as claimed. As the product is further refined and tested, I fully expect the lateral lengths to increase significantly. I believe that the ViperDrill system is a very useful and competent product that can be used for various applications in the oilfield and other areas. I can see its beneficial use in vertical wells where water coning or nearby water is a problem; for reducing frac growth and also size by significantly increasing the initial perf/wing length; for remedial well work where skin damage is a problem; for injection wells to reduce injection skin damage. I also believe that design can be beneficially used in certain horizontal wellbore applications to increase frac height or length with increased lateral/perf length because of the coil tubing/semi-rigid rotating drill string design. I am sure other potential application will also be identified."***

## *4.0 Technology Transfer Efforts*

The objective of technology transfer is to aggressively transfer our technology to independent oil companies and service companies. This was accomplished through direct contact with companies, discussions at regional trade associations such as the New Mexico Oil and Gas Association, and the Independent Petroleum Association of New Mexico, and through the following direct Technology Transfer activities:

Theses:

1. Xiao, Y.: "Reservoir Description and Simulation to Assess the Potential of Radial Jetted Stimulations to Enhance Oil Recovery, Case Study: Millman Field, Eddy County, New Mexico," M.S. thesis Petroleum Engineering, New Mexico Tech, August 2013.
2. Liu, X.:"Production Optimization of Lateral Placement by Using Computer Simulation," Masters thesis Petroleum Engineering, New Mexico Tech, July, 2012

Presentations:

1. Balch, R., (2015): "Field Testing and Diagnostics of Radial-Jet Well-Stimulation for Enhanced Oil Recovery from Marginal Reserves," RPSEA Onshore Technology Workshop, Canonsburg, Pennsylvania, October 27-28.
2. Balch, R., (2014): "Field Testing and Diagnostics of Radial-Jet Well-Stimulation for Enhanced Oil Recovery from Marginal Reserves," RPSEA Onshore Production Conference, Houston, Texas, June 17.
3. Ruan, T., and Balch, R., (2013): "Development of 3-Axis Acceleration DataLogger for Non-Wired Sensing and Recording of Wellbore Paths," The 2013 International Conference on Software Engineering and Computer Science (ICSECS'13), Yichang, Hubei, China, September 27-29.
4. Balch, R., (2013): "Field Testing and Diagnostics of Radial-Jet Well-Stimulation for Enhanced Oil Recovery from Marginal Reserves," RPSEA Onshore Production Conference, Long Beach, California, October 17.
5. Balch, R., (2013): "Field Testing and Diagnostics of Radial-Jet Well-Stimulation for Enhanced Oil Recovery from Marginal Reserves," RPSEA Onshore Production Conference, Wichita Kansas, June 28.
6. Balch, R., (2012): "Field Testing and Diagnostics of Radial-Jet Well-Stimulation for Enhanced Oil Recovery from Marginal Reserves," RPSEA Onshore Production Conference, Houston, Texas, November 29.

Paper:

1. Balch, R., Ruan, T., Savage, M., and Harvard, J. (2016): **SPE 180410-MS**. "Field Testing and Validation of a Mechanical Alternative to Radial Jet Drilling for Improving Recovery in Mature Wells," SPE Western Regional Meeting, Anchorage, AK, May 23-16, 2016.

A target goal of RSPEA is to spend 1.5% of project funds on technology transfer activities. Figure 113 tracks the progress of that goal.

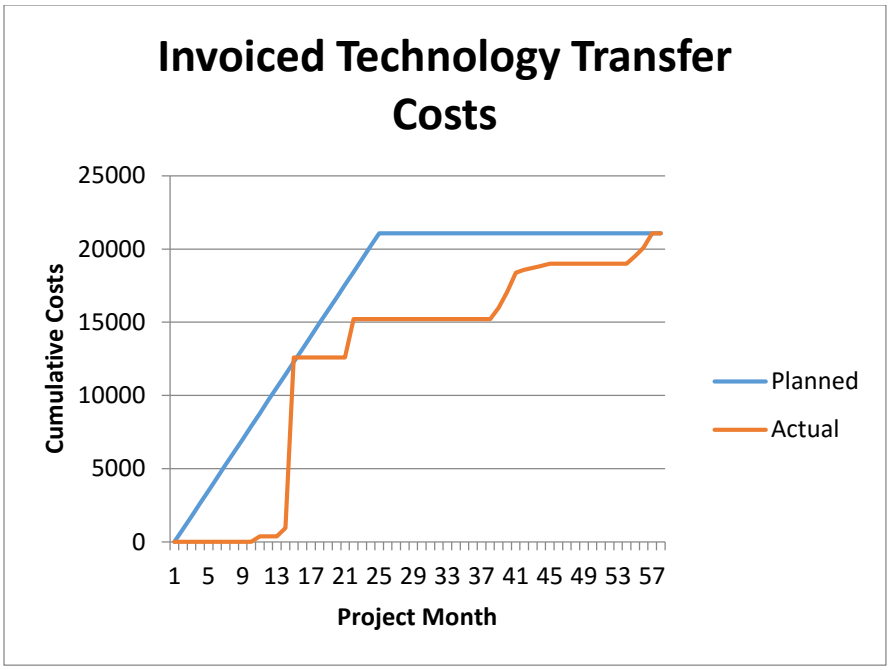


**Figure 113. Invoiced technology transfer by project month**

## *5.0 Conclusions*

The project was able to successfully test both the drilling system and the DataLogger used to measure the laterals. Field results were in part predicted by simulation studies, which examined the sensitivity of mature producing wells to stimulation using the Viper Drill. To optimize the treatments deployed during field studies, diagnostic technologies were developed and field-tested for monitoring the lateral placement: Sensors for measuring acceleration and direction were integrated with coiled tubing for monitoring the placement of laterals, laboratory studies with reservoir modeling using flow simulators were carried out to optimize the lateral placement, and the technical feasibility and economic efficiency of using these treatments for production enhancement in different types of reservoirs were evaluated through computer simulation and field demonstration.

Numerical simulation with Eclipse and CMG simulators modeled the effects of emplacing 30 ft long, 1 in. diameter laterals using three grid models utilizing combinations of square and radial grids with refinements along the lateral trajectories. Expected incremental oil was modeled at ~30% for four laterals in one production interval. Field sites in SE New Mexico were selected in the San Andres/Grayburg and Delaware formations and prototype designs of the location sensor were made utilizing durable piezoelectric sensors and chip based gyroscopes to measure deviations from vertical; these sensors are very similar to those found in many modern electronics devices, such as smart phones. The drilling system and sensors were both tested while

placing a total of 29 laterals of up to 32 ft in length in two wells between May and October of 2015.

In all 30 laterals were emplaced in two wells varying in length from 2 ft to 32.5 ft. As a result of fine tuning of the drilling system through five months of off-and-on field work, the system was reliably placing laterals of 32 ft in length at the end of the project, and that limit was based on the length of ViperDrill drill string components that were available, rather than any technical limit of the technology.

A small, on-system DataLogger was developed to measure the laterals post-drilling, to allay a frequent concern of small operators likely to use the technology, "How do I know where it went?" The DataLogger is small (20 mm D × 15 mm L) and can record 3-axis gyro and 3-axis acceleration for 2+ hours. A user-friendly Data Processing Tool has been successfully developed, which includes data transformation, algorithms and filters for length computing path, and data visualization functions. Field-testing has proven that the DataLogger can work, and errors on longer laterals, measured at an appropriate pull speed can are on the order of 10%.

## *6.0 Recommendations*

To further improve the DataLogger hardware, firmware and Data Processing Tool, a number of factors should be observed:

1. Keep tracking new technologies and new products in MEMS sensor, flash memory and lithium cell batteries
2. Continue optimization of algorithms and parameters of the Data Processing Tool box, including the acquisition of more data sets, and some preferably through jetted laterals.
3. Once the design is final, the DataLogger should be assembled/soldered by a professional manufactory on one PCB to improve the quality and reduce the size of the instrument.

## *7.0 REFERENCES*


Abdel-Ghany, M.A., Siso, S. and Hassan, A.M. 2011. New Technology Application, Radial Drilling Petrobel, First Well in Egypt. Presented at the 10th Offshore Mediterranean Conference and Exhibition, Ravenna, Italy, 23-25 February.

Broadhead, R., Zhou, J. and Raatz, W. 2004. Play Analysis of Oil Reservoirs in the New Mexico Part of the Permian Basin: Enhanced Production Through Advanced Technologies. Open file report 479, July, 2004.

Chen, H. 2009. *Engineering Reservoir Mechanics*, unpublished course manuscript, Dept. of Petroleum Engineering, Socorro: New Mexico Tech.

Ertekin, T., Abou-Kassem, J.H., and King, G.R. 2011. *Basic Applied Reservoir Simulation*, Textbook Series Vol. 7, SPE, Richardson, Texas.

Hall, H.N. 1953. Compressibility of Reservoir Rocks. *AIME* **198**: 309-311. SPE-953309-G. http://dx.doi.org/10.2118/953309-G.

Harvard, Jeff, 2012. Personal communication, Core analysis and structural tops for Millman field.

Malone, M., Nelson, S. and Jackson, R. 2000. Enzyme Breaker Technology Increases Production, Grayburg-Jackson Field, Southeast New Mexico; A Case History. Presented at the SPE Permian Basin Oil and Gas Recovery Conference, Midland, Texas, 21-23 March. SPE-59709-MS. http://dx.doi.org/10.2118/59709-MS.

McCain Jr., W.D. 1991. Reservoir-Fluid Property Correlations - State of the Art. *SPE Res Eng* (May 1991): 266-272.

Whitson, C. and Brule, M. 2000. *Phase Behavior*. SPE Monograph Series Vol. 20. SPE.

Standing, M. B. (1977). *Volumetric and phase behaviour of oil field hydrocarbon systems.* Richardson, TX: SPE.

Xiao, Y.:"Reservoir Description and Simulation to Assess the Potential of Radial Jetted Stimulations to Enhance Oil Recovery, Case Study: Millman Field, Eddy County, New Mexico," M.S. thesis Petroleum Engineering, New Mexico Tech, August 2013.

***Data Sheets and other materials used in chip development***

Silicon Storage Technologies, Inc, "64Mbit SPI Serial Dual I/O Flash," 2010, 2-10.

Microchip Technology Inc, "MPLAB X IDE ", 2012.

Microchip Technology Inc, "XC8 programming manual ", 2012.

Microchip Technology Inc, "PIC12F1840 data sheets," 2011.

Microchip Technology Inc, "PIC16F1825 data sheets," 2012.

STMicroelectronics Group of companies,LIS331HH data sheet, 2009.

Mark Pedley, "High Precision Calibration of a Three-Axis Accelerometer, 2013.3.22

http://web.mit.edu/evt/summary_battery_specifications.pdf "A Guide to Understanding Battery Specifications"

http://en.wikipedia.org/wiki/List_of_battery_sizes, " List of battery sizes"

http://www.vectornav.com/support/library?id=86

http://www.issi.com/WW/pdf/IS25LP032-064-128.pdf , “IS25LP128 128M-BIT 3V Serial Flash Memory datasheet ”,10/3/2014

InvenSense Inc., MPU-9250 Product Specification Revision 1.0,2014

InvenSense Inc., MPU-9150 Product Specification Revision 4.0, 2012